ANISOTROPIC NANO-COLLOIDS MADE BY NOVEL ELECTRIFIED CO-JETTING AND THEIR POTENTIAL APPLICATIONS

by

Kyung-Ho Roh

A dissertation submitted in partial fulfillment
of the requirements for the degree of
Doctor of Philosophy
(Macromolecular Science and Engineering)
in The University of Michigan
2008

Doctoral Committee:

Assistant Professor Joerg Lahann, Chair
Professor Sharon C. Glotzer
Professor David C. Martin
Associate Professor Nicholas Kotov

To my parents,
my wife Hyunjung,
my son Justin Joonsang,
and my God Jesus Christ.

ACKNOWLEGMENTS

It is certainly a privilege and pleasure for an author to have the opportunity to thank the many people who made the work possible. I am not one of the exceptions.

First and foremost, I would like to thank my PhD supervisor, Dr. Joerg Lahann. He's always been a great mentor for my PhD. Every academic achievement of mine throughout the PhD years wouldn't have been possible without his guidance. He gave me this wonderful project, through which I could enjoy the excitement of creating an innovative ideas. I have learned and will continue trying to resemble his intuitive perceptiveness on science as well as his drive for greatness. I would like to thank Dr. David C. Martin for his support and guidance especially for the budding period of my thesis research. I hope that I could learn his openness in science for greater good. I would also like to thank the rest of the academic committee, Dr. Sharon C. Glotzer and Dr. Nicholas Kotov for their continuing support and encouragement.

I was lucky enough to spend my whole PhD years with three great researchers as officemates, labmates and still friends, Himabindu Nandivada, Dr. David Peng, and Dr. Hsien-Yeh Chen. I have to thank Dr. Mutsumi Yoshida. Many parts of my thesis certainly would not have been possible without her help and support. I learned a great deal of TEM techniques from Dr. Jihua Chen. I spent many enjoyable hours to better understand the electrified jetting process together with Sonsoles de Olano Biada, Sridhar

Valluri, and Srijanani Bhaskar and Yuan Ma. I cannot mention here all the vibrant discussions and willing help I received from our Lahann lab, MRG, Solomon lab, Burns group, and neighboring Kotov group members. But thank you all.

I would also like to thank my Macro people. I have to thank Nonna Hamilton for her devotion to help our program, encouragement and prayer for my success. I am grateful to Dr. Richard Laine for his support and guidance as the Program Director.

I am also grateful to many people off-site campus. I would like to thank all the members of Korean Church of Ann Arbor for the prayer and support. And I wish to thank all of my Korean friends for uncountable reasons. Lastly, and most importantly, I wish to thank my parents and my wife. Their love is what I am now.

There is one more being to thank. And he is the only reason and purpose of all this. He is Jesus Christ, my Lord.

TABLE OF CONTENTS

LIST OF FIGURES

LIST OF SCHEMES

LIST OF TABLES

ABSTRACT

In this dissertation, the novel applicability of the electrified jetting process for the control of materials distribution in nanometer scale is demonstrated. Simultaneous jetting of two or three distinct polymer solutions through jetting capillaries in a side-by-side geometry was employed to create biphasic or triphasic nanocolloids. The resulting nanocolloids consist of two or more separate compartments, which generates anisotropy. Various materials such as biomolecules, functionalized polymers, and inorganic nanocrystals were selectively incorporated into the individual phases of the nanocolloids. Selective surface modifications and chemical reactions combined with electrified co-jetting enabled demonstration of the novel concept of directional cell-membrane labeling. Selective incorporation of superparamagnetic nanocrystals in one hemisphere of nanocolloids opened a new route to control the orientation of a nano building block. The potential applications of these anisotropic nanocolloids with unique functionalities include drug delivery, bio-imaging, and novel displays.

CHAPTER 1

INTRODUCTION

1.1 Overview

In this thesis, a new concept of using simultaneous jetting of two or more parallel jetting solutions (electrified co-jetting) for the production of anisotropic multiphasic nano-objects was proposed. In order to prove this concept by appropriately designed experiments, general working parameters of the conventional electrified jetting for the control over sizes and shapes of resulting nano-objects were initially studied. Various aqueous polymer solutions were used for the initial biphasic jetting experiments, where successful encapsulation of two or three different biomolecules within distinct individual phases of a single nanosphere was demonstrated.To apply this unique anisotropy in biomedical applications, water-stabilization of the biphasic nanocolloids were performed. After initial biocompatibility of the biphasic nanocolloids was evaluated *in vitro*, directional specific labeling of cell-membrane was demonstrated as a unique biomedical application taking advantage of the particle anisotropy. For that purpose, chemical conjugation of the jetting polymers with functional ligands and selective surface modification of the biphasic nanocolloids was critical. Finally, design of biphasic objects was extended to encompass the composite structure with nanocrystals. Encapsulation of functional nanocrystals, especially magnetic nanocrystals in this thesis, into the polymeric biphasic nanocolloids in an anisotropic manner enables unique building blocks

that possess multiple functionalities. The summarized contents of following chapters are as follows.

In the following two sections of Chapter 1, a literature review is provided to summarize the previous efforts on the synthesis of anisotrpic objects. In addition, the basic principles of electrified jetting process are introduced and relatively recent developments of the process are presented, especially with regard to the use of dual capillary setup in electrified jetting. Initial studies on the morphology control by altering jetting parameters are presented as preliminary experimental results for electrified jetting of a single jetting liquid.

In Chapter 2, simultaneous jetting of two or more parallel solutions (electrified co-jetting) will be introduced as a new process for the production of multiphasic micro/nano- objects. As a novel proposal, the concept of biphasic jetting should first be proven. In order to incorporate two different components in each side of the jet, capillaries feeding two different jetting liquids should be employed in a side-by-side fashion. Similary number of jetting capillaries and jetting solutions were extended to three. Various aqueous polymer solutions were selected and used for the initial biphasic and triphasic jetting experiments, where the proposed concept of electrified co-jetting was proven by showing that two or three different biomolecules were successfully encapsulated within distinct individual phases of a single nanospheres. Characterization of the biphasic/triphasic character after the jetting will be an important issue. In order to distinguish one phase from the other, appropriate materials should be selected considering the origin of contrast for different characterization methods. Different fluorescent dyes will be incorporated in each phase for confocal microscopy, and materials with different electron density will be employed to give contrast in transmission electron microscopy.

In Chapter 3, water-stabilization of nanocolloids prepared by electrified jetting will be discussed, in order to render this unique nanocolloids more useful in many applications where expose to aqeous environment is critical. For a biomedical application where the nanocolloids function in a biological entity, the stability of the nanocolloids in physiological condition would be a prerequisite. Among many possible crossliking mechanisms, thermal imidization was selected. As aqueous solutions of poly(acrylamide-*co*-acrylic acid) were compatible with electrified co-jetting process to ensure the production of multiphasic nanocolloids, the colloids could simply be cured in an elevated temperature to induce the imdization reaction between carboxylic acid groups and amide groups in the polymer backbone chains to form imide linkages. The stability of biphsic morphology as well as the integrity of the colloidal suspension was examined. The water-stable nanocolloids described in this chapter serve as platform for the further application studies.

In chapter 4, anisotropic nanocolloids as platforms for the biological applications were proposed and tested. For the first part of this chapter, the basic biocompatibility the water-stable biphasic nanocolloids developed in chapter 3 was tested *in-vitro*. This intial biocompatibility confirms that the nanocolloids bear relatively low cytotoxicity for a certain range of tested doses. It also allows us to properly modify the nanocolloids for the specific applications. The second part of this chapter describes novel concept of direction-specific labeling of cell membrane by use of biphasic nanocolloids. In order to eliminate nonspecific interactions between the bare nanocolloids and the celluar membranes, the surface of the nanocolloids were modified with PEG chains. By introducing cell-specific antibody molecules in one hemisphere of the colloidal particle, the specific association could be made in a direction-specific manner. The selective surface modifications, the feasibility of which was already propsed in the previous

chapters, were performed in multiple steps by use of famous biotin-streptavidin linker groups.

In chapter 5, encapsulating the functional nanocrystals, especially magnetic nanocrystals, in an anisotropic manner by electrified co-jetting is proposed for the production of unique building blocks that possess multiple novel functionalities. The synthesis of nanocrystals that have desirable characteristics and the preparation of stable suspensions of nanocrystals as the jetting solutions become the critical part of the chapter.

Chapter 6 will be dedicated to conlusions and summary of the proposed future work. The basic investigation of liquid motion inside of jetting cone in conjunction with critical physical parameter of the jetting liquids would be necessary for pseudo-universal application of electrified co-jetting process. Possible optimization of the electrified jetting process is suggested for the production of nanoobjects with narrower size distribution. Leveraging multi-bore needle, more sophisticated design of the nanometer-sized building block is possible. Relatively easier production of multiphasic nanofibers by use of electrified co-jetting process is proposed and briefly discussed. And a few applications of multiphasic nanoobjects are suggested with background rationale.

1.2 Background and Literature Review

In numerous studies on organic micro/nano-objects such as polymeric micelles,(*1-3*) liposome,(*4-6*), microspheres(*7-9*) and also on the semiconductor quantum dots and nanocrystals,(*10-18*) control over their sizes and shapes has been extensively investigated. However they are mostly isotropic in terms of the material distribution within the particle. Comparably, the development of micro/nano-objects with anisotropic material distributions has been less explored. In this thesis, the development of a novel electrified co-jetting process as a drastically different syntetic route for anisotropic objects in micron and submicron scale is reported.

1.2.1 Anisotropic Objects

Regardless of the synthetic approach, the development of anisotropic biphasic objects possessing two distinct phases may establish significant advances in nanotechnology with broad impact in areas such as microelectronics and biotechnology. Potential for selective modification of each side of the biphasic object makes this system very attractive and versatile for electronic and biomedical applications.

Quite a comprehensive review on various synthetic procedures for so-called Janus-type micro/nano-particles appreared in 2004.(*19*) Summarized methods include dual-supplied spinning disk technique that is used by Gyricon display medium.(*20*) By use of simple Rayleigh instability, bichromal balls of approximately 100 μm in diameter were synthesized.(*21*) Further introduction of electronic bipolar character made them controllable electronically.

Various surface modification techniques for the introduction of anisotropy include surface modification with partial masking,(*22-25*) selective deposition,(*26, 27*)

microcontact printing,(*28, 29*) surface modification through partial contact with reactive media,(*30-32*) and template-assisted self-assembly.(*33, 34*) However, these monolayer-based methods have main limiations in the amount of particles that can be produced per batch. As the precursor particle sizes become smaller, especially into the nanometer scale, this limitation become more serious due to the enourmous increase in the necessary surface areas. In order to circumvent this drawback, several methods have been suggested. The first approach is to use curved surfaces or interfaces for the increased template suface. Emulsions (liquid-liquid interface),(*35*) solidified paraffin droplets,(*36*) and microbeads (solid-solid interface)(*37*) were further used for partial masking and selective surface modifications.

For some of the selected pairs of materials, there are known strategies to fabricate dumbbell-, snowman- or acron-like nanoparticles that are biphasic with material distribution anisotropy. These methods include controlled phase separating crystallization from precursor core-shell particles,(*38, 39*) and selected surface nucleation.(*40-42*) However, it is difficult to apply these methods for new pairs of materials due to the strict requirements in thermodynamics of controlled phase separation and crystallization.

Similar phase separation approach has been employed for biphasic polymer particle synthesis.(*43-48*) The seeded polymerization technique is a variation of emulsion polymerization, which takes advantage of the unique thermodynamics of polymers. The two polymers are immiscible to each other, while the starting two monomers may be miscible to each other, or one monomer may be miscible with the polymer of the other component. Therefore, the phase separation occurs during the emulsion polymerization, resulting in nanoparticles with anisotropic geometry and material distribution. Perro *et al.* performed similar seeded polymerization for polystyrene in the presence of silica particles.(*49*) By dissolving the polystyrene phase of the resulting snowman-like particles

before and after the necessary surface modification steps (protection-deprotection per particle), another bulk process for the production of Janus particle in large scale was successfully proposed.

Rainer *et al.* employed polystyrene-*b*-polybutadiene-*b*-poly(methyl methacrylate) and similar polystyrene-*b*-polybutadiene-*b*-poly(methacrylic acid) triblock copolymers for the synthesis of Janus micelles.(*50, 51*) These triblock copolymers have well-defined bulk morphologies due to their unique micro-phase separations. After following the selective crosslinking reaction of core polybutadiene blocks, dissolution of the bulk materials yielded Janus micelle.

Finally, creation of much larger (diameters of 50~150 microns) biphasic and multiphasic particles with monodisperse size distributions was made possible with the recent advancement of microfluidics. By use of flow focusing technology,(*52-54*) microdroplets containing chromophore molecules and biomolecules in separate phases were generated and cured by appropriate crosslinking mechanisms.(*55-58*)

1.2.2 Electrohydrodynamic Process

General Features

Electrified jetting is a process to develop liquid jets having a micro/nanometer-sized diameter, using electrohydrodynamic forces. This well-established process has been employed by two distinct categories of technical processes, electrospraying and electrospinning (Scheme 1.1). Intrinsically, these two processes have much in common in terms of experimental setup and the principal mechanisms for generating an electrified jet from the jetting liquids. In details, when high electrical potential differences (typically

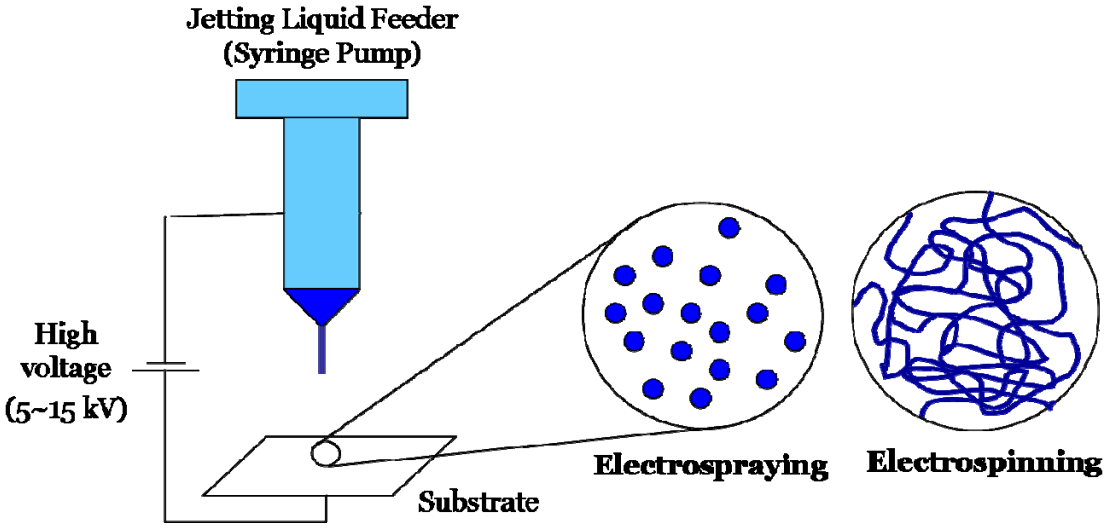

Scheme 1.1 Typical experimental setup of electrified jetting. Jetting solution is fed in a controlled flow rate by syringe pump. When a the liquid droplet coming out of the jetting capillary is electrostatically charged by applying high voltage source, the droplet deforms (Taylor cone). Above a certain critical voltage for a certain jetting liquid, a thin thread of liquid (liquid jet) is ejected from the tip of the cone. Depending on the characteristics of the jetting liquids and working parameters, the liquid jet either breaks down to aerosol-type or maintains its continuous form. In special cases where the solvents evaporate fast enough during the jetting, the solutes solidify in the form of micro/nano-sphere or nanofibers.

several thousand volts) are applied between liquids that are fed through a capillary and a collecting substrate, the electric field can generate a jet from the charged liquid.

Since electrified jetting is a electrohydrodynamic process of producing a liquid jet, the properties of the jetting liquid and operating parameters are closely related to each other. In addition, if the jetting liquid is not one-component but a mixture of more than two compounds, the jetting liquid is a solution and naturally, the properties of the solution are governed by several parameters of the solvent and solutes. As summarized in Figure 1.1, liquid properties, solution parameters, and operating parameters are interconnected in understanding and controlling this process.(*59-61*)

In fact, electrified jet, the electrostatically charged liquid thread, is produced only under a particular condition (*i.e.*, under certain combinations of the liquid and operating parameters). As previously mentioned, the jetting occurs only above the ciritical

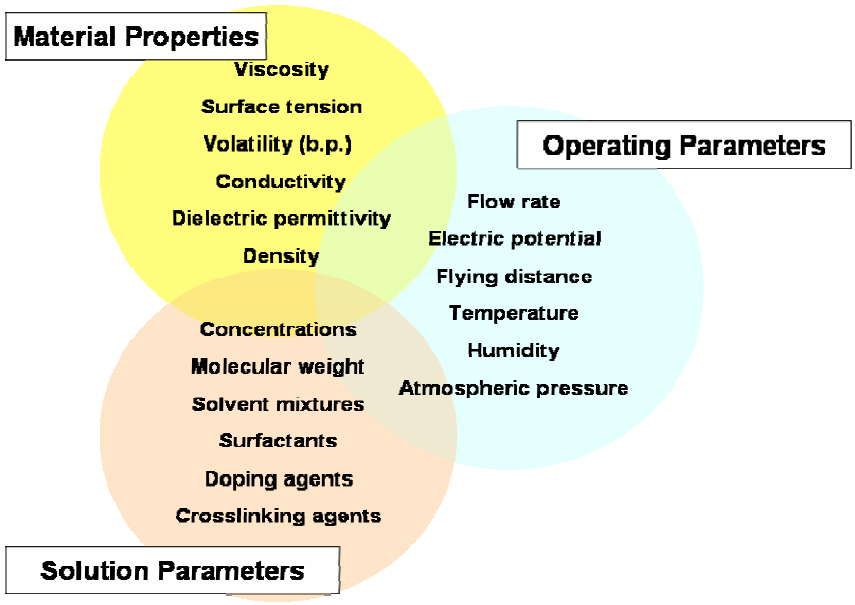

Figure 1.1 Material properties of jetting liquids and parameter windows that are governing the process of electrified jetting. Most parameters are interrelated to each other.

electrical voltage, for a jetting solution with a certain set of liquid properties. In other words, there are many other functioning modes in electrohydrodynamic processes.

First in electrospraying, this electrohydrodynanmic process is used for the continuous production of liquid droplets. The jetting liquids are usually Newtonian - such as in the case of low molecular weight compounds like water or organic solvents - and are a very dilute solution of macromolecules.(*62*) Since Zeleny's observations(*63, 64*) of several functioning modes leading to the production of aerosols with very different characteristics, several other modes and accomplished considerable theoretical and experimental works have been reported.(*65, 66*) More recently, Cloupeau *et al.* published several reports summarizing a classification of functioning modes of electrospraying.(*67, 68*) They categorized the main functioning modes of electrospraying as dripping, microdripping, cone-jet, multijet, simple jet, ramified jet, and spindle mode (Scheme 1.2) .

First, the dripping mode (Scheme 1.2a) occurs in the lowest range of applied voltage. The flow of jetting liquid fed through the capillary drops via surface tension and gravitation even without an application of electric field. When the volatage is applied between the hanging drop and the collecting substrate, the electric field attracts the liquid drop towards the substrate. At the same time, the repulsion forces between the charges on the surface of the droplet acts oppositely to the surface tention. As a result, the dripping frequency rises and the droplet size decreases as the applied volage is increased. Sometimes, this dripping mode generates not only the main drops but also one or several smaller satellite droplets per main drop. Also, this dripping mode sometimes alternates with the cone-jet mode that will be discussed below. This phenomena is attributed to the fact that the shape of pendant droplet changes over the dripping mode. At some point of

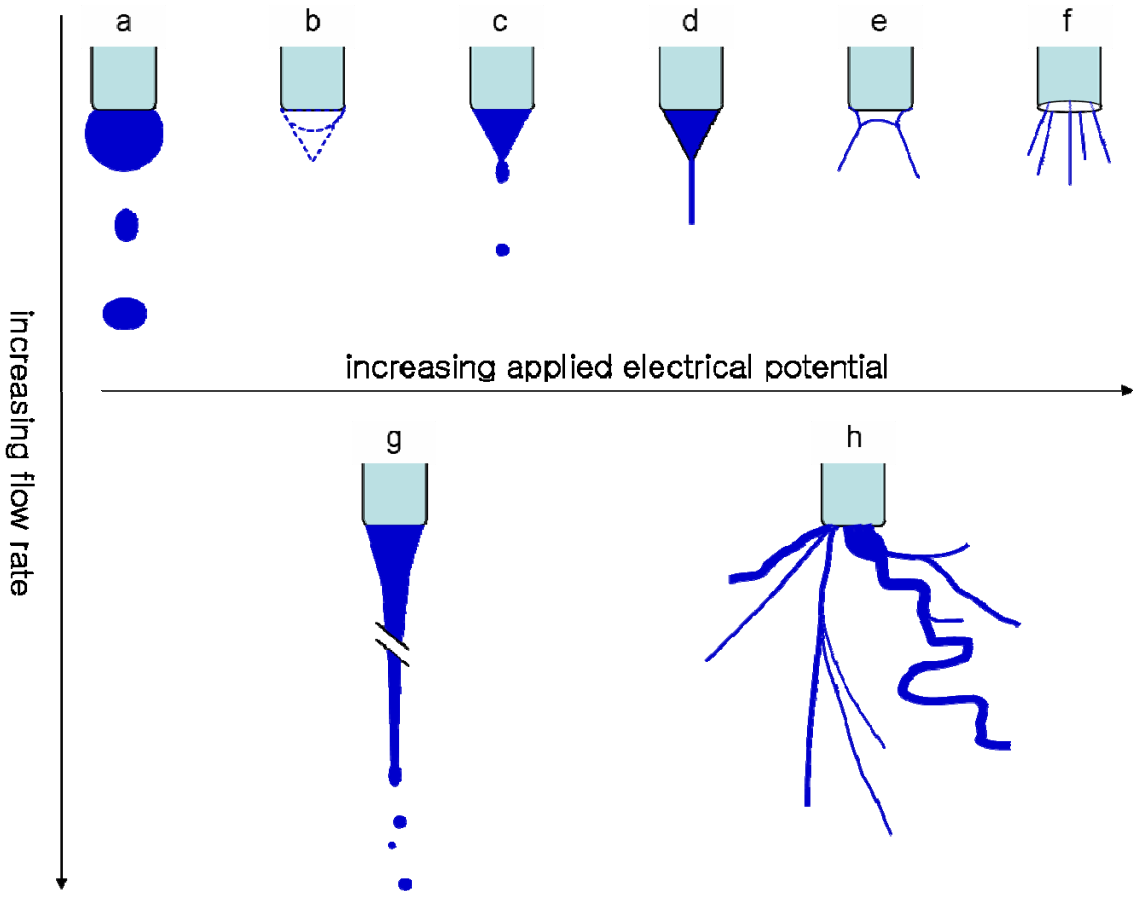

Scheme 1.2 Various functioning modes of electrohydrodynamic process. (a) dripping, (b) intermittent cone-jet, (c) microdripping, (d) cone-jet, (e-f) multijet or multiple cone-jet, (g) stable jet, and (h) ramified jet mode.

dripping mode, the electric field at the tip of the pendant droplet becomes high enough to generate a liquid jet.

In general, when the applied voltage is in an intermediate range (between dripping and cone-jet mode) at a relatively low flow rate, a certain jetting liquid possess intermittent cone-jet mode (Scheme 1.2b) or microdripping mode (Scheme 1.2c). When the voltage is slightly lower than than to produce stable cone-jet mode, the pendant droplet can alternate between the angled and the round shape. In the meantime, the jet is

ejected in a regular interval. The microdripping mode has been reported in a relatively smaller number of cases. Kozhenkov *et al.* clearly demonstrated the presence of this mode by high speed imaging,(*69, 70*) the droplet was directly generated out of the pendant cone rather than a thread of liquid, but the size of the droplet was clearly smaller than the case of regular dripping mode.

The cone-jet mode (Scheme 1.2d) has been regarded as the particularly interesting mode among these many functioning modes, as this mode typically produces monodisperse aerosols within a very wide range of average drop sizes including the submicron range. This mode can be described as follows: when an electric potential of a few kilovolts is applied, the force balance between electric field and surface tension makes the meniscus of the pendent droplet assume a conical shape - the so called the Taylor cone.(*71*) After surface charges of the cone go beyond the stabilizing effect of the surface tension (the Rayleigh limit), fission of the jet occurs. The ejected liquid jet is eventually fragmented by several instabilities and forms a spray of droplets. The shape of the cone can be either concave or convex. And the jet formation may occur at the very apex of the cone for jetting liquids with relatively high conductivities, whereas the jet formation region can extend to the edge of the capillary in the case of the liquids with lower conductivities. This cone-jet mode can be achieved for a certain range of applied potential and flow rate; however, maintenance of liquid mass balance in and out of the cone is essential for a stable cone-jet mode. If the applied potential is high enough to consume more liquid to generate jets than the liquid flow coming into the cone, the cone will eventually disappear. In the opposite case, if the inlet liquid flow into the cone is more than the outlet liquid flow as a jet, the cone will grow in volume and eventually break and drip. For a certain balanced pair of flow rate and applied potential, the diameter of the jet decreases as flow rate and corresponding applied potential decreases.

The length of the jet increases with the viscosity of the jetting liquid. In an extreme case where the jet does not break into droplets and rather forms a continuous fiber, the process is called electrospinning. A large part of the research in electrospraying involves this cone-jet mode, either for experimental(*72*) or theoretical work.(*73*) Among the various applications, production of charged gas phase ions of bio-macromolecules for mass spectroscopy is one of the most important and widely used.(*62*)

At a higher voltage, the various forms of cone-jet mode, so-called multijet (Scheme 1.2e) or multicone-jet (Scheme 1.2f), might appear. The higher surface charge causes the jet to erupt from multiple ejection points.

When the flow rate is sufficiently high, the liquid always forms a jet, regardless of the presence of an electric field. When an electrical voltage is accompanied with this critical high flow rate, the acceleration of the jet is achieved (simple jet mode, Scheme 1.2g). For a region of relative low volages, the jet is similar to the cone-jet but with a larger diameter. As the voltage increases, so do the jet ramifications (Scheme 1.2h).

Another possible functioning mode for electrospraying is the spindle mode. In this mode, the droplet formation occurs both from the tip of the pendant droplet and from the breakage of the jet. This mixture of the several functioning modes intrinsically generate droplets with broad size distribution.

As briefly mentioned above, the basic experimental setup of electrospinning is similar to electrospraying. This similarity, especially in the cone-jet mode, results from the fact that both the formation of the Taylor cone and the emission of the jet from the apex of the cone are essential to both processes. However, in electrospinning, the jet of viscous liquid is elongated until the diameter is several orders smaller than the initial value without fragmentation. The enhanced surface-to-volume ratio expedites solvent evaporation, and the polymers are solidified as nanofibers. The advantage of using a

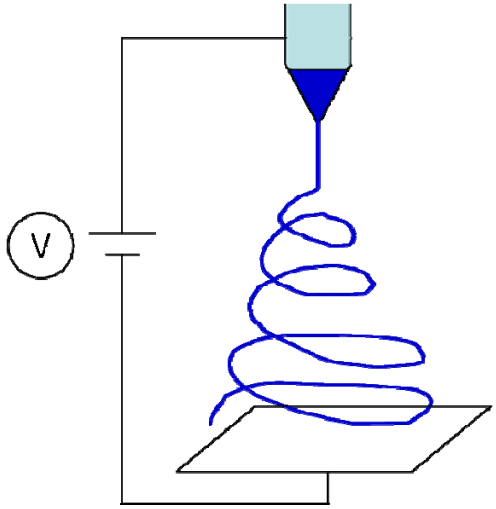

Scheme 1.3 Whipping instability of the jet during the electrospinning process. This rapid whipping motion is critical for the generation of ultrathin nanofibers.

polymer solution as a jetting liquid is that the polymer can form a stable nanoobject after solvent evaporation without any further sol/gel treatment.

The dripping mode, cone-jet mode, and stable jet mode, which have been introduced for the elctrospraying process, are simillary present in the application of viscoelestic jetting solutions for the electrohydrodynamic process. However, the characteristic production of fibers with the submicron-scale diamters from the electrospinning process has been almost exclusively achieved in the cone-jet mode (including the varied multi-jet and multicone-jet mode). Previously, the thin fibers were thought to be the result of numerous ramifications of the jet during the elctrohydrodynamic process. However, the Rutledge and the Reneker groups investigated the working mechanisms and principles of the electrospinning process theretically as well as experimentally,(*60, 61, 74-87*) and showed that the rapidly whipping jet, the convective instability accompanying with the cone-jet mode, is critical for the elongation of the jet and formation of ultrathin solid fibers (Scheme 1.3).

The idea of using an electric field to spin fibers from charged polymer melts or solutions was first reported in the 1930s. Electrospinning has seen dramatic revival of interest in recent years because of its potential to produce ultra-fine nanofibers with diameters that are a few orders of magnitude smaller than those produced by conventional spinning. As Huang *et al.* summarized in their review paper, almost one-hundred different polymers (mostly in the form of solution with solvent but melts in smaller number of cases) have been successfully electrospun to form nanofibers.(*88*) The polymer solutions that have been used as jetting liquid for the production of nanofiber can be summarized in terms of the solvent used, one of the important independent solution paramenters (Table 1.1).

Table 1.1 Jetting solutions of selected commodity polymers and their solvents.

Solvent	Polymer
Formic acid	Nylon 6,6[54]
	Nylon 4,6[55]
	Silk / fibronectin[56]
Dimethyl formamide	polyurethanes[54, 57]
	polyacrylonitrile[58]
	polyalactic acid[59]
	polystyrene[60, 61]
Dimethyl accetamide	polybezimidazole[54, 62]
	polyamide[63]
Tetrahydrofuran	polystyrene[60, 64]
	polymethylmethacrylate[60]
	poly vinyl phenol[65]
Chloroform	polycarbonate[60]
	polymethylmethacrylate[60]
Dichloromethane	poly(L-lactic acid)[66-68]
	poly vinyl carbazole[66]
Distilled water	polyvinyl alchol[69, 70]
	polyethylene oxide[29, 36, 71, 72]
Tolunene	polystyrene[60]
Methyl ethyl ketone	polystyrene[39]
Hydrochloric acid	collagen-PEO[73, 74]
Carbon disulfide	polystyrene[60]
Acetone	poly methyl methacrylate[60]
	cellulose acetate[75]
Acetic acid	cellulose acetate[75]
Ethanol	poly(2-hydroxyethyl methacrylate)[61]
Hexafluoro-2-propanol	polyehter imide[61]
Tetrahydrofuran:Dimethylforamide (9:1)	poly(ferrocenyldimethylsilane)[76]

Electrified Jetting with Coaxial Core-Shell Capillary

In the experimental setup described above for the conventional electrified jetting, uniaxial single capillary is employed for the feeding of jetting liquid. In one of the seminal papers, Loscertales *et al.* showed that this core-shell geometry can be employed in electrospraying to produce stable jets of immiscible liquids with core-shell geometry.(*89*) In this case, a monodisperse aerosol with an outer liquid encapsulating an inner liquid was produced even after the jet was broken up into a small droplets.

Moreover, this core-chell geometry became one of the major breakthoughs in the electrospinning as well.(*90*) By use of coaxial core-shell geometry, which feeds different outer and inner liquids, various coated and hollow nanofibers were created. Greiner *et al.* employed similar compound capillary and polymer-polymer solution pairs and polymer-metal salt solution pairs to produce core-shell nanofibers.(*91*) This process also was exploited together with sol-gel chemistry to produce inorganic vesicles and hollow nanofibers (nanotubes).(*92-95*) In these examples, the inner liquid served as a liquid template, and the outer liquid underwent a sol-gel transition during the flight from the capillary to the collecting substrate. Though inner and outer liquids are either immiscible or poorly miscible to each other in these studies, the authors noted that if the sol-gel transition is faster than the mixing of the two liquids, one can use miscible liquid pairs for this experimental setup. The advantage of using this core-shell capillary is not only on the generation of hollow and coated nanofibers but also on the fact that this method can be applied for materials which cannot be electrospun to form nanofibers otherwise. Yu *et al.* showed that relatively low concentration solution of poly(aniline sulfonic acid) and *Bombyx mori* silk can be used as core-liquid and successfully electrospun by help of viscoelasticity of shell-liquid of poly(vinyl alcohol) (PVA) and poly(ethylene oxide)

(PEO) solutions. Li *et al.* also successfully electrospun solution of a popular conjugated polymer, poly[2-methoxy-5-(2-ethylhexyloxy)-1,4-phenylenevinylene] (MEH-PPV), which could not be electrospun without the co-spinning of poly(vinyl pyrrolidone) (PVP) solution in the shell capillary.(*96*)

Electrified Jetting with Sidy-by-Side Capillary

Another basic configuration of dual capillary is the side-by-side capillary setup rather than core-shell geometry. Gupta *et al.* leveraged this capillary setup in electrospining to minimize the complicated thermodynamic and kinetic aspects of mixing in the production of fibers with miscible components.(*97*) Two pairs of polymer solutions, PVC/PVDF and PVC/Extane®, were employed to achieve bicomponent fibers. Field Emission Scanning Electron Microscopy (FESEM) in conjunction with Energy Dispersive Spectroscopy (EDS) analysis was used to characterize these fibers. The results showed clear coexistence of different polymer components in these fibers. However, the mixing ratio was not uniform even in one fiber due to the instability of the cone-jet mode in the electrospinning process.

Although the exact capillary geometry was not clearly reported, Madhugiri and co-workers also presented synthesis of polymer/molecular sieves composite fibers by use of similar dual syringe setup in electrospinning.(*98*) They employed conjugated polymer, MEH-PPV solution in one syringe and molecular sieve gel in the other syringe for the simultaneous jetting. The resulting composite showed blue shift in electroluminescence compared to the pure MEH-PPV nanofiber, which may be attributed to the prevention of aggregation of polymer chains by presenting silica mesoporous nanospacer.

More controlled utilization of the side-by-side geometry in electrospinning appeared in 2007. The authors electrospun SnO_2 and TiO_2 presursor solutions through

each side of side-by-side dual capillary and successfully produced anisotropic bicomponent nanofibers.(*99*) Both phases of SnO_2 and TiO_2 were exposed to the surface of the bicomponent fiber with the heterojunction interface in between. The resulting bicomponent nanofiber showed better photocatalytic activity due to the better charge separation (prevention of recombination) and efficient electron-hole utilization in catalytic activity. This work is the first example of using the sidy-by-side dual capillary for the generation of material anisotropy in nanometer scale following our original report in 2005, as described in Chapter 2.

1.3 Preliminary Experiments of Single Solution Electrified Jetting

When polymer solutions are employed as jetting liquids, roughly three different regimes can be designated for electrified jetting depending on the polymer concentrations. At the two extreme concentration regions, *i.e.*, very dilute concentration (such as below overlap concentration, c*) and fairly concentrated concentration (above c*), jetting can be categorized as electrospraying and electrospinning, respectively. Very dilute polymer solutions are similar to low molecular weight liquids (usually solvents) in terms of their viscoelasticity. The capillary break-up of the jet occurs easily to form droplets, so as to produce unimolecular macromolecule ions as in the case of application of mass spectrometry. However at higher concentrations, the capillary break-up of the jet is difficult to achieve due to the strain hardening of the polymer solution in elongational flow. During this persistence, solvent evaporation is accelerated by the elongation of the jet and eventually the jet solidifies as a fine fiber. At intermediate concentrations, beaded fibers have been observed in several cases.(*61, 87, 100-102*) This structure is sometimes referred to as beads-on-string morphology.

Poly(ethylene oxide) (PEO) solutions are one of the best studied systems, which show this morphology.(*61, 100, 101*) This unique structure is a result of competition between the elongational force of the electric field and the surface tension of the jetting liquid. Since the size and shape of the beads and string can be controlled by adjusting various liquid parameters and operating parameters, PEO solutions of concentrations in range for this morphology was selected as a starting system to investigate the parameter windows.

From previous studies,(*61, 100, 101*) viscosity, charge density, and surface tension of the jetting solutions have been identified as key factors affecting this

morphology. Viscosity and surface tension of solutions can be changed by solution parameters such as the molecular weight of polymer, concentration, and addition of other components such as co-solvents and surfactants. Charge density can be controlled by the addition of doping agents (i.e. ionizing salt) and operational parameters such as electrical potentials and neutralizing ion generation.

PEO (average viscosity molecular weight 600,000 g/mol) was purchased from Aldrich (St. Louis, MO, USA). Using distilled water as a basic solvent, solutions were prepared by magnetic stirring at room temperature. After 24 hours of dissolution, non-dissolved precipitates were removed by centrifugation and filtration. The polymer solutions were fed by a syringe pump equipped with 1ml syringe. Electrodes were connected directly to the metal capillary tip (0.3 mm diameter) of the syringe and the aluminum foil as a conducting substrate (collector). Between the two electrodes, a high-voltage supply with positive DC voltage with generating capability of up to 30 kV was connected. The distance between the electrodes was 25 cm and applied electric potential was 8 kV unless otherwise specified. Characterization of morphology of resultant objects was performed using a Scanning Electron Microscope (Model XL 30) manufactured by Phillips.

In order to familiarize with the technique, some of the experimental results presented in a previous article(*61*) were repeated and confirmed in the laboratory. As shown in Figure 1.2, increased viscosity due to increased concentration of polymer results in i) larger bead diameter, ii) longer distance between the beads, iii) larger fiber diameter, and iv) changes in shape of the beads from sphere to spindle-like.

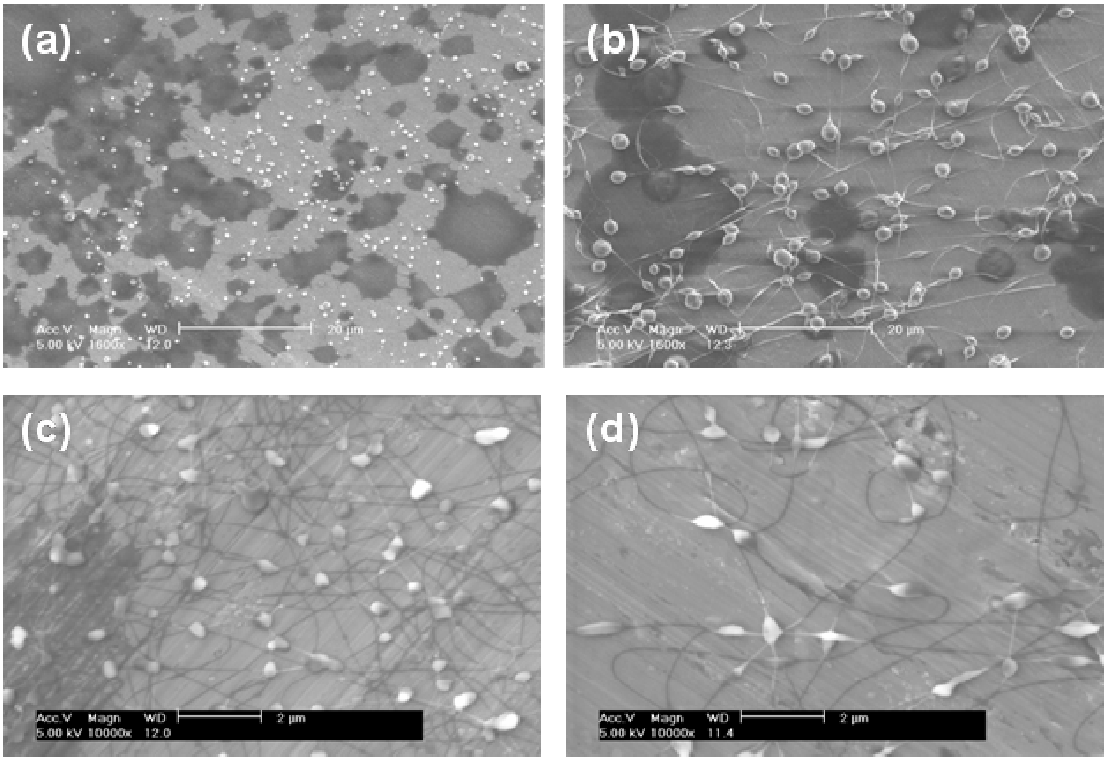

Figure 1.2 Variations of beads-on-string morphology of electrospun PEO by changing concentrations; (a) and (b): PEO solutions in mixed solvents of ethanol/water (4/6 by volume), (c) and (d): PEO solutions in distilled water; (a) and (c): 1 %, (b) and (d): 2 % by weight.

In addition to the perspectives of previous research on electrospinning, important operational parameters were confirmed in accordance with previous papers on electrospraying. Size and size distributions of the droplets in electrospraying with cone-jet mode are known to be highly dependent on the flow rate (pumping rate of the jetting liquids).(*103*) At a fixed flow rate, the size distributions consist of one or several modes with respect to the bead diameter. At minimum flow rate, the number of modality of the distributions and diameter of the droplet were also minimal.

When the flow rate is changed, the electric field must be adjusted by changing either distance or electric potential between the electrodes in order to sustain a stable cone-jet mode. Higher flow rate should be accompanied by a higher electrical field for

mass balance of jetting liquids. As shown in Figure 1.3, at higher flow rates (0.5 ml/h and 0.25 ml/h), several modes of droplets with larger diameters were observed as dark flat spot. This is attributed to the incomplete solvent evaporation from droplets before they reach the substrate, which results wet and flat droplets on the substrate.

To control morphologies by changing the process regimes from electrospraying to electrospinning and the intermediate, viscosity of the jetting liquid could be altered. The viscosity is governed by polymer concentration and molecular weight. As such, rough morphology diagram for the aqueous solutions of poly(ethylene oxide) was created (Figure 1.4). Ten data points were achieved by examining each resulting morphologies from the electrified jetting of 10 different jetting solutions that consisted of polymers of different molecular weights in different concentrations (for MW 20k, 5.0, 10, 20 %, for 100k, 1, 10, 20 %, for 600k, 0.2, 2, 6%, and for 5M, 1 % (w/v)), and approximate lines were drawn based on the data points. As expected, we observed the production of

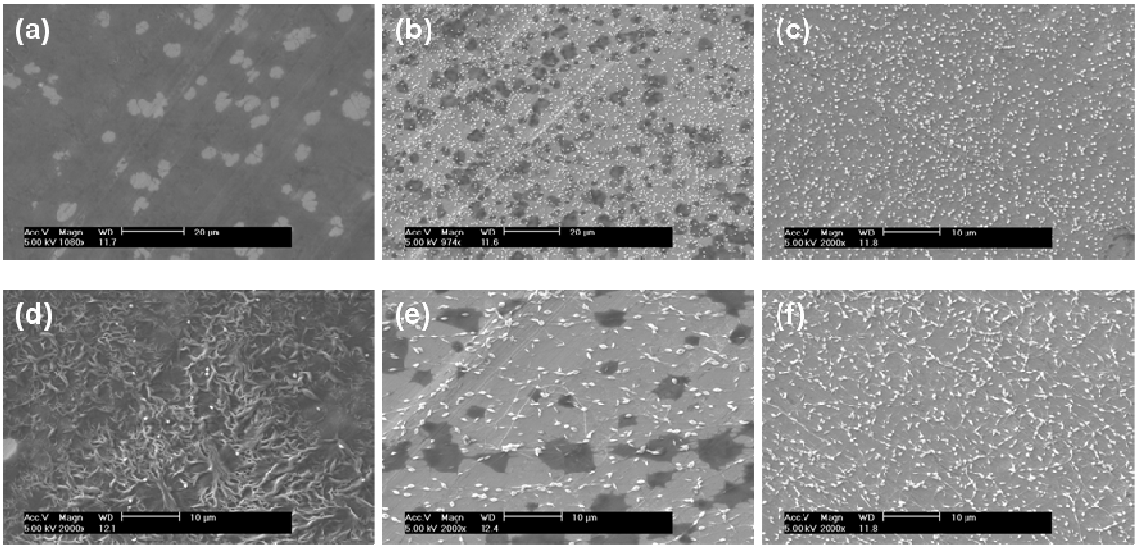

Figure 1.3 Variations of beads-on-string morphology of electrospun PEO by changing flow rate; (a), (b) and (c): PEO solutions in distilled water 0.5 % by weigh, and (d), (e) and (f): 2 % by weight; (a) and (d): 0.5 ml/ hour, (b) and (e): 0.25 ml/hour, and (c) and (f): 0.05 ml/hour.

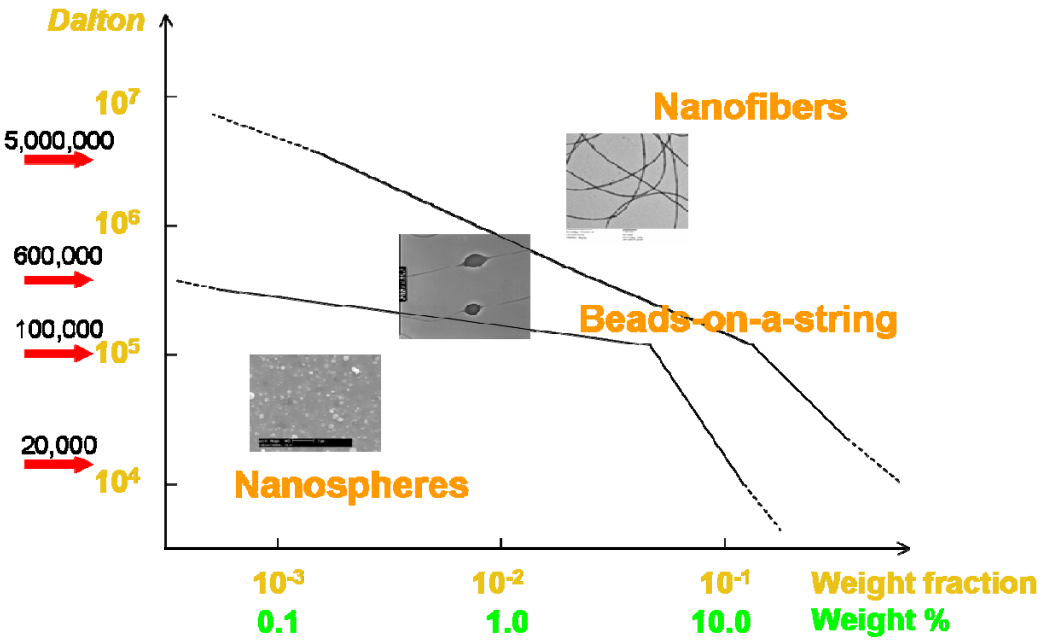

Figure 1.4 Morphology diagram of nanoobjects produced by electrified jetting of aqueous solutions of polyethylene oxides (PEOs). Ten different pairs of molecular weight and concentration were examined for the acutual morphologies, and approximate line was drawn to extrapolate the diagram.

nanospheres in low concentration and small molecular weight, and nanofibers in high concentration and large molecular weight solutions. In between, beads-on-a-string morphologies were formed.

These findings in the morphological control over the resulting nano-objects obtained by electrified jettings of aqueous based polymer solution agrees well with previous reports.(*61, 82, 104-106*) The parameter windows for the generation of stable cone-jet mode and the resulting beads-on-a-string morphology, which are determined by these preliminary experiments, will serve as the platform for further electrified co-jetting experiments described in chapter 2.

References

1. K. Mortensen, J. S. Pedersen, *Macromolecules* **26**, 805 (Feb, 1993).
2. K. Kataoka, G. S. Kwon, M. Yokoyama, T. Okano, Y. Sakurai, *Journal of Controlled Release* **24**, 119 (May, 1993).
3. B. Chu, *Langmuir* **11**, 414 (Feb, 1995).
4. R. L. Juliano, D. Stamp, *Biochemical and Biophysical Research Communications* **63**, 651 (1975).
5. D. Papahadjopoulos *et al.*, *Proceedings of the National Academy of Sciences of the United States of America* **88**, 11460 (Dec, 1991).
6. Y. Liu *et al.*, *Nature Biotechnology* **15**, 167 (Feb, 1997).
7. S. Freiberg, X. Zhu, *International Journal of Pharmaceutics* **282**, 1 (Sep, 2004).
8. J. Hanes, J. L. Cleland, R. Langer, *Advanced Drug Delivery Reviews* **28**, 97 (Oct, 1997).
9. N. K. Varde, D. W. Pack, *Expert Opinion on Biological Therapy* **4**, 35 (Jan, 2004).
10. N. Pinna, K. Weiss, J. Urban, M. P. Pileni, *Adv Mater* **13**, 261 (2001).
11. L. Manna, D. J. Milliron, A. Meisel, E. C. Scher, A. P. Alivisatos, *Nat Mater* **2**, 382 (2003).
12. R. C. Jin *et al.*, *Science* **294**, 1901 (2001).
13. V. F. Puntes, K. M. Krishnan, A. P. Alivisatos, *Science* **291**, 2115 (2001).
14. N. Malikova, I. Pastoriza-Santos, M. Schierhorn, N. A. Kotov, L. M. Liz-Marzan, *Langmuir* **18**, 3694 (2002).
15. K. Boal *et al.*, *Nature* **404**, 746 (2000).
16. R. K. Saini *et al.*, *J Am Chem Soc* **125**, 3617 (2003).
17. S. P. Wang, N. Mamedova, N. A. Kotov, W. Chen, J. Studer, *Nano Lett* **2**, 817 (2002).
18. S. H. Sun, H. Zeng, *Journal of the American Chemical Society* **124**, 8204 (Jul, 2002).
19. A. Perro, S. Reculusa, S. Ravaine, E. B. Bourgeat-Lami, E. Duguet, *Journal of Materials Chemistry* **15**, 3745 (2005).
20. http://www2.parc.com/hsl/projects/gyricon/. (accessed Feb. 2008).
21. N. K. Sheridon *et al.*, *Proceeding of the IDRC, SID/IEEE* (Sep, 1997).
22. Z. N. Bao *et al.*, *Chemistry of Materials* **14**, 24 (Jan, 2002).
23. V. N. Paunov, *Langmuir* **19**, 7970 (Sep, 2003).
24. V. N. Paunov, O. J. Cayre, *Advanced Materials* **16**, 788 (2004).
25. C. Casagrande, P. Fabre, E. Raphael, M. Veyssie, *Europhysics Letters* **9**, 251 (Jun, 1989).
26. E. Hugonnot, A. Carles, M. H. Delville, P. Panizza, J. P. Delville, *Langmuir* **19**, 226 (Jan, 2003).
27. H. Takei, N. Shimizu, *Langmuir* **13**, 1865 (Apr, 1997).

28. O. Cayre, V. N. Paunov, O. D. Velev, *Chemical Communications*, 2296 (Sep, 2003).
29. H. Y. Koo, D. K. Yi, S. J. Yoo, D. Y. Kim, *Advanced Materials* **16**, 274 (Feb, 2004).
30. K. Nakahama, H. Kawaguchi, K. Fujimoto, *Langmuir* **16**, 7882 (Oct, 2000).
31. L. Petit, E. Sellier, E. Duguet, S. Ravaine, C. Mingotaud, *Journal of Materials Chemistry* **10**, 253 (Feb, 2000).
32. L. Petit, J. P. Manaud, C. Mingotaud, S. Ravaine, E. Duguet, *Materials Letters* **51**, 478 (Dec, 2001).
33. L. Nagle, D. Fitzmaurice, *Advanced Materials* **15**, 933 (Jun, 2003).
34. Y. D. Yin, Y. Lu, Y. N. Xia, *Journal of the American Chemical Society* **123**, 771 (Jan, 2001).
35. H. W. Gu, Z. M. Yang, J. H. Gao, C. K. Chang, B. Xu, *Journal of the American Chemical Society* **127**, 34 (Jan, 2005).
36. L. Hong, S. Jiang, S. Granick, *Langmuir* **22**, 9495 (Nov, 2006).
37. M. Lattuada, T. A. Hatton, *Journal of the American Chemical Society* **129**, 12878 (Oct, 2007).
38. M. Giersig, T. Ung, L. M. LizMarzan, P. Mulvaney, *Advanced Materials* **9**, 570 (Jun, 1997).
39. H. W. Gu, R. K. Zheng, X. X. Zhang, B. Xu, *Journal of the American Chemical Society* **126**, 5664 (May, 2004).
40. S. Reculusa *et al.*, *Chemistry of Materials* **14**, 2354 (May, 2002).
41. T. Teranishi, Y. Inoue, M. Nakaya, Y. Oumi, T. Sano, *Journal of the American Chemical Society* **126**, 9914 (2004).
42. H. Yu *et al.*, *Nano Letters* **5**, 379 (Feb, 2005).
43. I. Cho, K. W. Lee, *Journal of Applied Polymer Science* **30**, 1903 (1985).
44. M. Okubo, T. Yamashita, H. Minami, Y. Konishi, *Colloid and Polymer Science* **276**, 887 (Oct, 1998).
45. H. R. Sheu, M. S. Elaasser, J. W. Vanderhoff, *Journal of Polymer Science Part a-Polymer Chemistry* **28**, 653 (Feb, 1990).
46. H. M. Ni, G. H. Ma, M. Nagai, S. Omi, *Journal of Applied Polymer Science* **76**, 1731 (Jun, 2000).
47. J. W. Kim, R. J. Larsen, D. A. Weitz, *Journal of the American Chemical Society* **128**, 14374 (Nov, 2006).
48. G. Kim, A. Sousa, D. Meyers, M. Shope, M. Libera, *Journal of the American Chemical Society* **128**, 6570 (May, 2006).
49. A. Perro *et al.*, *Chemical Communications*, 5542 (Nov, 2005).
50. R. Erhardt *et al.*, *Macromolecules* **34**, 1069 (Feb, 2001).
51. R. Erhardt *et al.*, *Journal of the American Chemical Society* **125**, 3260 (Mar, 2003).
52. A. S. Utada *et al.*, *Science* **308**, 537 (2005).
53. S. Q. Xu *et al.*, *Angewandte Chemie-International Edition* **44**, 724 (2005).
54. L. Martin-Banderas *et al.*, *Small* **1**, 688 (Jul, 2005).
55. T. Nisisako, T. Torii, T. Higuchi, *Chemical Engineering Journal* **101**, 23 (2004).

56. T. Nisisako, T. Torii, T. Takahashi, Y. Takizawa, *Advanced Materials* **18**, 1152 (May, 2006).
57. Z. H. Nie, W. Li, M. Seo, S. Q. Xu, E. Kumacheva, *Journal of the American Chemical Society* **128**, 9408 (Jul, 2006).
58. R. F. Shepherd *et al.*, *Langmuir* **22**, 8618 (Oct, 2006).
59. J. M. Deitzel, J. Kleinmeyer, D. Harris, N. C. B. Tan, *Polymer* **42**, 261 (2001).
60. Y. M. Shin, M. M. Hohman, M. P. Brenner, G. C. Rutledge, *Polymer* **42**, 9955 (2001).
61. H. Fong, I. Chun, D. H. Reneker, *Polymer* **40**, 4585 (1999).
62. J. B. Fenn, M. Mann, C. K. Meng, S. F. Wong, C. M. Whitehouse, *Science* **246**, 64 (1989).
63. J. Zeleny, *Proceedings of the Cambridge Philosophical Society* **18**, 71 (May, 1916).
64. J. Zeleny, *Physical Review E* **10**, 1 (1917).
65. A. G. Bailey, *Electrostatic Spraying of Liquids* (Wiley, New York, 1988), pp.
66. B. Vonnegut, R. L. Neubauer, *Journal of Colloid Science* **7**, 616 (1952).
67. M. Cloupeau, B. Prunetfoch, *Journal of Electrostatics* **25**, 165 (Oct, 1990).
68. M. Cloupeau, B. Prunetfoch, *Journal of Aerosol Science* **25**, 1021 (Sep, 1994).
69. V. I. Kozhenkov, A. A. Kirsh, N. A. Fuks, *Colloid Journal of the Ussr* **36**, 1061 (1974).
70. V. I. Kozhenkov, N. A. Fuks, *Uspekhi Khimii* **45**, 2274 (1976).
71. G. Taylor, *Proc R Soc Lond* **A280**, 383 (1964).
72. A. Gomez, K. Q. Tang, *Physics of Fluids* **6**, 404 (Jan, 1994).
73. J. F. Delamora, I. G. Loscertales, *Journal of Fluid Mechanics* **260**, 155 (Feb, 1994).
74. M. Ma, Y. Mao, M. Gupta, K. K. Gleason, G. C. Rutledge, *Macromolecules* **38**, 9742 (2005).
75. J. H. Yu, S. V. Fridrikh, G. C. Rutledge, *Advanced Materials* **16**, 1562 (2004).
76. M. M. Hohman, M. Shin, G. Rutledge, M. P. Brenner, *Physics of Fluids* **13**, 2201 (Aug, 2001).
77. M. M. Hohman, M. Shin, G. Rutledge, M. P. Brenner, *Physics of Fluids* **13**, 2221 (Aug, 2001).
78. Y. M. Shin, M. M. Hohman, M. P. Brenner, G. C. Rutledge, *Applied Physics Letters* **78**, 1149 (Feb, 2001).
79. S. V. Fridrikh, J. H. Yu, M. P. Brenner, G. C. Rutledge, *Physical Review Letters* **90** (Apr, 2003).
80. J. Doshi, D. H. Reneker, *Journal of Electrostatics* **35**, 151 (1995).
81. J. J. Ge *et al.*, *Journal of the American Chemical Society* **126**, 15754 (2004).
82. H. Q. Hou *et al.*, *Chemistry of Materials* **17**, 967 (2005).
83. H. F. Jia *et al.*, *Biotechnology Progress* **18**, 1027 (2002).
84. D. H. Reneker, I. Chun, *Nanotechnology* **7**, 216 (1996).
85. D. H. Reneker, A. L. Yarin, H. Fong, S. Koombhongse, *Journal of Applied Physics* **87**, 4531 (2000).

86. A. L. Yarin, S. Koombhongse, D. H. Reneker, *Journal of Applied Physics* **89**, 3018 (2001).
87. X. Fang, D. H. Reneker, *Journal of Macromolecular Science-Physics* **B36**, 169 (1997).
88. Z. M. Huang, Y. Z. Zhang, M. Kotaki, S. Ramakrishna, *Composites Science and Technology* **63**, 2223 (Nov, 2003).
89. I. G. Loscertales *et al.*, *Science* **295**, 1695 (2002).
90. Y. Dzenis, *Science* **304**, 1917 (2004).
91. Z. C. Sun, E. Zussman, A. L. Yarin, J. H. Wendorff, A. Greiner, *Advanced Materials* **15**, 1929 (2003).
92. G. Larsen, R. Velarde-Ortiz, K. Minchow, A. Barrero, I. G. Loscertales, *Journal of the American Chemical Society* **125**, 1154 (2003).
93. I. G. Loscertales *et al.*, *Journal of the American Chemical Society* **126**, 5376 (2004).
94. D. Li, Y. N. Xia, *Nano Letters* **3**, 555 (2003).
95. D. Li, Y. N. Xia, *Nano Letters* **4**, 933 (May, 2004).
96. D. Li, A. Babel, S. A. Jenekhe, Y. N. Xia, *Advanced Materials* **16**, 2062 (Nov, 2004).
97. P. Gupta, G. L. Wilkes, *Polymer* **44**, 6353 (2003).
98. S. Madhugiri, A. Dalton, J. Gutierrez, J. P. Ferraris, K. J. Balkus, *Journal of the American Chemical Society* **125**, 14531 (2003).
99. Z. Y. Liu, D. D. L. Sun, P. Guo, J. O. Leckie, *Nano Letters* **7**, 1081 (Apr, 2007).
100. R. Jaeger, M. M. Bergshoef, C. M. I. Batlle, H. Schonherr, G. J. Vancso, *Macromolecular Symposia* **127**, 141 (Feb, 1998).
101. R. Jaeger, H. Schonherr, G. J. Vancso, *Macromolecules* **29**, 7634 (Nov, 1996).
102. F. Vollrath, D. T. Edmonds, *Nature* **340**, 305 (Jul, 1989).
103. J. Rosellllompart, J. F. Delamora, *Journal of Aerosol Science* **25**, 1093 (Sep, 1994).
104. L. Huang, K. Nagapudi, R. P. Apkarian, E. L. Chaikof, *Journal of Biomaterials Science-Polymer Edition* **12**, 979 (2001).
105. H. J. Jin, S. V. Fridrikh, G. C. Rutledge, D. L. Kaplan, *Biomacromolecules* **3**, 1233 (2002).
106. P. K. Kahol, N. J. Pinto, *Synthetic Metals* **140**, 269 (2004).

CHAPTER 2

ELECTRIFIED CO-JETTING

2.1 Biphasic Jetting

The materials in this section of Chapter 2 are adapted from previously reported data in "Biphasic Janus Particles with Nanoscale Anisotropy, *Nature Materials* (2005) 4, 759-763", by K. –H. Roh, D. C. Martin, J. Lahann; and have been slightly modified.

2.1.1 Introduction

Recent advances in the field of nanotechnology have fueled the vision of future devices spawned from tiny functional components that are able to assemble according to a master blueprint.(*1*) In this concept, the controlled distribution of matter or "patchiness"(*2*) is important for creating anisotropic building blocks and introduces an additional design parameter - beyond size and shape.(*3, 4*) Although the reliable and efficient fabrication of building blocks with controllable materials distributions will be of interest for many applications in research and technology, their synthesis has been addressed only in a few specialized cases.(*5, 6*) Here we show the design and synthesis of polymer-based particles with two distinct phases. The biphasic geometry of these Janus particles is induced by the simultaneous electrohydrodynamic jetting(*7-9*) of parallel polymer solutions under the influence of an electrical field. The individual phases can be independently loaded with biomolecules or selectively modified with

model ligands, as confirmed by confocal microscopy and transmission electron microscopy. The fact that the spatial distribution of matter can be controlled at such small length scales will provide access to previously unknown anisotropic materials. This novel type of nanocolloid may enable the design of multicomponent carriers for drug delivery, molecular imaging, or guided self-assembly.

2.1.2 Methods

Materials and Preparation of Jetting Solutions

PEO (MW 600 kD), PAA (MW 250 kD), PSS (MW 200 kD), and PEI (MW 750 kD), and the model biomolecules, FITC-dextran (MW 250 kD) and rhodamine-B-dextran (MW 70 kD) were purchased from Aldrich, Inc., USA. Amino-dextran (MW 500 kD) and BODIPY® FL, SE were purchased from Molecular Probes Inc., USA.

Each jetting solution was prepared by dissolution of the components in distilled water (reported as percentage of weight per volume). For the PEO solutions, centrifugation and filtration were performed prior to use. All other solutions were used without further purification.

Characterization of Jetting Solutions

Reported molecular weights are average values and are based on the product descriptions provided by the suppliers. All solutions used as jetting liquids were fully characterized with respect to their fluid properties. Zero-shear solution viscosity was measured using a Low Shear 30 rheometer (Contraves, Zürich, Swiss). Surface tension was measured using a CAHN Dynamic Contact Angle Analyzer and conductivity was

determined using an Orion 105 Plus Conductivity Meter (both: Thermo Electron Corp., USA.) All measurements were performed at 20 °C under ambient conditions.

Electrified Jetting with a Single Capillary

Jetting solutions were stored in a 1ml syringe (Becton, Dickinson and Company, NJ, USA). The flow rate was controlled by a syringe pump (KDS100, KD Scientific Inc., MA, USA) with a control step size of 10 μl/hour. A conducting single capillary (Precision stainless steel tips, 21guage, 0.5 inch long, EFD Inc., RI, USA) was connected via the tip of the syringe and further attached to the cathode of the high voltage supply. The electron voltage was controlled in the range of 5-15 kV. A square piece of aluminum foil was connected to the anode as a collecting substrate. For samples examined with the confocal microscope, glass slides were placed on top of the aluminum foil (counter-electrode). In all cases, the distance between the electrodes was adjusted vertically in the range of 5 to 25 cm.

Electrified Jetting with Side-by-Side Dual Capillaries

The experimental setup for biphasic jetting was similar to that used for single-phase jetting as described above, except for the configuration of the capillary setup through which the two jetting liquids were fed: Using the dual syringe applicator assembly (FibriJet® SA-0100, Micromedics, Inc., MN, USA), two 1 ml syringes were controlled by a single syringe pump. Each syringe was loaded with a specific jetting solution. The two syringes were connected to a dual channel tip ((FibriJet® SA-0105, Micromedics, Inc., MN, USA), which had two capillaries with dimensions of 26 gauge

and 3 inch in length. These dual capillaries were covered with a transparent plastic tube that confined the two capillaries in a side-by-side orientation.

Confocal Microscopy

Images were taken with a SP2 confocal laser scanning microscope (Leica, USA) on the substrate containing the nanocolloids. To detect incorporated biomolecules, an Ar/ArKr laser (wavelength 488 nm) and a GreNe laser (wavelength 543 nm) were used to excite FITC-dextran and rhodamine-B-dextran, respectively. The detection wavelength range for each fluorescence emission was confined to 508-523 nm for FITC and 580-595 nm for rhodamine B. The same lasers were used for excitation of BODIPY® and rhodamine B during the selective chemical modification experiment. The detection wavelength range for fluorescent emission was confined to 500-535 nm for BODIPY® and 570-630 nm for rhodamine B.

Electron Microscopy

TEM images were obtained using a 2010 STEM (JEOL, JAPAN) with an accelerating voltage of 200 kV. All TEM samples were prepared by direct jetting onto a carbon film on top of a copper grid (400 mesh, Ted Pella, Redding CA, USA), which was mounted onto the counter-electrode. SEM images were obtained using a XL30 FEG SEM (Philips, USA) at 5 kV. SEM samples were prepared by direct jetting onto a piece of 1 square inch of aluminum foil used as counter-electrode, and were examined by SEM without further coating with a conductive layer.

Size Distribution Measruement

Based on the SEM images, bead diameters were determined. For beads with spindle-like shapes, lengths were separately measured both along the fiber axis and perpendicular to the main axis. The arithmetic mean value of those two diameters was used to obtain the histogram.

Selective Surface Modification

For surface modification, the substrate containing the nanocolloids was immersed in BODIPY® dye solution dissolved in n-hexane (5 ppm). The succinimidyl ester groups of the dye reacted within 15 min selectively with the amino groups of the particles to form a stable amide bond. After reaction, particles were immersed in excess of clean hexane for 90 min to wash out unreacted dye and visualized using confocal microscopy.

2.1.3 Results and Discussions

The compositions of the jetting solutions that were prepared and used in this study is summarized in Table 2.1. For each solution, a few physical parameters (viscosity, surface tension, and conductivity) that are believed to be critical in the electrified jetting process were characterized and summarized in Table 2.2.

Previous work in the area of electrohydrodynamics has resulted in isotropic materials made from single-phase polymer solutions,(*9-13*) blends,(*14*) and hybrid materials,(*15-17*) as well as coaxial fibers(*16, 17*) and core/shell particles.(*17-20*) In response to the applied electrical field, the liquid drop at the tip of the nozzle is distorted into a narrow cone (Taylor cone).(*7*) The electrical field further induces a stretching process that leads to the formation of a nanometer thick polymer thread, which - in conjunction with solvent evaporation - accounts for most of the size reduction.

Table 2.1 Compositions of the jetting solutions used in Chapter 2.1.

Solutions	Components in distilled water (w/v)
1	Polyethylene oxide (Mw = 600,000 g mol^{-1}) 2%, rhodamine-B-labeled dextran (Mw = 70,000 g mol^{-1}) 0.5%
2	Polyethylene oxide (Mw = 600,000 g mol^{-1}) 2%, FITC-labeled dextran (Mw = 250,000 g mol^{-1}) 0.5%
3	Polyethylene oxide (Mw = 600,000 g mol^{-1}) 2%, amino-dextran (Mw = 500,000 g mol^{-1}) 0.5%
4	Polyacrylic acid (Mw = 200,000 g mol^{-1}) 10% and rhodamine- B-labeled dextran (Mw = 70,000 g mol^{-1}) 1.5%
5	Polyacrylic acid (Mw = 200,000 g mol^{-1}) 10% and FITC-labeled dextran (Mw = 250,000 g mol^{-1}) 1.5%
6	Polystyrene sulfonate sodium salt (Mw = 200,000 g mol^{-1}) 1.5% and polyethylene oxide (Mw = 600,000 g mol^{-1}) 1%
7	Polyethylene imine (Mw = 750,000 g mol^{-1}) 0.9% and polyethylene oxide (Mw = 600,000 g mol^{-1}) 1%

Table 2.2 Summary of physical properties of the jetting solutions used in Chapter 2.1. * Nomenclature of solutions are same as summarized in Table 2.1.

Solutions*	Viscosity (mPa·s)	Surface tension (mN m^{-1})	Conductivity (μS cm^{-1})
1	40.83	60.43	114
2	40.88	60.58	104
3	45.21	59.92	119
4	26.92	65.16	3,620
5	30.66	68.08	3,540
6	21.15	49.97	4,520
7	13.07	61.01	261

During our electrohydrodynamic processing experiments, a laminar flow of two distinct polymer solutions was pumped at suitable flow rates, typically in the range of μl/min, through a modified nozzle with side-by-side geometry (Figure 2.1a).(*21, 22*) The side-by-side geometry was selected over previously reported coaxial geometries,(*16-20*) because of the bipolar polymer/polymer interface that was maintained between two jetting fluids throughout the nozzle until electrified jetting occurred. Figure 2.1b shows a micrograph of the outlet region of the nozzle. In this set-up, the biphasic character of the jetting liquid continued throughout the droplet (Figure 2.1a) and resulted in a single liquid thread that was formed at the interface of the two jetting solutions. Under certain conditions (polyethylene oxide solutions in distilled water), we observed a vortex at the tip of the liquid cone (Figure 2.1b, inlet). The spontaneous formation of vortices has been previously observed during electrified jetting of organic solvents,(*23*) which had

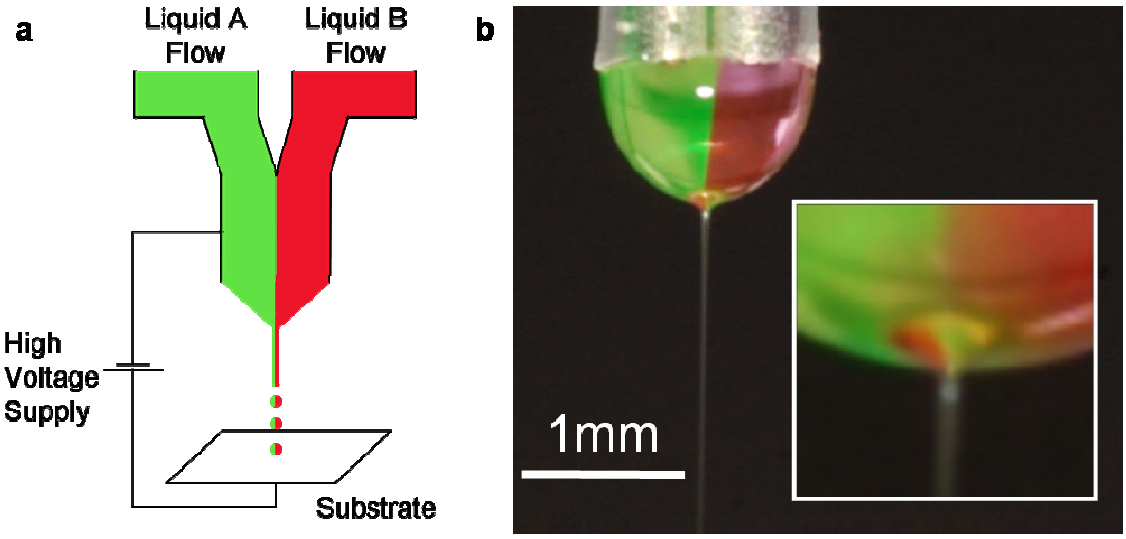

Figure 2.1 Biphasic electrified jetting using side-by-side dual capillaries. a: Schematic diagram of the experimental setup used for electrohydrodynamic processing. When exposed to an applied electric potential (5 to 15 kV depending on the jetting conditions), the bipolar jetting liquid experiences an electrical field that was formed between the tip of the liquid and the counter-electrode (collecting substrate). For certain parameter combinations, well-structured biphasic Taylor cones were observed at the tip of the nozzle; consisting of two aligned fluid phases. b: Digital image of a typical biphasic Taylor cone with jet. Poly(ethylene oxide) (PEO, MW 600 kD) dissolved in distilled water (2 % (w/v)) was used in both jetting fluids. Each phase was labeled by addition of 0.5 %(w/v) of a fluorescent dye, i.e. fluorescein isothiocyanate-conjugated dextran (green) and rhodamine-B-conjugated dextran (red). The inlet shows a detailed image of the swire-like jet ejection point. The formation of the vortex was reproducible and did not seem to interfere with the actual synthesis of the biphasic particles. The scale bar is 1 mm.

substantially lower viscosities (<10 mPa•s) and electrical conductivities (0.5 μS cm^{-1})(*23*) than the aqueous polymer solutions used in this study. The formation of the vortex was reproducible and did not seem to interfere with the actual synthesis of biphasic particles. In our jetting experiments, the liquid jets ejected from a Taylor cone could either be fragmented to particles or be sustained and elongated in the form of continuous fibers. As previously reported for one-phasic systems,[10-12] the differences in the final morphologies were mainly determined by properties of the jetting liquids (viscosity,

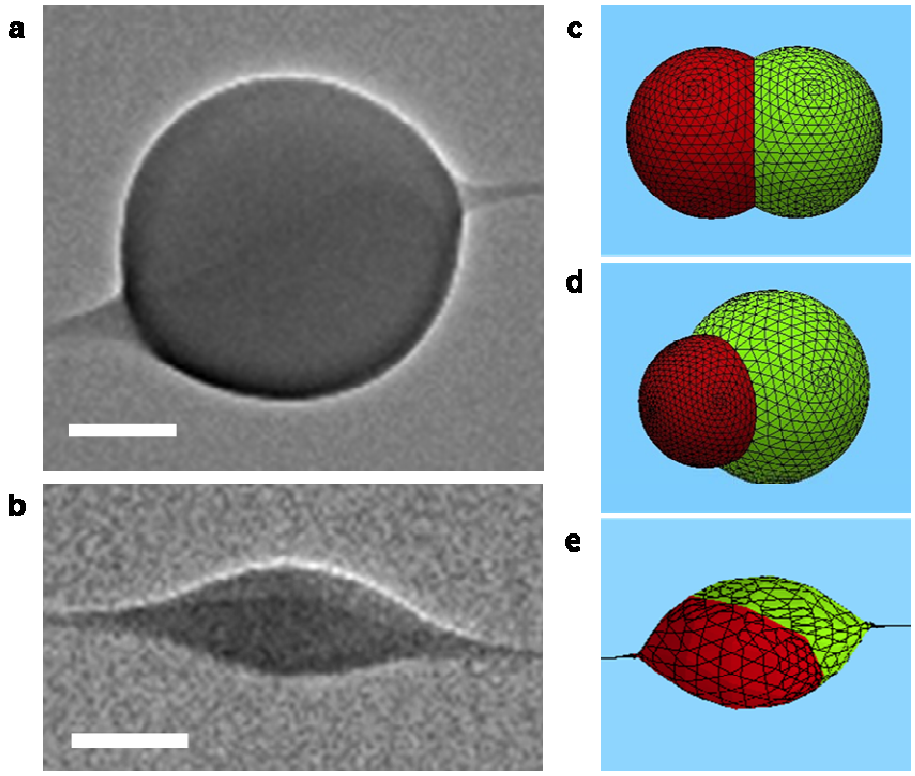

Figure 2.2 Biphasic anisotropy examined by TEM and Modeling. a and b: The jetting solution is composed of 1.0 %(w/v) of PEO (MW 600 kD) in each side. Dark contrast was due to poly(styrene sulfonate), sodium salt (PSS, Aldrich Inc., USA), which was included in one jetting solution. Poly(ethylene imine) (PEI, Aldrich Inc., USA) was added to the other jetting solution. Scale bar is 100 nm. c, d and e: Particle morphologies shown for the case that two jetting liquids reach the thermodynamic equilibrium state. For $\gamma_{AV} \approx \gamma_{BV}$, a peanut-like geometry, c, ($V_A = V_B$ and $\gamma_{AB} > 0$) or an eyeball-like geometry, d, ($V_A = 4V_B$ and $\gamma_{AB} > 0$) can be obtained; e, spindle-like geometry ($V_A = V_B$ and $\gamma_{AB} = 0$) was obtained by enforcing boundary conditions that tether the two halves of the droplet between two opposing solid surfaces.

conductivity, and surface tension) and electrohydrodynamic parameters (applied field strengths, flow rates); and could be controlled with relative ease.

One objective of our initial experiments was to determine whether biphasic particles with sub-micrometer diameters are accessible through electrohydrodynamic jetting. In a series of experiments, we fabricated biphasic objects from a dilute aqueous

solution of a polyethylene oxide (PEO, MW 600 kD). The morphology of the objects was characterized by transmission electron microscopy (TEM). Depending on the choice of process parameters, the shape of the objects was varied and both discontinuous particles and long fibers could be observed. Figures 2.2a and 2.2b show characteristic TEM micrographs of biphasic particles prepared from two jetting fluids: (1) 1 % PEO and 1.5 % sodium polystyrene sulfonate (PSS, MW 200 kD) and (2) 1 % PEO and 0.9 % polyethylene imine (PEI, MW 750 kD). PSS characterized by the dark contrast in TEM images was selectively found in one phase revealing the biphasic character. Most of the poyethylene oxide-based objects had diameters between 100 and 400 nm and were connected through nanofibers with approximate diameters below 10 nm. In the case of polyacrylic acid (PAA, MW 250 kD, 10 %), discontinuous particles as small as 170 nm were observed. Because our Janus particles are larger than traditional nanoparticles,(*3-6*) but smaller than typical colloids, we will refer to them as nanocolloids.

Although potential shapes of biphasic nanocolloids are largely unknown, modeling studies may provide means to estimate what stable structures can be expected. The geometry of a biphasic droplet was estimated using the Surface Evolver program developed by Ken Brakke at Susquehanna University.(*24*) During electrohydrodynamic jetting, nano-objects emerge from fluid droplets with predictable geometries. At equilibrium, a fluid droplet composed of a phase A and a phase B has three characteristic free surface energies: the surface free energy of the phase A/vapor interface (γ_{AV}), the surface free energy of the phase B/vapor interface (γ_{BV}), and the surface free energy of the phase A/phase B interface (γ_{AB}). For our experimental system, γ_{AV} is similar to γ_{BV} and the equilibrium geometry of the resulting biphasic nanodroplets will mainly be determined by γ_{AB} and the relative volumes of the phases A and B. For $\gamma_{AB} = 0$ and equal amounts of A and B, the equilibrium state is a sphere, with phase A in one hemisphere

and phase B in the other. With increasing γ_{AB}, the sphere pinches down in the middle to reduce the interfacial area between phases A and B. This creates a bicomponent particle with a peanut-like geometry (Figure 2.2c). For nanodroplets with different volumes of phases A and B, eyeball-like envelopes are formed (Figure 2.2d). Figure 2.2e shows an example of a stable biphasic structure for $\gamma_{AB} = 0$. To a first approximation ($\gamma_{AB} \geq 0$), particle envelopes and interfaces of modeled nanodroplets and particles realized in practice (Figures 2.2a and 2.2b) were in good agreement. It can therefore be assumed that the predicted structures establish thermodynamic energy minima, towards which the nanocolloids will tend to converge during electrified jetting. Nonetheless, the TEM pictures also reveal some differences. For instance, the peanut-like structure of Figure 2.2c was not realized in practice, which may indicate that the particles were indeed not fully converged into the equilibrium shape. Observed discrepancies between model and experiment can be attributed to the contribution of additional factors, such as solidification due to solvent loss, or fluid relaxation during electrohydrodynamic processing.

Based on the results of simulation and experiment, we concluded that (1) the overall shape of the biphasic nanocolloids resembles shapes previously observed for single-phasic nanoparticles;(*10-13*) (2) preferential compartmentalization is due to the manipulations of the liquid phase and the interface is maintained throughout jetting and solidification; and (3) the nano-objects represent solidified intermediates. The apparent divergence from the equilibrium shape may provide opportunities to extend the method to the fabrication of biphasic particles with a wide range of non-equilibrium shapes, but may also be a potential source of inhomogeneities in nanocolloids' geometries. So far, these

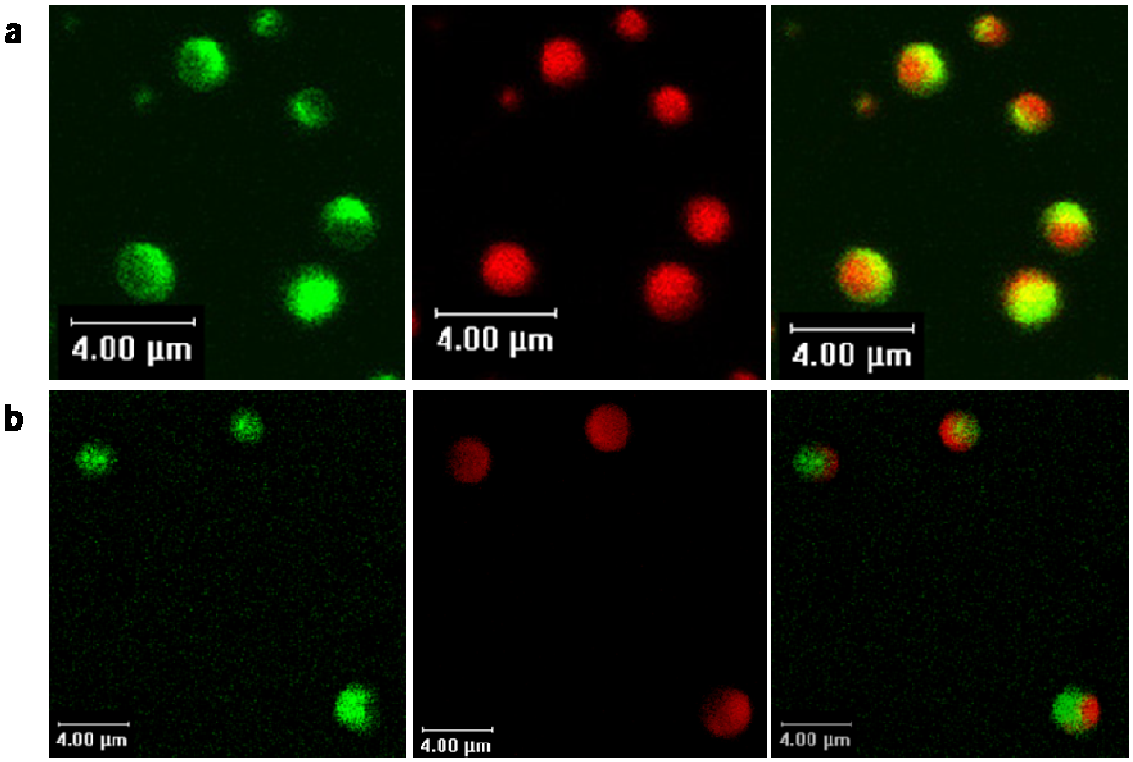

Figure 2.3 Encapsulation of biomolecules in dipolar fashion. Two distinct polymer systems based on polyethylene oxide (a) and polyacrylic acid (b) were used as biphasic carriers. Color-encoded biomolecules (FITC-dextran, green, and rhodamine-B-dextran, red) were incorporated in individual sides. Confocal micrographs of biphasic particles shown at the fluorescence emission range of FITC and rhodamine B. The overlays of these two phases reveal the biphasic character of the nanocolloids. For confocal microscopy, particles with diameters above 1 micron were selected for best imaging results.

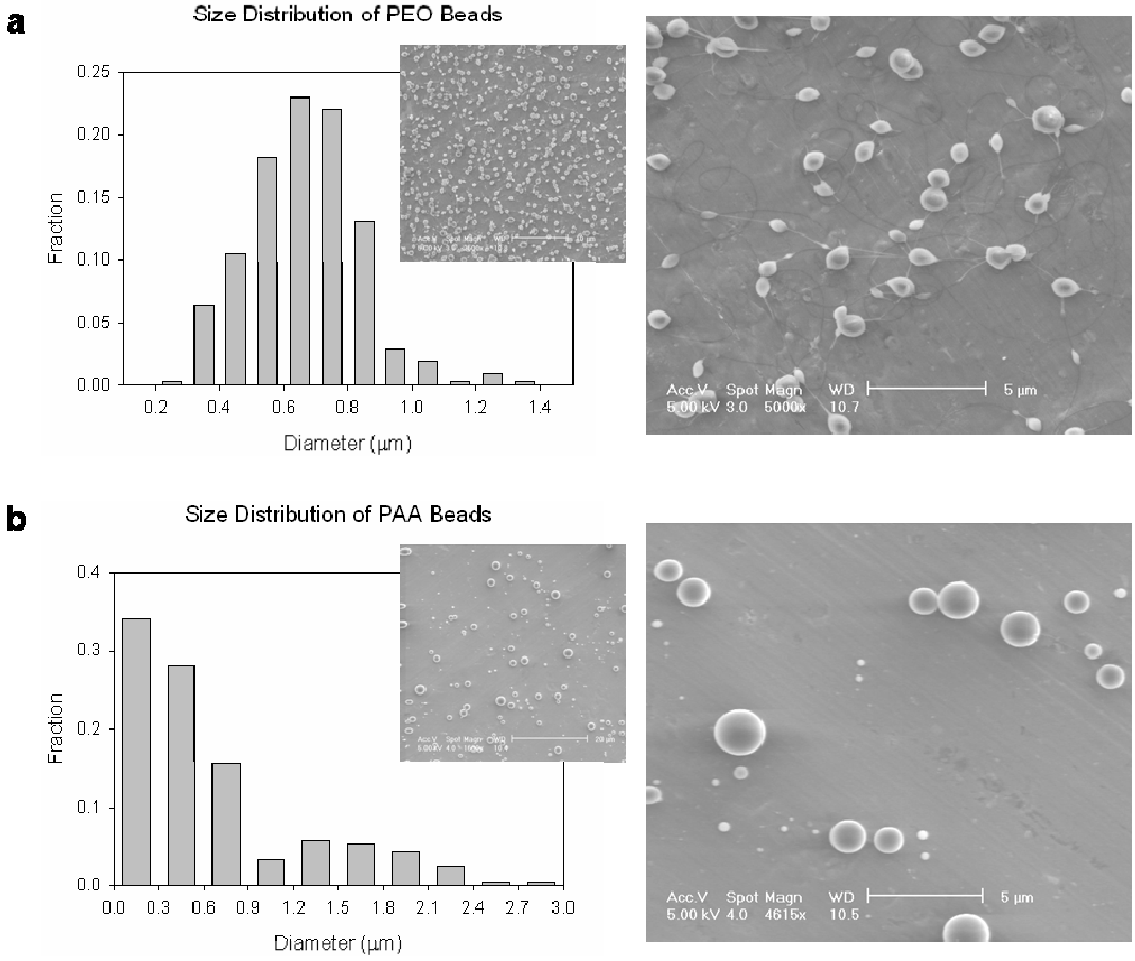

Figure 2.4 Size distributions of PEO (a) and PAA (b) biphasic particles determined from the SEM images (shown as inlets). Typical SEM images of higher magnifications show that PEO particles are linked with fine fibers (beads-on-a-string), while PAA particles have perfectly spherical envelopes. Scale bars of inlets are 10 microns (a) and 20 microns (b) and of enlargements are 5 microns.

phenomena have only been studied for water-based systems and further studies are warranted to establish the limits of these correlations; especially for systems that use organic solvents with lower surface free energies.

Some applications may require particles to act as selective carriers for two or more independent ingredients, such as molecular probes or drugs. To address the question of whether electrohydrodynamic jetting can be used to create Janus particles that

can function as multi-component carriers, we loaded the jetting fluids with two different model molecules; one in each phase. Using confocal laser scanning microscopy (Figures 2.3a and 2.3b), both molecules were identified based on their characteristic fluorescence emissions: (1) FITC-labeled dextran (green fluorescence); and (2) rhodamine-B-labeled dextran (red fluorescence). The confocal micrographs suggest that the two macromolecules preferentially compartmentalized within the particles. This finding was independent of whether we used polyethylene oxide (PEO) or polyacrylic acid (PAA) as base polymer. The superposition of the images in Figures 2.3a and 2.3b indicates the biphasic character of the particles along a thin interface that appears yellow in the confocal micrographs. The particles were further examined by scanning electron microscopy to determine particle shapes and sizes (Figures 2.4). Particles made of PEO were spindle-like and had an average diameter of 660 nm and a relatively narrow size distribution (standard deviation: 180 nm), while PAA particles had perfectly spherical envelopes and were discontinuous. Analysis of the histogram (Figure 2.4b) revealed a broader size distribution for PAA nanocolloids. A large subpopulation of the PAA particles consisting of about 80% of all nanocolloids was smaller than 1 micron in diameter. For this subpopulation, the average diameter was (402 ± 209) nm. It has been shown in the past that hydrodynamic focusing can greatly improve the monodispersity of colloids,(*20, 25, 26*) although less is known for submicron-size particles.(*19*) Nevertheless, the implementation of similar refinements may lead to biphasic nanocolloids with narrower size distributions.

Once the ability of biphasic particles to act as carriers for multiple components was demonstrated, we directed our study towards the selective modification of one specific particle phase. Selective modification, i.e. the ability to independently address only one of the two phases, will result in biphasic particles with distinct surface

properties. The enhanced anisotropy, in turn, will be essential to a directed assembly of hierarchical structures or devices (controlled patchiness). This type of selective chemical modification will also be instrumental to the use of biphasic particles in targeted drug delivery.

To elucidate the possibility of selective modification of patches of the biphasic nanocolloids, we conducted a series of experiments, wherein we added a small amount of an amino-functionalized polymer to one of the jetting fluids prior to electrohydrodynamic processing. In the example shown in Figure 2.5a, single-phasic nanocolloids were prepared via electrohydrodynamic processing of solutions composed of PEO (Mw 600,000 g mol^{-1}, 2 %) and amino-dextran (Mw 500,000 g mol^{-1}, 0.5 %). The free amine groups of the resulting particles were subsequently modified with 4,4-difluoro-5,7-dimethyl-4-bora-3a,4a-diaza-s-indacene-3-propionic acid, succinimidyl ester (BODIPY® FL, SE) ligands following a modified reaction protocol developed for conjugation and immobilization of biomolecules.(*27*) After chemical modification, the amino-modified nanocolloids showed homogenously distributed green fluorescence, indicating efficient binding of the ligand throughout the entire particle. In a second series of experiments, the nanocolloids were loaded with a rhodamine-dextran instead of the amino-dextran. No fluorescence associated with the BODIPY® ligands was observed suggesting that unspecific binding of the ligands to the nano-objects did not occur. In contrast, red fluorescence caused by the rhodamine-dextran was found throughout the reference particles (Figure 2.5b).

We concluded from these results that the amino groups were available for selective modification via amide formation and that the binding was of covalent nature, rather than based on unspecific interactions. We finally prepared biphasic nanocolloids with an amino-dextran in the first phase and a rhodamine-dextran in the second phase.

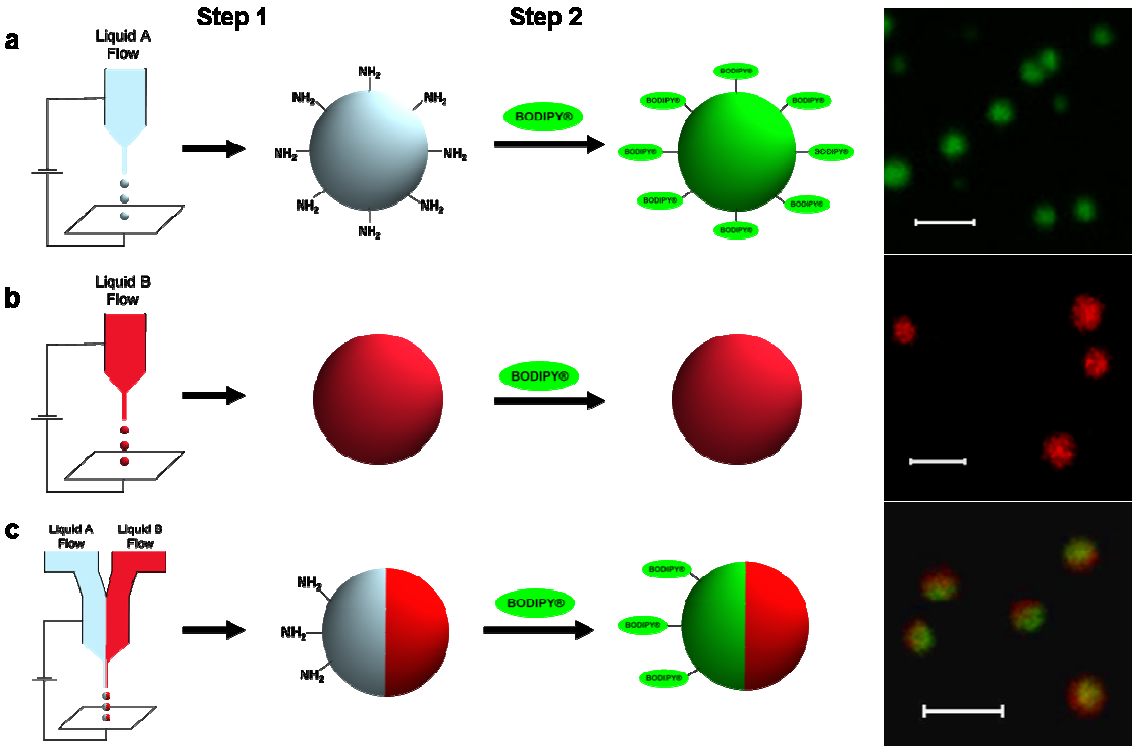

Figure 2.5 Scheme of the selective chemical modification. Jetting liquid A is a mixture of PEO (MW 600 kD, 2% (w/v)) and amino dextran (MW 500 kD, 0.5 % (w/v)) dissolved in distilled water. In jetting liquid B, rhodamine-B-dextran (MW 70 kD, 0.5 % (w/v)) is used instead of amino dextran. Confocal images are overlays of green and red fluorescence emission images. (a) Single jetting experiment with liquid A. The surface is modified via reaction between amine groups and BODIPY® dye molecules. (b) Single jetting experiment with liquid B. Only red fluorescent is observed due to rhodamine B originally incorporated in the jetting solution. No fluorescent due to BODIPY® is detected. **c**: Selective chemical modification of one side of the biphasic nanoparticles. Both, green fluorescent emission due to reacted BODIPY® dye and red fluorescent emission due to incorporated rhodamine B are observed and reveal the biphasic character of the nanocolloids. The data confirm that the reaction of the biphasic particles with the BODIPY® ligand results in selective binding to only one phase. For confocal microscopy, particles with diameters around 1 micron were selected for best imaging results. All scale bars are 2 microns.

After reaction with the BODIPY® ligand, nanocolloids were examined by confocal microscopy. The resulting micrographs (Figure 2.5c) confirm selective binding of the BODIPY® ligand to the amino-dextran containing phase only.

2.1.4. Conclusions

The concept of using small-scale fluid manipulation to fabricate solid materials with otherwise difficult to obtain properties has recently started to emerge as a promising theme in materials prcessing.(*19, 25, 26*) We have now extended this concept to the fabrication of anisotropic Janus particles with well-defined distributions of matter. Larger, colloidal Janus particles(*28*) accessible through dewetting,(*29*) microcontact printing,(*30*) or gel trapping(*28*) have been studied because of their potential as photonic crystals or electrolyte sensitive gels. To fabricate biphasic nanocolloids we now utilized an electrohydrodynamic jetting process that may be compatible with a wide range of commodity polymers.(*9*) Future research may be directed towards enhancement of the bipolarity of the particles, improved monodispersity, and the development of alternative anisotropic geometries including multiphasic nano-objects. The fact, that nanocolloids with controlled distributions of matter have been created, raises hope that these findings will, with further study, have implications in drug delivery, molecular imaging, electro-rheological fluids, and the fabrication of smart displays.

2.2 Triphasic Jetting

The materials in this section of Chapter 2 are adapted from previously reported data in "Triphasic Nanocolloids, *Journal of the American Chemical Society* (2006) 128, 6796-6797" by K. –H. Roh, D. C. Martin, J. Lahann; and have been slightly modified.

2.2.1 Introduction

One of the major challenges in current nanotechnology is the control of materials distribution at ultra-small length scales, potentially leading to multicompartmental nanoparticles. As introduced in Chapter 1, the simplest versions thereof are two-sided particles, so called Janus particles, which are believed to be of importance for designing active nanostructures or as functional elements in future device generations.(*31*) Previously known methods to create this geometries were summarized in Chapter 1, including surface modification with partial masking,(*30, 32, 33*) selective deposition,(*34, 35*) microcontact printing,(*36*) template-assisted self-assembly,(*37, 38*) emulsion polymerization,(*39*) surface nucleation,(*6, 40, 41*) or the derivation from core-shell particles.(*42, 43*)

Most of these approaches are intrinsically limited to binary systems making the fabrication of multi-compartmental nanoparticles an exceptional challenge. New and radically different approaches are needed to realize their efficient synthesis. The results shown in Chapter 2.1 serves as a first step towards the fabrication of multi-phasic nanocolloids.(*44*) In Chapter 2.2, extension of the concept of electrified co-jetting to the simultaneous manipulation of three liquid flows is proposed; thereby establishing a versatile and simple avenue towards triphasic nanocolloids, i.e. nanocolloids with three distinct compartments.

2.2.2 Methods

Materials

PEO, PAA, FITC-dextran (MW 250 kD), rhodamine-B-dextran (MW 70 kD) and Atto655-NHS (N-Hydroxysuccinimide)-ester dye were purchased from Aldrich, Inc., USA. PAAm-*co*-AA (MW 200 kD) was purchased from Polysciences, Inc. USA. Alexa Fluor® 647-conjugated bovine serum album (BSA) (MW 66 kD) and amino-dextran (MW 70 kD) were purchased from Molecular Probes, Inc., USA.

Solution Preparation

To purify the PEO solutions, centrifugation and filtration were performed prior to use. The other solutions were used without further purification. Every solution was prepared by dissolution of the components with distilled water (reported as percentage of weight per volume). Every fluorescent dye-conjugated biomolecule except Atto 655-conjugated dextran was used as purchased. Atto 655-dextran was prepared by 2 hour reaction between 50 mg of amino dextran and 0.35 mg of Atto 655-NHS-ester dye in 5 ml of distilled water followed by membrane dialysis and lyophilization.

Electrified co-jetting

Each of three jetting solution was stored in a 1 ml plastic syringe (Becton, Dickinson and Company, NJ, USA). The flow rate was controlled by a syringe pump (KDS100, KD Scientific Inc., MA, USA) in the range of μl/min. Three parallel capillaries were assembled by putting three conducting needles (20 gauges, 5 cm long) as described in the main text. A transparent plastic tube was used to encircle three

capillaries together. Positive voltage was applied with high potential generator (ES30P, Gamma High Voltage Research, Inc., USA).

Thermal imidization

Reaction were performed at 175 ^{o}C for 3 hours in a convection oven before the stabilized nanocolloids were suspended in water. When necessary, 5 minutes of tip-type sonication was performed to prepare well suspended nanocolloids.

Confocal laser scanning microscopy

Images were taken with a SP2 CLSM (Leica, USA). Each fluorescent dye was excited with different lasers (Ar/ArKr laser at 488 nm for FITC, GreNe laser at 543 nm for Rhodamine B and HeNe laser at 633 nm for Alexa Fluor® 647 or Atto 655). Individual phases were observed in separate windows for their characteristic emission wavelength ranges (505-535 nm for FITC, 570-610 nm for Rhodamine B and 655-700 nm for Alexa Fluor® 647 or Atto 655). For a better phase distinction, the colors for each observation channel were digitally designated differently from the actual emission colors (blue, green and red for FITC, Rhodamine and Alexa Fluor 647 or Atto 655 respectively).

Scanning electron microscopy

Images were obtained using XL30 FEG SEM (Philips, USA) at 5 kV. SEM samples were prepared by direct jetting onto a piece of 1 square inch aluminum foil as a substrate, and were seen by SEM without coatings of conductive layer.

Size distribution measurement

Based on the SEM images, bead diameters were measured. For PEO beads with spindle-like shapes, lengths were separately measured both along the main axis and perpendicular to the main axis, and the arithmetic mean value of those two diameters was used to obtain the histogram.

2.2.3 Results and Discussions

In the electrohydrodynamic processing experiments herein, a laminar flow of three distinct polymer solutions was pumped at suitable flow rates, typically in the range of μl/min, through a modified nozzle with side-by-side geometry.(*21, 22, 44*) The schematic diagram of Figure 2.6a shows three parallel jetting capillaries used in a

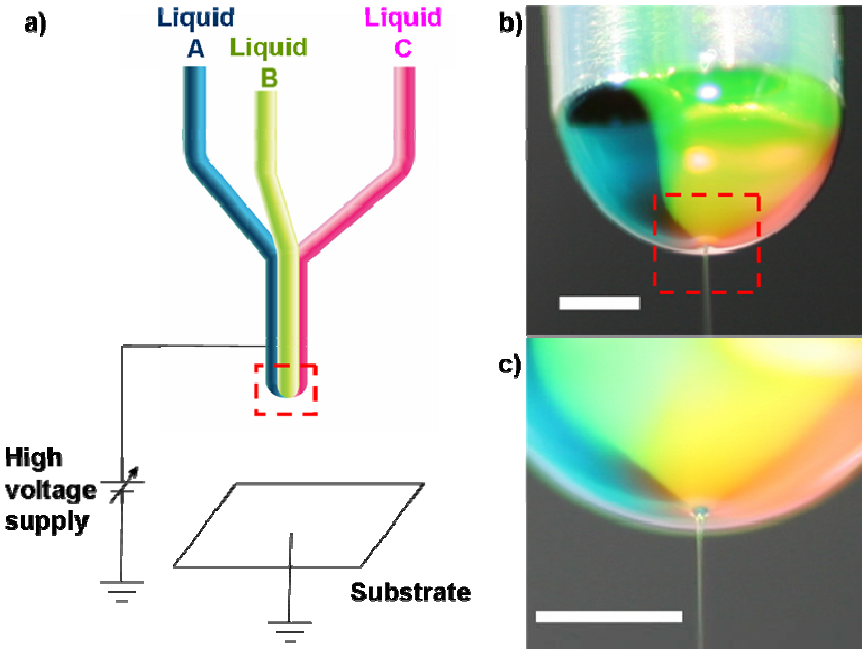

Figure 2.6 (a) Typical electrified jetting setup with triple side-by-side capillaries. (b) Actual photograph of the capillary outlet region designated with dotted line in (a). (c) Enlarged photograph of the jet ejection point designated with dotted line in (b). Scale bars are 500 μm.

conventional electrified jetting setup. The capillaries are aligned to form a triangular cross-sectional geometry. Because the laminar flow regime extends through the needles into the outlet region, droplets with three distinct interfaces can be formed. Figure 2.6b shows an image of the outlet region during the jetting process, which consists of three fluid flows (applied electric potential is approximate 10 kV). The green, red, and blue jetting solutions are composed of polyethylene oxide (PEO, MW 600,000 g/mol) mixed with different dyes: Fluorescein-conjugated dextran (green), Rhodamine B-conjugated dextran (red), and Alexa Fluor® 647-conjugated bovine serum albumin (blue). From the digital image (Figure 2.6b) and the enlargement shown in Figure 2.6c it is apparent that the three phases are maintained throughout the pendant droplet. Moreover, the digital image reveals a single liquid thread contemplating the interface between the three phases. The electrified co-jetting conditions were selected to ensure that the liquid jets ejected from the Taylor cone were fragmented to particles rather than extended to nanofibers. Nevertheless, the co-jetting approach should be similarly extendable to the fabrication of tri-compartmental nanofibers. Once the polymer thread is elongated under the influence of the accelerating electrical field, "instant" evaporation of the solvent and solidification occurs. Much of the appeal of the electrified co-jetting approach stems from the fact that solid nanocolloids are fabricated by manipulation of fluids, which can often be controlled in a simpler and more precise manner than solids.

Once the triphasic nanocolloids were prepared, confocal laser scanning microscopy (CLSM) and scanning electron microscopy (SEM) was used for characterizations (Figures 2.7a and 2.7b). In the CLSM experiments, each fluorescent dye was excited with different lasers and the individual compartments were observed in separate windows. As shown in the overlay of the three confocal images (Figure 2.7a), the biomacromolecules loaded in each jetting liquid remain compartmentalized to form separate phases. Although a range of different nanocolloidal architectures and interfaces is typically observed, the triangular geometry of the multi-phasic nanocolloids shown in Figure 2.7a appeared to be predominant. Figure 2.7b shows a SEM picture of PEG-based nanocolloids, which were still linked by fine polymer threads with diameters of the order of ten nanometers (beads-on-a-string morphology).

In principle, jetting of polymer solutions under the influence of electrohydrodynamic forces can be applied to a wide range of commodity polymers. In addition to the PEO-based system, we also processed jetting fluids based on polyacrylic acid (PAA) and polyacrylamide-*co*-polyacrylic acid (*45*)(PAAm-*co*-AA). The use of

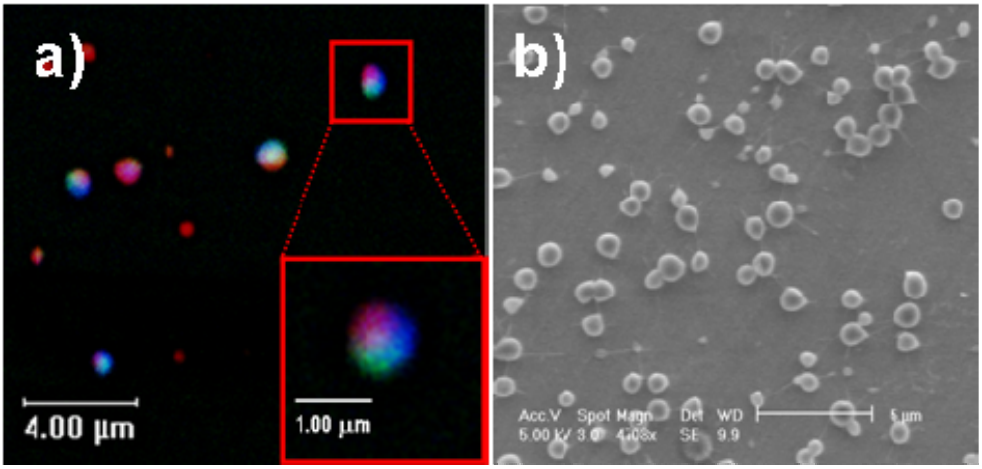

Figure 2.7 Confocal laser scanning microscopy image (a) and scanning electron microscopy (b) of PEO based triphasic particles.

aqueous solutions for electrified co-jetting leads to nanocolloids that are inevitably water-soluble. Studying triphasic nanocolloids in aqueous environments will therefore require an extra modification step to stabilize the nanocolloids. Similar stabilization of polymer-based structures has been achieved by photochemical(*46*) or thermal crosslinking.(*47, 48*) To stabilize the triphasic nanoclolloids, we turned to the thermal imidazation, i.e., the temperature-induced crosslinking of carboxylic acid groups of PAA with amide groups of PAAm.(*49*) Thermal imidization proved to be an effective way to stabilize the PAA- and PAAm-based nanoparticles.

To probe the stability of cross-linked tri-compartmental particles in aqueous solutions, we incorporated differently colored macromolecular dyes into the aqueous

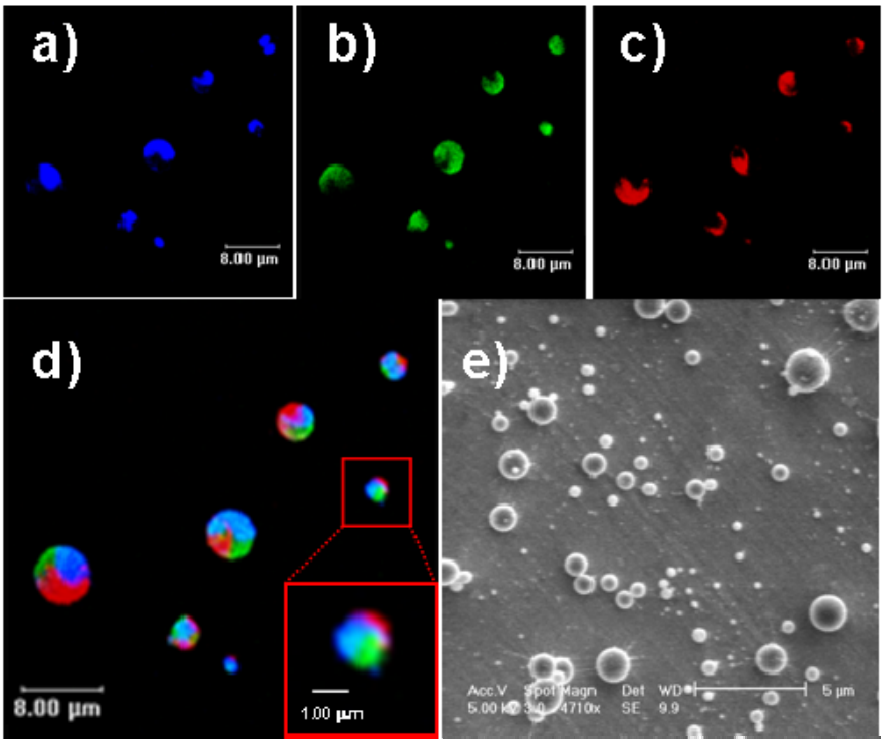

Figure 2.8 Confocal laser scanning microscopy images (a-d) and scanning electron microscopy (e) of colloidal particles made of P(AAm-*co*-AA) and PAA; the individual phases containing biomolecules tagged with FITC (a), Rhodamine B (b) and Alexa Fluor® 647 (c) and their overlay (d).

solutions of poly(acrylamide-*co*-acrylic acid, sodium salt) (MW 200 kD, 10% acrylic acid residues) and polyacrylic acid (MW 250kD). After co-jetting and subsequent thermal crosslinking, the nanocolloids were imaged by CLSM. In Figures 2.8a-c, individual compartments can be distinguished based on their characteristic fluorescent emission wavelength range; confirming that the biomolecules are localized in only a portion of each nanocolloidal particle even after the thermal treatment and re-suspension. The overlay of the three images (Figure 2.8d) further reveals predominant presence of each macromolecular dye in only one single phase. Occasionally, interfacial areas were observed, where two ore more colors coexisted. These limited findings suggest that some interfacial diffusion occurred during electrohydrodynamic processing and/or solidification. Once the nanocolloids are formed, intercompartmental diffusion of the macromolecular dyes is effectively prohibited by the formation of interpenetrating network between the cross-linked polymer matrixes and the biomacromolecular dyes. The integrity of the particles and the separate compartments of the dyes were maintained intact without dissolution or diffusion for an observed period of a few days.

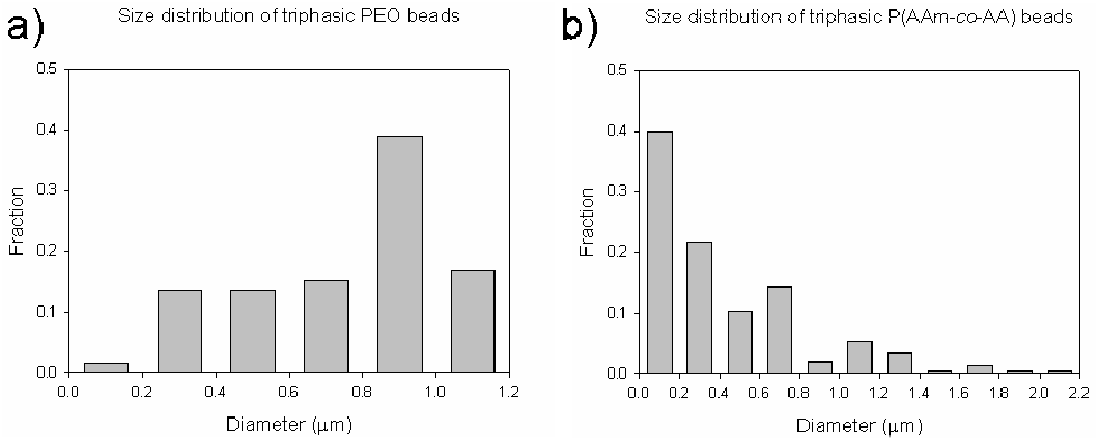

Figure 2.9 Size distributions of triphasic PEO (a) and P(AAm-co-AA) (b) colloids.

SEM analysis was performed on the tricomparmental PAA- and PAAM-based nanocolloids to complement the CLSM experiments. The SEM image shown in Figure 2.8e indicates that PAA- and PAAm-based nanocolloids are disconnected objects with close to perfectly spherical shapes. The mean diameter is about 430 nm with standard deviation of 400 nm. It should be noted that all size distributions were reported as observed, and no optimization with respect to controlling the size distributions was undertaken (Figure 2.9). To narrower size distributions and to approach the goal of a close to monodisperse size control, the combination of microfluidics-based hydrogynamic focusing and the use of polymers with a narrower molecular weight distribution should be persued in further studies.

2.2.4. Conclusions

In summary, we have shown that macro-scale fluid manipulation can be utilized for the fabrication of anisotropic nanoparticles with multiple compartmentalization. The fact that these novel nanocolloids are fabricated by electrified co-jetting suggests that the proposed technology may be broadly applicable to a wide range of different polymers

and polymer composites. Nevertheless, the detailed understanding of multi-component nano-objects will need to be developed, before the exciting potential of triphasic nanocolloids in self-assembly processes or for the development of novel imaging probes can be evaluated. Once the technological hurdles are overcome, multiphasic nanoparticles, such as the triphasic nanocolloids of this study, could be of great interest for applications in the fields of drug delivery, molecular imaging, and smart displays.

References

1. S. C. Glotzer, *Science* **306**, 419 (2004).
2. Z. L. Zhang, S. C. Glotzer, *Nano Letters* **4**, 1407 (2004).
3. L. Manna, D. J. Milliron, A. Meisel, E. C. Scher, A. P. Alivisatos, *Nature Materials* **2**, 382 (2003).
4. N. Malikova, I. Pastoriza-Santos, M. Schierhorn, N. A. Kotov, L. M. Liz-Marzan, *Langmuir* **18**, 3694 (2002).
5. J. F. Hulvat, S. I. Stupp, *Advanced Materials* **16**, 589 (2004).
6. T. Teranishi, Y. Inoue, M. Nakaya, Y. Oumi, T. Sano, *Journal of the American Chemical Society* **126**, 9914 (2004).
7. G. Taylor, *Proceedings of the Royal Society of London Series a-Mathematical and Physical Sciences* **280**, 383 (1964).
8. J. Zeleny, *Proceedings of the Cambridge Philosophical Society* **18**, 71 (May, 1916).
9. Y. Dzenis, *Science* **304**, 1917 (2004).
10. D. H. Reneker, I. Chun, *Nanotechnology* **7**, 216 (1996).
11. H. Fong, I. Chun, D. H. Reneker, *Polymer* **40**, 4585 (1999).
12. Z. Jun, H. Q. Hou, A. Schaper, J. H. Wendorff, A. Greiner, *E-Polymers* (Mar, 2003).
13. J. Zeng *et al.*, *Journal of Applied Polymer Science* **89**, 1085 (2003).
14. E. H. Sanders, R. Kloefkorn, G. L. Bowlin, D. G. Simpson, G. E. Wnek, *Macromolecules* **36**, 3803 (2003).
15. Z. C. Sun, E. Zussman, A. L. Yarin, J. H. Wendorff, A. Greiner, *Advanced Materials* **15**, 1929 (2003).
16. I. G. Loscertales *et al.*, *Journal of the American Chemical Society* **126**, 5376 (2004).
17. G. Larsen, R. Velarde-Ortiz, K. Minchow, A. Barrero, I. G. Loscertales, *Journal of the American Chemical Society* **125**, 1154 (2003).
18. I. G. Loscertales *et al.*, *Science* **295**, 1695 (2002).
19. C. Berkland, D. W. Pack, K. Kim, *Biomaterials* **25**, 5649 (2004).
20. C. Berkland, E. Pollauf, D. W. Pack, K. Kim, *Journal of Controlled Release* **96**, 101 (2004).
21. P. Gupta, G. L. Wilkes, *Polymer* **44**, 6353 (2003).
22. S. Madhugiri, A. Dalton, J. Gutierrez, J. P. Ferraris, K. J. Balkus, *Journal of the American Chemical Society* **125**, 14531 (2003).
23. A. Barrero, A. M. Ganan-Calvo, J. Davila, A. Palacio, E. Gomez-Gonzalez, *Physical Review E* **58**, 7309 (1998).
24. http://www.susqu.edu/facstaff/b/brakke/evolver/evolver.html.
25. A. S. Utada *et al.*, *Science* **308**, 537 (2005).
26. S. Q. Xu *et al.*, *Angewandte Chemie-International Edition* **44**, 724 (2005).

27. G. T. Hermanson, *Bioconjugate Techniques* (Academic Press Inc., San Diego, CA, 1995), pp.
28. J. R. Millman, K. H. Bhatt, B. G. Prevo, O. D. Velev, *Nature Materials* **4**, 98 (2005).
29. Y. Lu *et al.*, *Journal of the American Chemical Society* **125**, 12724 (2003).
30. V. N. Paunov, O. J. Cayre, *Advanced Materials* **16**, 788 (2004).
31. A. Perro, S. Reculusa, S. Ravaine, E. B. Bourgeat-Lami, E. Duguet, *Journal of Materials Chemistry* **15**, 3745 (2005).
32. Z. N. Bao *et al.*, *Chemistry of Materials* **14**, 24 (Jan, 2002).
33. V. N. Paunov, *Langmuir* **19**, 7970 (Sep, 2003).
34. E. Hugonnot, A. Carles, M. H. Delville, P. Panizza, J. P. Delville, *Langmuir* **19**, 226 (Jan, 2003).
35. H. Takei, N. Shimizu, *Langmuir* **13**, 1865 (Apr, 1997).
36. O. Cayre, V. N. Paunov, O. D. Velev, *Chemical Communications*, 2296 (Sep, 2003).
37. L. Nagle, D. Fitzmaurice, *Advanced Materials* **15**, 933 (Jun, 2003).
38. Y. D. Yin, Y. Lu, Y. N. Xia, *Journal of the American Chemical Society* **123**, 771 (Jan, 2001).
39. A. Pfau, R. Sander, S. Kirsch, *Langmuir* **18**, 2880 (Apr, 2002).
40. S. Reculusa *et al.*, *Chemistry of Materials* **14**, 2354 (May, 2002).
41. H. Yu *et al.*, *Nano Letters* **5**, 379 (Feb, 2005).
42. M. Giersig, T. Ung, L. M. LizMarzan, P. Mulvaney, *Advanced Materials* **9**, 570 (Jun, 1997).
43. H. W. Gu, R. K. Zheng, X. X. Zhang, B. Xu, *Journal of the American Chemical Society* **126**, 5664 (May, 2004).
44. K. H. Roh, D. C. Martin, J. Lahann, *Nature Materials* **4**, 759 (2005).
45. K.-H. Roh, M. Yoshida, J. Lahann, *Langmuir* **23**, 5683 (2007).
46. C. Roffey, *Photogeneration of Reactive Species for UV-Curing* (Wiley, New York, 1997), pp.
47. J. M. Chapman *et al.*, *Journal of Pharmaceutical Sciences* **73**, 1482 (1984).
48. J. H. Maguire, K. H. Dudley, *Analytical Chemistry* **49**, 292 (1977).
49. S. Y. Yang, M. F. Rubner, *Journal of the American Chemical Society* **124**, 2100 (2002).

CHAPTER 3

WATER STABILIZATION OF ANISOTROPIC NANOCOLLOIDS

The materials in this chapter are adapted from previously reported data in "Water-Stable Biphasic Nanocolloids with Potential Use as Anisotropic Imaging Probes, *Langmuir* (2007) 23, 5683-5688", by K. –H. Roh, M. Yoshida, J. Lahann; and have been slightly modified.

3.1 Introduction

Recent advances in the field of nanobiotechnology are pointing towards the design of functional probes that are able to self-orientate relative to a cellular surface; thereby encoding - and ultimately revealing - useful biological information.(*1*) In this concept, the controlled distribution of matter or "patchiness"(*2, 3*) is important for creating anisotropic building blocks and introduces an additional design parameter - in addition to particle geometry.(*4*) As summarized in detail in Chapter 1, a series of methods have been recently reported on the fabrication of anisotropic particles.(*5-20*)

As described in Chapter 2, alternative route towards the design and synthesis of polymer-based nanoparticles with two or multiple distinct phases, which exploits electrified co-jetting was pursued.(*21, 22*) It was shown that individual phases of the Janus particles can be independently loaded with biomolecules or selectively modified with model ligands.(*21, 22*) In this co-jetting process, the use of water-based jetting

solutions has various advantages, such as the secure working environments, which simplifies scale-up of the manufacturing process, the compatibility with biomolecules, or the appropriate volatility of water for the generation of nanocolloids under ambient conditions. However, the intrinsic water-solubility of the resulting nanocolloids may become a limitation for several biological applications, including the use as imaging probes. It is therefore highly desirable to develop water-soluble polymer systems that are compatible with biphasic jetting, but can be further cross-linked to ensure stability in the physiological environments.

In this Chapter, the synthesis and characterization of water-stable biphasic nanocolloids are demonstrated. Electrified co-jetting of two aqueous polymer solutions followed by a thermal crosslinking step was used to create water-stable biphasic nanocolloids. For this purpose, aqueous solution mixtures of poly(acrylamide-co-acrylic acid) and polyacrylic acid were employed as jetting solutions. When the biphasic nanocolloids created by side-by-side electrified co-jetting were thermally treated, a crosslinking reaction occurred between amide groups and carboxylic groups on the polymer backbones to form stable imide groups. Infrared spectroscopy was employed to confirm the reaction. The quality and the integrity of the resulting biphasic nanocolloids were examined by confocal laser scanning microscopy, flow cytometry analysis, and dynamic light scattering. Selective encapsulation of two biomolecules in each phase of the biphasic colloids was maintained even after the thermal reaction and suspension in aqueous environment. Well-dispersed spherical colloids with stable dye loadings in each hemisphere were kept intact and without aggregation or dissolution for several weeks. Finally, biphasic nanocolloids were selectively surface-modified with a biotin-ligand resulting in water-stable particles to ensure binding of proteins to a single hemisphere only.

3.2 Methods

Materials

PAA, FITC-dextran (MW 70 kD), Rhodamine-B-dextran (MW 70 kD) and Atto-655-NHS (N-Hydroxysuccinimide)-ester were purchased from Sigma-Aldrich Inc., USA. PAAm-co-AA was purchased from Polysciences, Inc. USA. Biotin-dextran (MW 70 kD) and amino-dextran (MW 70 kD) were purchased from Molecular Probes, Inc., USA. Streptavidin conjugated with tetramethylrhodamine isothiocyanate (TRITC) was purchased from Pierce Biotechnology, Inc. USA. All chemicals were used as received without further purification.

Preparation of Jetting Solutions

Jetting solutions of PAAm-co-AA and PAA were prepared by mixing two pre-dissolved pure polymer solutions to prepare the final concentrations mentioned in the main text. Fluorescence-labeled dextrans or biotin-dextran were added into the solution as indicated. Prior to preparing the solutions for flow cytometry, Atto-655 dye was conjugated with dextran by 2 hour reaction between 50 mg of amino dextran and 0.35 mg of Atto-655-NHS-ester in 5 ml of distilled water followed by membrane dialysis and lyophilization.

Biphasic Jetting

Two 1 ml syringes were controlled by a single syringe pump. Each syringe was loaded with a specific jetting solution. The two syringes were connected to a dual channel tip ((FibriJet® SA-0105, Micromedics, Inc., MN, USA), which had two capillaries with dimensions of 26 gauges and 3 inches in length. These dual capillaries were covered with

a transparent plastic tube that confined the two capillaries in a side-by-side orientation. Positive voltage was applied with high potential generator (ES30P, Gamma High Voltage Research, Inc., USA) between the dual capillaries and a piece of aluminum foil (about 10 square inches) as a collecting substrate.

Thermal Imidization and Collection of Biphasic Nanocolloids

Biphasic nanocolloids were treated at 175 ^{o}C for various times using a convection oven. After crosslinking of the colloids, the material was harvested with a sharp razor blade. The collected particles were suspended in water for stabilization tests.

Confocal Laser Scanning Microscopy

About 50 μl of collidal suspensions were placed between two cover slips. For confocal microscopy, we used a SP2 CLSM (Leica, USA). Each fluorescent dye was excited with different lasers (Ar/ArKr laser at 488 nm for FITC, GreNe laser at 543 nm for Rhodamine B/TRITC) and individual phases were observed in separate windows based on their characteristic emission wavelengths.

Flow Cytometry Analysis of Biphasic Nanocolloids

Four separate samples of colloids were prepared; nanocolloids without any dye, loaded only with FITC-dextran, loaded only with Atto-655-dextran, or biphasic nanocolloids containing FITC- or Atto-655-dextran in each of the two phases, respectively. The nanocolloids were re-suspended in PBS and analyzed using a FACSCalibur (BD Biosciences, San Jose, CA) at the University of Michigan Flow Cytometry Core Facility, equipped with 488 nm Argon and 635 nm Helium-Neon lasers. Signals from FITC- and Atto 655-conjugated dextran were resolved in FL1 (excitation by

488 nm laser with 530/30 bandpass filter) and FL4 (excitation by 635 nm laser with 661/16 bandpass filter) channels, respectively. For each sample, 20,000 events were collected. Data acquisition was performed using CellQuest Pro (BD Biosciences) and analysis was performed using WinMDI (Scripps Research Institute, La Jolla, CA, USA). Results are displayed as density plots of FL1 versus FL4 intensities.

Dynamic Light Scattering

The normalized autocorrelation function of colloids particle density fluctuations was measured at room temperature. Thermally crosslinked nanocolloids were suspended in PBS (pH = 7.4). The colloids concentration was 400 ppm. The incident laser with a wavelength of 488 nm was used. The compact goniometer system in conjunction with a multitau correlator (ALV-5000E, Langen, Germany) was employed. The measurement was performed at angle of 90 degrees. The specimen was allowed to equilibrate for 10 min before the measurement.

Selective Conjugation of Streptavidin to Biphasic Nanocolloids

The biphasic particles loaded with FITC-dextran and biotin-dextran in each hemisphere were produced by electrified co-jetting followed by thermal crosslinking for one hour at 170 $^{\circ}$C. After 3 mg of the particles were suspended in 1 ml of PBS, 20 μl of an aqueous buffer solution of TRITC-streptavidin (0.5% w/v) was added and the samples were incubated for 5 hours at room temperature with gentle stirring. Unbound or non-specifically adsorbed streptavidin was separated from the biphasic nanocolloids by centrifugation. This process was repeated three times.

3.3 Results and Discussions

Scheme 3.1 outlines the experimental design as well as the reaction mechanism of the thermal imidization reaction used for crosslinking. Thermal imidization is a reaction between a carboxylic acid group and an amide group to form an imide group under the influence of elevated temperatures.(*23, 24*) This reaction has been used for the creation of water-stable films(*25*) and bulk structures composed of polyacrylamide (PAAm) and polyacrylic acid (PAA) in solid state.

To elucidate the applicability of this approach for stabilizing biphasic nanocolloids, we conducted a series of electrified co-jetting experiments with aqueous solutions of polymers that have suitable functional groups for corsslinking via imidization. A mixture of PAA (MW 250 kD) and poly(acrylamide-*co*-acrylic acid, sodium salts) (PAAm-*co*-AA, MW 200 kD, 10% acrylic acid residues) was used as the

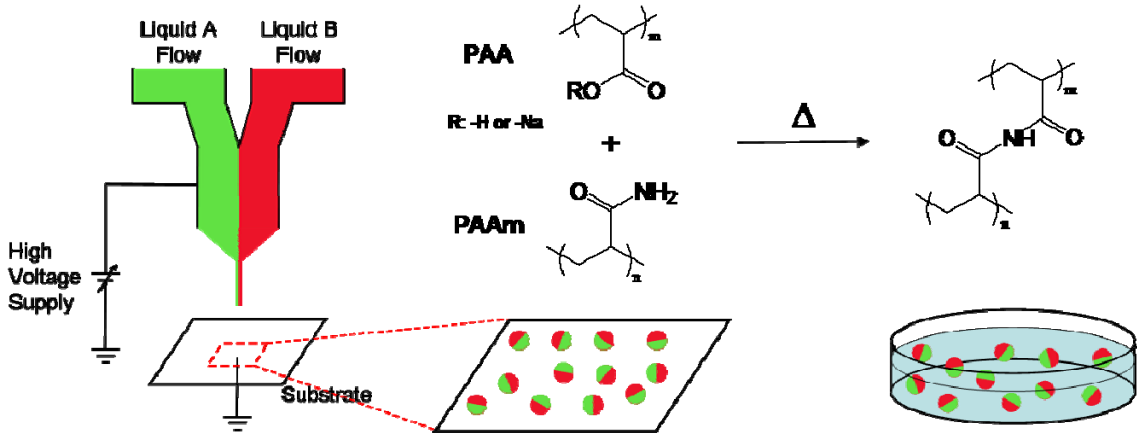

Scheme 3.1 Biphasic co-jetting and subsequent thermal imidization. Jetting liquid A and B are composed of PAA and PAAm-*co*-PAA in water. Liquid A and B are additionally containing FITC-conjugated dextran and Rhodamine B-conjugated dextran, respectively. After the electrified jetting, the resulting biphasic nanocolloids were thermally treated to crosslink the polymer chains. After the reaction, biphasic nanocolloids were stable in water for extended periods of time.

basis of the jetting solutions. For the biphasic co-jetting, both sides of the jetting solutions were composed of a mixture of PAA and PAAm-*co*-AA with varying additions of fluorescence-labeled biomacromolecules. Initially, a series of experiments to establish appropriate ratios of PAA and PAAm-*co*-AA was conducted. The basic limits for the co-jetting concentrations were extrapolated by examining the jetting behavior of the individual polymers. For PAAm-*co*-AA, spherical colloids were observed below about 5% (w/v), while polymer concentration of PAA had to be below 10 % (w/v). In a typical experiment, we used a polymer mixture of 5% PAAm-*co*-AA and 1% PAA. Furthermore, we incorporated FITC-conjugated dextran (MW 250 kD) in one side of the jetting solution and Rhodamine B-conjugated dextran in the other phase. The addition of macromolecular dyes allowed us to track the individual compartments and to assess the stability of the interface between the two compartments. After co-jetting of the two polymer fluids, the biphasic nanocolloids were exposed to elevated temperatures to induce crosslinking. Finally the biphasic nanocolloids were harvested from the substrate and aqueous nanocolloidal suspensions were prepared.

During the course of the thermal treatment, FTIR measurements were used to confirm and monitor the thermal imidization reaction for various mixing ratios and reaction conditions. Without thermal treatment, the biphasic nanocolloids readily dissolved in aqueous media. In contrast, thermal treatment had a profound impact on the stability of the biphasic nanocolloids in aqueous environments. Figure 3.1 shows a series of FTIR spectra recorded for nanocolloids made from the mixture of 5% PAAm-*co*-AA and 1% PAA solutions. All the samples were directly jetted onto a piece of gold substrate and the FTIR reflectance was measured after each reaction time at 175 °C. After 60 min, the characteristic C=O stretching band (amide I around 1673 cm^{-1}) and the

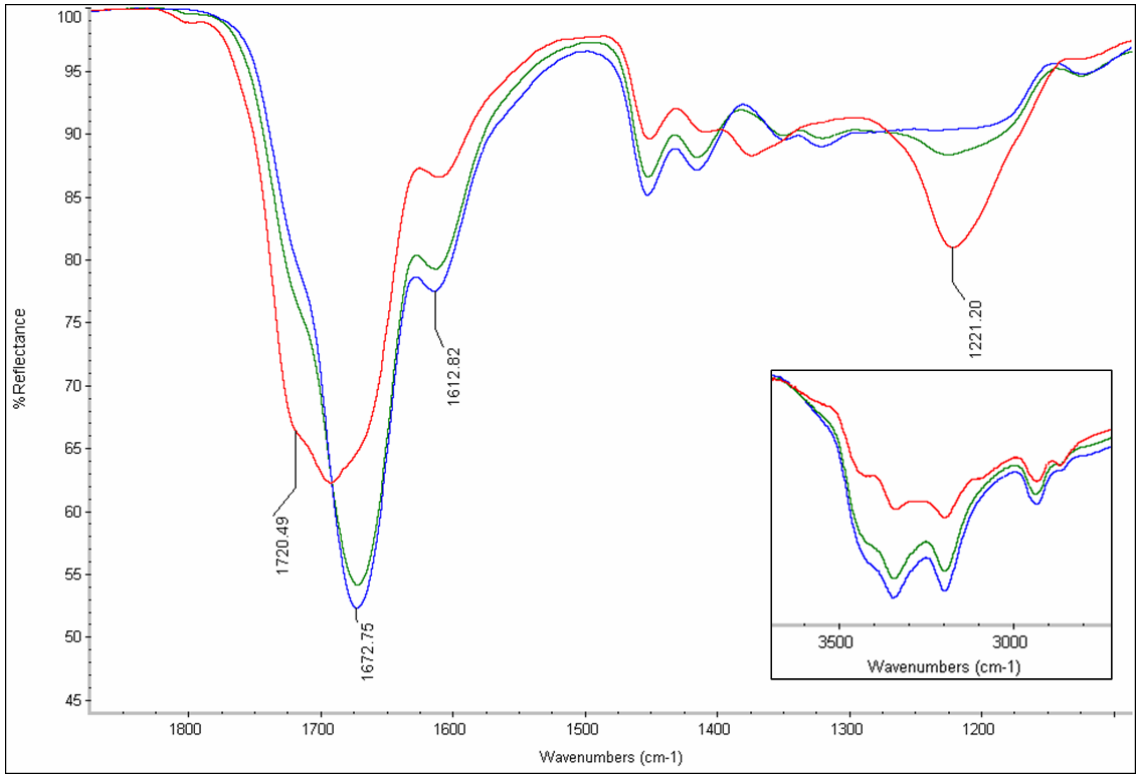

Figure 3.1 FTIR reflectance spectra of a PAA/PAAm nanocolloid for different reaction times. The blue spectrum was recorded for nanocolloids prepared by jetting on top of gold substrate before the thermal crosslinking reaction, while the green and red spectra were measured for the same colloids after an 1 hour and a 12 hour reaction at 175°C, respectively.

C-NH band of amide group (amide II around 1613 cm^{-1}) decreased, while bands characteristic for the imide groups appeared near 1720 cm^{-1} and 1221 cm^{-1}. Both, N-H and O-H stretching bands of amide and carboxylic acid groups simultaneously decreased indicating the consumption of these functional groups during amide formation (inset of Figure 3.1). After 180 min, substantial conversion was observed revealing considerable crosslinking of the biphasic nanocolloids. After 12 hours, the majority of the carboxylic acid and amide groups were converted into imide groups. Based on these results, we concluded reaction times between 60 and 180 min to be optimum. Under these conditions, a substantial portion of the amide groups was converted into imide groups, while reducing the potential of side reactions, such as oxidation, due to excessive thermal treatment.

Next, we assessed the biphasic character of the nanocolloids using confocal laser scanning microscopy (CLSM). Figure 3.2 shows the CLSM images of biphasic nanocolloids exposed to an aqueous bulk after thermal imidization for crosslinking. In order to observe fluorescence indicting the presence of dye-conjugated dextran molecules incorporated in each side, the individual phases were observed in separate wavelength windows (505-535 nm for FITC and 570-610 nm for Rhodamine B). As clearly observed

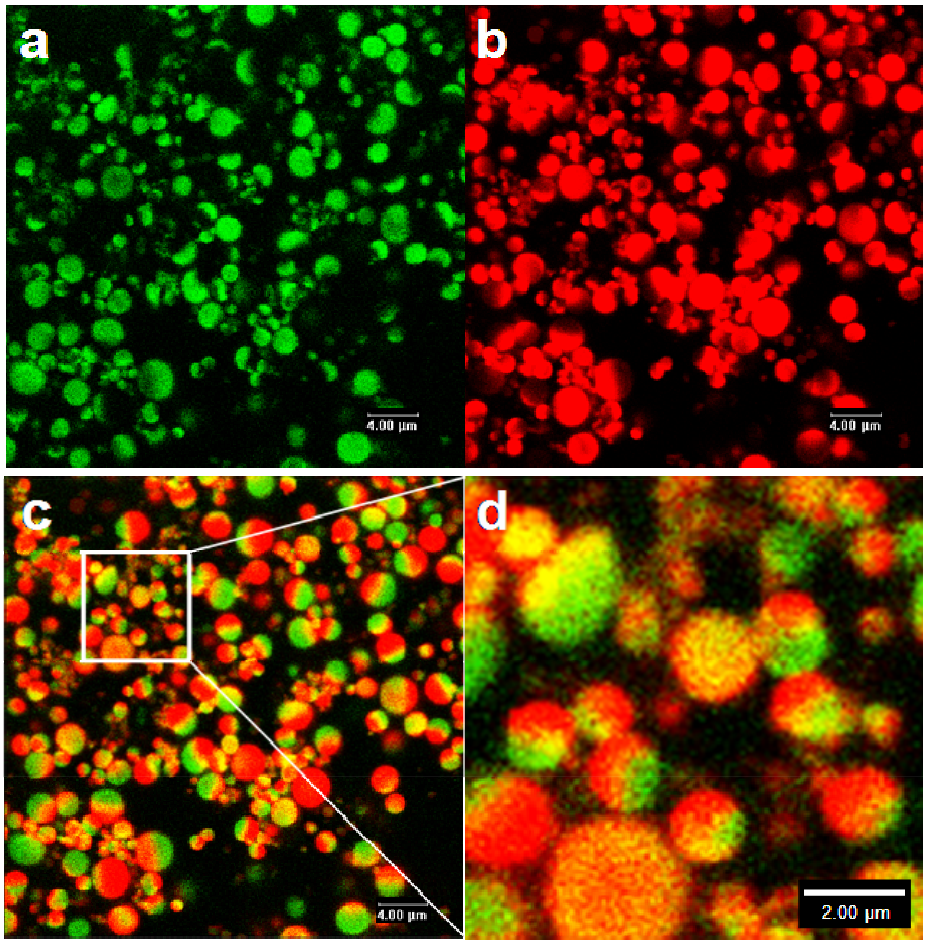

Figure 3.2 Confocal laser scanning microscope images of thermally crosslinked biphasic nanocolloids after 2-week exposure in PBS buffer. Fluorescence intensities are originated from FITC (a) and Rhodamine B (b) conjugated dextrans, which are selectively encapsulated in each phase; (c) is the overlay of the two phases; (d) is an enlargement of a selected area of (c). Scale bars are 4 µm (a-c) and 2 µm (d).

from individual phases and the overlay of the two phases, the fluorescence-labeled dextrans incorporated in each phase showed little interfacial diffusion or mixing after thermal reaction, even after being exposed to water for an extended period of time. Moreover the confocal images indeed confirmed that crosslinking for 60 min at 175 $^{\circ}$C suffices to stabilize the biphasic nanocolloids. In fact, biphasic nanocolloids, made from the solution of 5% PAAm-*co*-AA and 0.5% PAA and suspended in PBS, maintained their biphasic character during the 15-week observation period used in this study. Moreover, close to perfect spherical envelopes were observed for the nanocolloids. Even though some aggregates were observed when the collected particles were initially exposed into an aqueous environment, simple sonication for less than 5 minutes was in all cases sufficient to disintegrate the aggregated particles and to form well-dispersed nanocolloids. These experiments suggest that the thermal reaction occurs not between the individual particles to form permanent aggregates, but only intraparticularly to stabilize the structure of individual particles. These results were confirmed for various mixing ratios of PAAm-*co*-AA and PAA.

The images of biphasic nanocolloids from CLSM suggest that almost the entire population of the nanocolloids consists of two separate phases. Even particles that appear to consist of a single phase when a snapshot through one focal plane is taken usually reveal a second phase when the focal plane is changed. In addition to CLSM, flow cytometry was used for high-throughput characterization of the biphasic nature of individual nanocolloids. For this experiment, biphasic nanocolloids and three control groups of nanocolloids (empty nanocolloids and two types of monophasic nanocolloids) were prepared. Figure 3.3 shows four density plots of the corresponding nanocolloids: empty nanocolloids containing no dye (c), monophasic nanocolloids containing only a single dye (a and d), and biphasic nanocolloids containing both dyes (b). The three

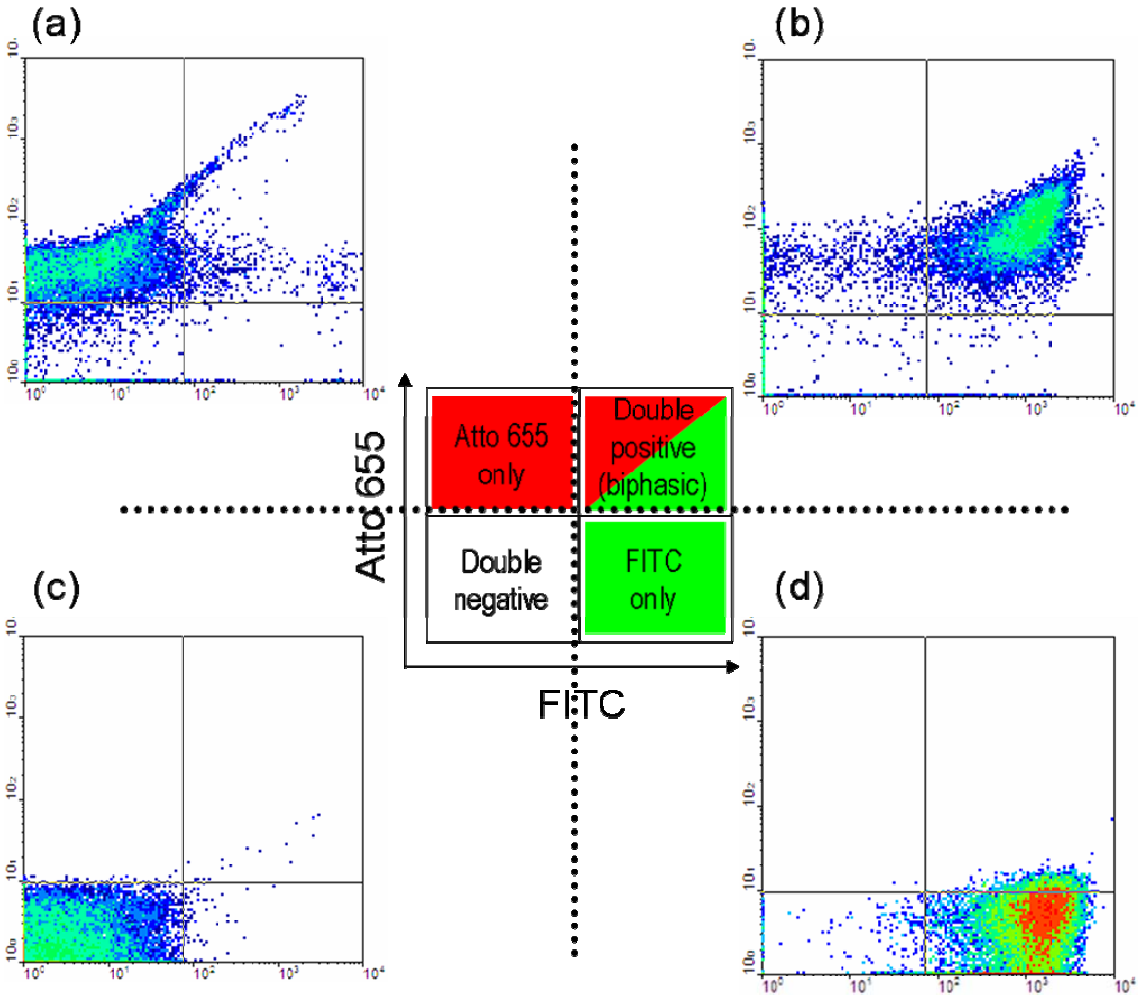

Figure 3.3 Flow cytometry analysis of nanocolloids. Four separate density plots are corresponding to the nanocolloids containing no dye (c), only FITC-dextran (d), only with Atto 655-dextran (a), or both FITC- and Atto 655-dextrans in each of the phases (b). Signals from FITC- and Atto 655-conjugated dextrans were resolved in FL1 (excitation by 488 nm laser with 530/30 bandpass filter) and FL4 (excitation by 635 nm laser with 661/16 bandpass filter) channels, respectively. The central scheme explains the four quadrants in each density plot – a two by two matrix of differing intensities of FITC and Atto 655.

density plots from the control groups were used to determine the appropriate cut-off fluorescent signal values for the two dyes. This setting is used to divide the negative signals from the positive. FITC and Atto 655 were selected as two fluorescent dyes,

because there is minimal overlap between the emission spectra of these two dyes. This is important when determining accurate values for the fluorescent cut-off signals that define each of the four quadrants. The empty nanocolloids without any dyes fall in the lower left quadrant, because they were negative for both FITC and Atto 655. Correspondingly, the majority of nanoparticles loaded with either FITC- or Atto 655-dyes alone were confined to their respective quadrants (upper left, lower right). When the biphasic nanocolloids, which were loaded with a different dye in each hemisphere, were examined, the vast majority of biphasic nanocolloids was located in the upper right quadrant, confirming the presence of fluorescence from both FITC and Atto 655 dyes in individual compartments of the biphasic nanocolloids. Nevertheless, a relatively broad distribution of fluorescence intensities was observed and made the accurate quantification somewhat difficult. The broad distribution of fluorescence intensities may be attributed to the relatively high polydispersity of the non-optimized nanocolloids used in this study. To further assess the size distribution of biphasic nanocolloids, dynamic light scattering (DLS) measurements were employed. This study was conducted with the further intention to examine the quality and the integrity of the colloidal suspensions stored for extended times.

Figure 3.4 shows the measured size distribution of the biphasic nanocolloids directly after suspension (black) and 3 days after the suspension (white). Both samples show unimodal distributions with average hydrodynamic radii of around 400 nm and standard deviations of about 270 nm. There were no significant changes in size distribution or distribution mode of the nanocolloids over time, which suggests that the integrity of the colloids was effectively maintained without aggregation formation or dissolution of the particles. Even though a fraction of the colloids settled by gravitation after they were initially suspended, simple hand shaking resulted in re-establishment of the suspension.

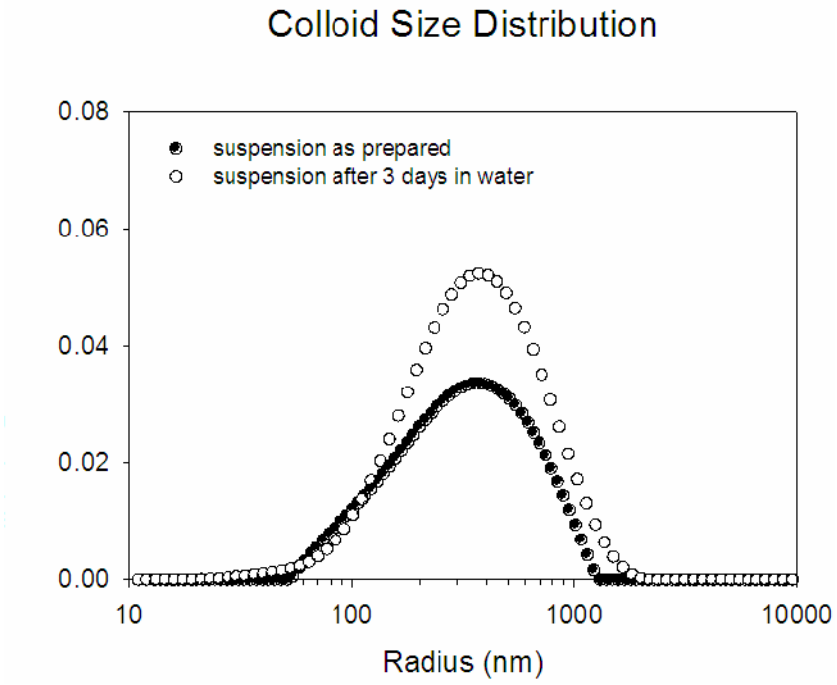

Figure 3.4 Dynamic light scattering measurement assessing the size distribution of biphasic nanocolloids suspended in PBS buffer for different periods of time (black: immediately after suspension, white: 3 days after suspension). Measured average radii are 414 and 427 nm with the standard deviations of 263 and 284 nm, for black and white, respectively.

When considering the use of biphasic nanocolloids as imaging probes, the ability to target a specific hemisphere with one type of biological ligands without simultaneously reacting the second hemisphere is important. If the targeting ligands are present in only one hemisphere of the particles, unique anisotropy of the two-colored imaging probes would become feasible. To demonstrate selective modification, we employed a simple bioconjugation strategy based on biotin and streptavidin. Biotin-modified dextran was incorporated in one jetting solution resulting in biphasic nanocolloids, which were

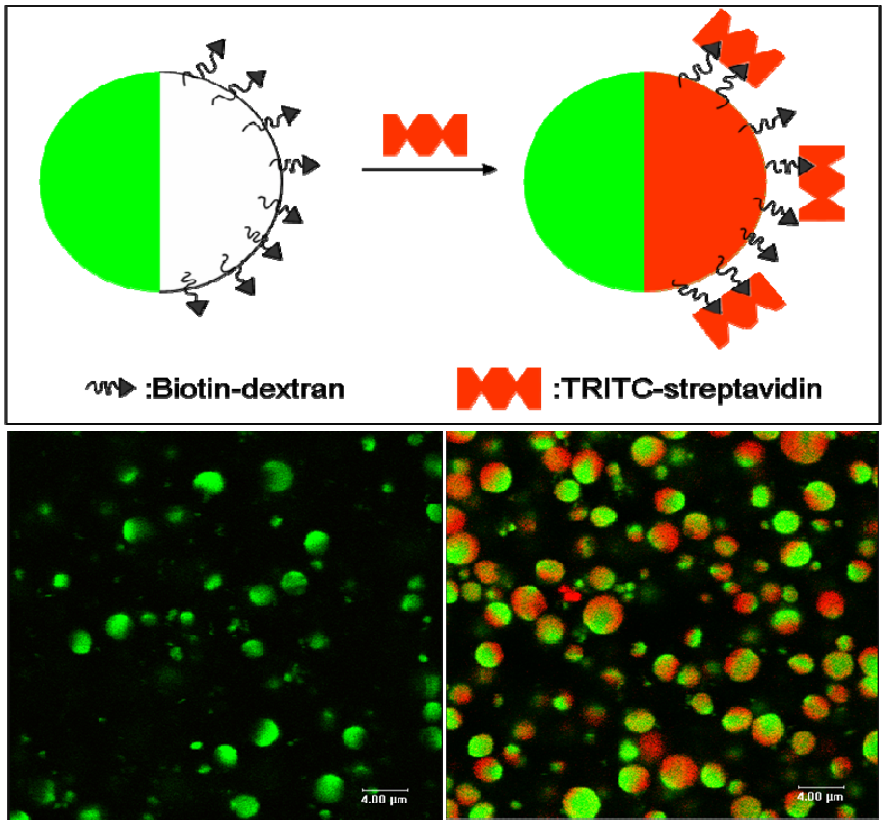

Figure 3.5 Scheme of bioconjugation and the corresponding CLSM images of surface-modified biphasic nanocolloids. The two jetting solutions were designed to contain FITC-dextran or biotin-dextran in one of the hemispheres. When these particles were subsequently incubated with TRITC-conjugated streptavidin, the hemisphere containing biotin (previously non-fluorescent) specifically bound to the protein, as indicated by the red fluorescence in these hemispheres (right). The CLSM images show selective binding of streptavidin to one hemisphere only.

biotinylated in a single hemisphere only. Subsequent reaction with fluorescence-labeled streptavidin was used to evaluate the specificity of this approach. Figure 3.5 shows the schematic description and CLSM images of biphasic particles before and after the modification via bioconjugation of fluorescence-labeled protein. The biphasic particles were produced by electrified co-jetting of two solutions containing FITC-dextran and biotin-dextran in each side. Prior to bioconjugation, the overlay image of FITC- and TRITC- channels of CLSM analysis shows that only one hemisphere of the particle is fluorescent (FITC emission). However, after incubation with TRITC-streptavidin and subsequent washing, only the originally dark hemisphere showed detectable emission at 613-685 nm. This finding indicates not only the selective presence of active biotin in one hemisphere of the original particles, but also the specific association of streptavidin to a single hemisphere of nanocolloids. Because each individual streptavidin molecule has four binding sites, further bioconjugation with biotinylated cell- or tissue-specific targeting ligands becomes indeed feasible through this relatively simple approach.

3.4 Conclusions

Biphasic nanocolloids are of great interest because of their potential for self-assembly, drug delivery, or biomedical imaging. These application require however the biphasic nanocolloids to be stable under physiological conditions. We have developed a simple technology to fabricated water-stable biphasic nanocolloids that involves electrified co-jetting of aqueous polymer solutions followed by conversion of the resulting polymer objects into stable nanocolloids by crosslinking via thermal imidization. Under the conditions of crosslinking, colorant loading as well as biphasic architecture of the nanocolloids were maintained. Selective modification of one

hemisphere renders the resulting nanocolloids anisotropic. The novel type of imaging probes may indeed be attractive for use as imaging probes.

References

1. S. A. Wickline, A. M. Neubauer, P. Winter, S. Caruthers, G. Lanza, *Arteriosclerosis Thrombosis and Vascular Biology* **26**, 435 (Mar, 2006).
2. L. Hong, A. Cacciuto, E. Luijten, S. Granick, *Nano Letters* **6**, 2510 (Nov, 2006).
3. Z. L. Zhang, S. C. Glotzer, *Nano Letters* **4**, 1407 (Aug, 2004).
4. S. C. Glotzer, *Science* **306**, 419 (2004).
5. A. Perro, S. Reculusa, S. Ravaine, E. B. Bourgeat-Lami, E. Duguet, *Journal of Materials Chemistry* **15**, 3745 (2005).
6. Z. N. Bao *et al.*, *Chemistry of Materials* **14**, 24 (Jan, 2002).
7. V. N. Paunov, *Langmuir* **19**, 7970 (Sep, 2003).
8. V. N. Paunov, O. J. Cayre, *Advanced Materials* **16**, 788 (2004).
9. E. Hugonnot, A. Carles, M. H. Delville, P. Panizza, J. P. Delville, *Langmuir* **19**, 226 (Jan, 2003).
10. H. Takei, N. Shimizu, *Langmuir* **13**, 1865 (Apr, 1997).
11. O. Cayre, V. N. Paunov, O. D. Velev, *Chemical Communications*, 2296 (Sep, 2003).
12. L. Nagle, D. Fitzmaurice, *Advanced Materials* **15**, 933 (Jun, 2003).
13. Y. D. Yin, Y. Lu, Y. N. Xia, *Journal of the American Chemical Society* **123**, 771 (Jan, 2001).
14. M. Giersig, T. Ung, L. M. LizMarzan, P. Mulvaney, *Advanced Materials* **9**, 570 (Jun, 1997).
15. H. W. Gu, R. K. Zheng, X. X. Zhang, B. Xu, *Journal of the American Chemical Society* **126**, 5664 (May, 2004).
16. S. Reculusa *et al.*, *Chemistry of Materials* **14**, 2354 (May, 2002).
17. T. Teranishi, Y. Inoue, M. Nakaya, Y. Oumi, T. Sano, *Journal of the American Chemical Society* **126**, 9914 (2004).
18. H. Yu *et al.*, *Nano Letters* **5**, 379 (Feb, 2005).
19. Z. H. Nie, W. Li, M. Seo, S. Q. Xu, E. Kumacheva, *Journal of the American Chemical Society* **128**, 9408 (Jul, 2006).
20. T. Nisisako, T. Torii, T. Takahashi, Y. Takizawa, *Advanced Materials* **18**, 1152 (May, 2006).
21. K. H. Roh, D. C. Martin, J. Lahann, *Nature Materials* **4**, 759 (2005).
22. K. H. Roh, D. C. Martin, J. Lahann, *Journal of the American Chemical Society* **128**, 6796 (2006).
23. J. M. Chapman *et al.*, *Journal of Pharmaceutical Sciences* **73**, 1482 (1984).
24. J. H. Maguire, K. H. Dudley, *Analytical Chemistry* **49**, 292 (1977).
25. S. Y. Yang, M. F. Rubner, *Journal of the American Chemical Society* **124**, 2100 (2002).

CHAPTER 4

BIOCOMPATIBLITY AND POTENTIAL BIOLOGICAL APPLICATION OF ANISOTROPIC NANOCOLLOIDS

4.1 Short-Term Biocompatiblity of Biphasic Nanocolloids

The materials in this section of chapter 4 are adapted from previously reported data in "Short-Term Biocompatibility of Biphasic Nanocolloids with Potential Use as Anisotropic Imaging Probes, *Biomaterials* (2007) 28, 2446-2456", by M. Yoshida, K. -H. Roh, J. Lahann; and have been slightly modified.

Advances in nanotechnology, in particular the development of nanoparticles, will result lead to the development of novel tools for biomedical research and clinical practice. Potential applications of nanoparticles include areas where combined therapy and imaging are needed. In this context, anisotropic nanoparticles may be especially attractive because they can deliver directional information due to differences in the nanoparticle/cell orientation. As shown in Chapter 3, water-stable biphasic nanoparticles were developed by use of simultaneous jetting of two different polymer solutions and subsequent thermal imidization. To determine the feasibility of using these anisotropic biphasic nanoparticles as imaging probes, short-term biocompatibility was evaluated using model cell culture systems. Presence of these biphasic nanoparticles, composed of 0.5% polyacrylic acid and 4.5% poly(acrylamide-*co*-acrylic acid), in culture did not

significantly affect proliferation of human endothelial cells and murine fibroblasts as determined by a colorimetric proliferation assay. Moreover, double staining of these cells with annexin V and propidium iodide and flow cytometry analysis indicated that cell viability was decreased only at the highest dose tested. Upon addition, biphasic nanoparticles were internalized by both cell types, as evidenced by orthogonal confocal laser scanning micrographs. Taken together, these results suggest biocompatibility of the biphasic nanoparticles in physiological systems and open the possibilities for receptor- or surface marker-mediated approach to improve specific targeting as imaging probes.

4.1.1 Introduction

Recent advances in nanotechnology have sparked the premise of novel tools for medical research and clinical practice. In particular, nanoparticles have gained much attention for their wide variety of potential applications. Uses of nanoparticles may range from diagnostics, such as imaging probes, to novel therapeutic modalities including controlled drug delivery systems.(*1-5*) Moreover, future nanoparticle designs may be able to simultaneously provide targeting capabilities, complex drug release profiles, and 'smart' imaging competence ("Theranostics" = combined ability for therapy and diagnosis).(*6*) Because of their subcellular dimensions, nanoparticles have been explored in various applications including cell labeling and imaging, such as magnetic resonance imaging.(*7-9*) These techniques are often used for in vivo applications where the particles are either attached to the cell surface(*10, 11*) or internalized by mechanisms including phagocytosis(*11*) and macropinocytosis(*12*). In both cases, targeting specificity is of importance, not only to image the targeted cells or organs, but also to avoid rapid clearance by the reticuloendothelial system.(*13-16*) However, without interventions to prevent particle uptake, nanoparticles are mostly internalized into cell vacuoles.(*8*) In

addition, excessive addition of nanoparticles to cells may lead to apoptosis, especially in cases where the nanocolloids are internalized via a receptor-mediated endocytosis, and result in the separation of the particles from the specific receptor.(*8*) Strong adhesion of nanoparticles to cell surfaces by a specific receptor may shelter the cells from endocytosis effects.(*17*) Nevertheless, internalization of particle probes may pose a major challenge during development of nanoparticles for imaging.(*18*) Future work is needed to expand the fundamental capabilities of nanoparticles and to widen the operational design space for subcellular imaging probes.

Anisotropic particles may be advantageous compared to their isotropic counterparts, as they are able to encode directional information and provide advanced multifunctionality. One essential design parameter for anisotropic imaging probes, in addition to size and shape,(*19, 20*) is the controlled distribution of matter.(*21*) While reliable and efficient fabrication of building blocks with anisotropic material distributions will be of interest for many biomedical applications, their synthesis has only been addressed in a few specialized cases.(*22, 23*) Selective surface modification methods have been performed for this purpose utilizing partial masking,(*24, 25*) selective deposition,(*26, 27*) and microcontact printing.(*28*) In addition, two-sided particles have been created by a range of methods including template-assisted self-assembly of particles,(*29, 30*) rearrangement or recrystallization of materials from precursor core–shell particles,(*31, 32*) phase separation in emulsion polymerization,(*33*) and partial or selective surface nucleation.(*23, 34, 35*)

In Chapter 2 and 3, a novel synthesis approach towards polymer-based particles with two distinct phases was demonstrated.(*36*) Because of their typical size range of 200 nm to several microns, they are referred as biphasic nanocolloids. To determine the fundamental feasibility of using these biphasic nanocolloids as anisotropic imaging

probes, short-term biocompatibility and stability in biological systems are the necessary initial criteria. Therefore in this section of Chapter 4, the short-term biocompatibility of the nanocolloids was tested using model cell culture systems. In particular, effect of biphasic nanocolloids on cell proliferation, viability, and uptake were investigated in details.

4.1.2 Methods

Synthesis of water-stable biphasic nanocolloids

The synthesis of biphasic particles used in this section follows the detailed methods described in Chapter 3. In brief, polymer solutions of 0.5% polyacrylic acid (PAA) (MW 250 kDa, Sigma, St. Louis, MO, USA) and 4.5% poly(acrylamide-co-acrylic acid, sodium salts) (PAAm-co-AA) (MW 200 kDa, 10% acrylic acid residues, Polysciences, Warrington, PA, USA) were prepared in double distilled water (ddH_2O). To enable monitoring of the biphasic nanocolloids by fluorescence, FITC (fluorescein isocyanate)-conjugated dextran (MW 250kDa, Sigma) or rhodamine B-conjugated dextran (MW 70 kDa, Sigma), or Cascade Blue-conjugated dextran (MW 10 kDa, Invitrogen, Carlsbad, CA, USA) were added at a final concentration of 0.3%. Following the electrified jetting, the biphasic nanocolloids were incubated at 175 ^{o}C for 3h to induce crosslinking by thermal imidization between carboxylic acid and amide groups to form an imide group.(*37, 38*) Prior to use, biphasic nanocolloids were suspended in ddH_2O and sonicated for 2min, washed 3 times, then resuspended in ddH_2O and UV sterilized for 30min.

Cell culture

Cryopreserved human umbilical vein endothelial cells (HUVECs) were purchased from Cambrex (Walkersville, MD, USA) and cultured in complete Endothelial Growth Media (Cambrex) containing 2% fetal bovine serum. Cryopreserved murine fibroblasts (NIH 3T3) were purchased from American Type Culture Collection (Manassas, VA, USA) and cultured in Dulbecco's modified Eagle's medium with 4mM Lglutamine, 1.5 g/L sodium bicarbonate and 4.5 g/L glucose (ATCC), and 10% bovine calf serum (ATCC), per manufacturer's directions. Both cell types were cultured in 75 cm^2 tissue culture-treated polystyrene (TCPS) flasks (Corning), maintained at 37 ^oC in a humidified atmosphere of 5% CO_2, and media replaced every other day until 80% confluency was reached. Cells were harvested from flasks with 0.25% trypsin/ethylenediaminetetraacetic acid solution (Sigma) and seeded at indicated densities for respective experiments.

Cell proliferation assay

The effect of biphasic nanocolloids on proliferation of HUVECs and NIH 3T3 cells was evaluated using a commercially available colorimetric cell proliferation assay (CellTiter 96s Aqueous One Solution Cell Proliferation Assay, Promega, Madison, WI, USA). Cells were detached from TCPS flask by trypsinization and resuspended in appropriate media and seeded at 2.5×10^4/well in triplicates in a 24-well TCPS plate (BD Falcon, Franklin Lakes, NJ, USA). Biphasic nanocolloids loaded with rhodamine B- and FITC-conjugated dextran were added at a dose of 0.01, 0.1, or 1 mg/10^6 initial number of cells seeded. At 4, 24, 48, 72, and 96 h after incubation with the biphasic particles, colorimetric reagent was added to each well per manufacturer's suggestions for additional 4 h for colorimetric development. To minimize any effect of the presence of the biphasic nanocolloids on absorbance readings, 200 mL of the supernatant was

transferred from each well to a 96-well plate, and absorbance at 490nm was recorded using a spectrophotometric plate reader (Molecular Dynamics). Cell culture media without any cells were used as background. This experiment was repeated 3 times and results are reported as average±standard deviation (S.D.).

Flow cytometry analysis of biphasic nanocolloid association with cells and cell viability

To determine the degree of cytotoxicity of biphasic nanocolloids on cell viability, HUVECs or NIH 3T3 cells were detached from flasks and plated into a 6-well TCPS plate (BD Falcon) at a density of 5×10^5/well in appropriate media. Cells were treated or not with 0.01, 0.1, or 1mg biphasic nanocolloids/10^6 initially seeded cells. After 24 h of treatment with biphasic nanocolloids, cells were detached from the surface using a non-enzymatic dissociation solution (Sigma), and washed 3 times in icecold HEPES binding buffer (10mM HEPES/NaOH, pH 7.4, 140 mM NaCl, 2.5mM $CaCl_2$) to remove any loosely associated biphasic nanocolloids. Cells were then resuspended in ice-cold HEPES binding buffer and stained with Alexa fluor 647-conjugated Annexin V and propidium iodide (PI) (Invitrogen) for 30 min. Samples were analyzed by FACSCalibur (BD Biosciences, San Jose, CA, USA) at the University of Michigan Flow Cytometry Core Facility, equipped with 488nm Argon and 635nm Helium–Neon lasers. Data acquisition was performed using CellQuest Pro (BD Biosciences) and analyzed using WinMDI (Scripps Research Institute, La Jolla, CA, USA).

Cell population with increased fluorescence resolved in FL1 channel (excitation by 488nm laser, 530/30 filter) was gated as cells with attached or internalized biphasic nanocolloids. This marker (M1) was established to include 5% of cell population from the negative control (cells cultured in the absence of biphasic nanocolloids). Proper

selection of this gate enabled assessment of the effect of increasing ratios of biphasic nanocolloids over initial cell numbers on the cellular association of biphasic nanocolloids. Signals from Alexa 647-conjugated Annexin V and PI were resolved in FL4 (excitation by 635 nm laser with 661/16 filter) and FL2 (excitation by 488 nm laser with 585/42 filter) channels, respectively. Cytotoxicity of biphasic nanocolloids on cells was evaluated by assessing the population in quadrants from Annexin V/PI double staining. Annexin V has a high affinity for phosphatidylserine, which is located on the cytoplasmic surface of the cell membrane in normal cells but becomes translocated to the extracellular side of the plasma membrane in apoptotic cells. Propidium iodide is a dye, which binds to nucleic acids, and is impermeant to live cells and apoptotic cells, but enters dead cells with compromised membrane integrity, staining the nucleic acids inside the cell. Thus, cells that do not show fluorescence from either Annexin V or PI are considered to be live, whereas those that are positive for Annexin V or both Annexin V and PI are considered to be apoptotic or dead, respectively. This experiment was repeated 3 times and numerical results are reported as average ± S.D., and representative histograms are shown.

Confocal laser scanning microscopy analysis of biphasic nanocolloid association to cells

To assess the morphology and the location of associated biphasic nanocolloids with respect to the cell membrane (internalized vs. surface-associated nanocolloids), confocal laser scanning microscopy (CLSM) was used. Coverslips (18mm) were coated with poly-L-lysine (Sigma) and placed at the bottom of a 12-well TCPS plate. Prior to cell seeding, coverslips were incubated for 1 h with appropriate media at 37 ^{o}C. After this incubation period, cells were seeded at a density of 5×10^{4}/well and biphasic nanocolloids

were added at 0.1 or 1 mg/10^6 initially seeded cells. After 4, 24, or 48 h of incubation with biphasic nanocolloids, coverslips were washed 3 times in Dulbecco's phosphate-buffered saline (Invitrogen) and fixed for 15 min in 4% paraformaldehyde (Fluka, St. Louis, MO, USA). Upon washing, cells were permeabilized with 0.5% Triton X-100 (Alfa Aesar, Ward Hill, MA, USA) and stained with rhodamine-conjugated phalloidin (Invitrogen) and counterstained with Hoechst 33342 (Invitrogen). After the final washing steps, the coverslips were mounted in Prolong Gold (Invitrogen), allowed to cure overnight at 4 ^{o}C, and visualized using Zeiss CLSM 510 confocal microscope (Zeiss) at Microscopy & Image Analysis Laboratory at the University of Michigan. For the visualization of biphasic nanocolloid uptake vs. surface adhesion, three-dimensional CLSM images were reconstructed from Z-stack images. This experiment was repeated 3 times and representative CLSM images are shown.

Glucose-6-phosphate dehydrogenase release

Cytotoxicity associated with biphasic nanocolloids was assessed by measuring release of cytosolic enzyme glucose-6-phosphate dehydrogenase (G6PD) from cells cultured in the presence or absence of various doses of particles into the media. This enzyme is released from damaged cells and its presence was detected using a commercially available fluorescent enzymatic assay (Vybrant Cytotoxicity Assay, Molecular Probes, Eugene, OR, USA). HUVECs or NIH 3T3 cells were cultured with or without 0.01, 0.1, or 1mg of biphasic particles/10^6 seeded cells for 24 h. To ensure that there was no effect of the fluorescent dyes leaching out from the particles on the fluorescent readings, media with or without nanocolloids were run in parallel. After the incubation period, media was cleared by centrifugation at 1200 rpm for 5min. Media from cells lysed with 0.5% Triton X for 5 min served as a positive control. Cleared media

was transferred to a 96-well plate in triplicates, and G6PD release was determined using Vybrant Cytotoxicity kit according to manufacturer's directions, and fluorescence readings were taken every 5 min for 30 min at 37 ^{o}C (ex: 544 nm, em: 590 nm) using a fluorescent plate reader (Molecular Dynamics). This experiment was repeated 3 times and results are reported as average±S.D.

Statistical analysis

Statistical analysis was performed using a general linear model ANOVA with Minitab software (Version 13.20, Minitab, State College, PA, USA). Unless otherwise indicated, p-values of 0.05 were considered significant. Experiments were repeated as indicated.

4.1.3 Results and discussion

While the effects of bulk biomaterials on cell function are beginning to be understood, much less is known about materials with subcellular dimensions.(*39-41*) However, because nano-sized materials may have different physicochemical properties than their corresponding bulk materials,(*42*) the understanding of influences arising from subcellular dimensions and unusual particle geometries has become increasingly important. For example, silicate mineral is considered benign while its fibrous form, asbestos, is carcinogenic, and other parameters including surface charge, size, and aspect ratio are thought to affect toxicity.(*43*)

Similarly, ultra-fine particles have been shown to be more cytotoxic than their microparticle counterparts.(*44*) In addition, shapes of carbon-based nanomaterials have been shown to affect cytotoxicity, where the nanomaterials in the filamentous form were less toxic compared to those in particle form.(*41*) Material shapes have been demonstrated as an important factor in determining the uptake of particulates,(*45*) which can influence cell viability.(*8*)

Given the unique geometry of these biphasic nanoparticles, their effect on model physiological systems might differ significant from known polymer particles and must be thoroughly evaluated prior to a more formal assessment of the use as imaging probes. In this study, human endothelial cells (HUVECs) and murine fibroblasts (NIH 3T3s) were selected as model cell culture systems because they are well characterized and are nonprofessional phagocytes. The polymer system for the fabrication of the biphasic nanocolloids, 0.5% PAA / 4.5% PAAm-*co*-AA, was chosen not only because they produced stable biphasic nanocolloids using the electrified jetting approach, but also because their respective components, PAAm (Aquamid, polyacrylamide hydrogel) and

PAA have been used in other studies, including human trials without revealing significant harmful effects.(*46-48*)

Regarding in vivo imaging of cells or tissues, biphasic nanocolloids may be preferentially attached to the surface of cells or internalized by cells depending on the application. In both cases, it is important to control the clearance of the imaging probes from systemic circulation by phagocytes and to target the correct cell or tissue type. For the study presented in this Chapter, the initial goal was to evaluate the interactions between biphasic nanocolloids and cells and to delineate cell surface adhesion versus cell uptake. To establish a baseline, nanocolloids were studied in the absence of specific ligands and without further surface modification.

Production and characterization of the biphasic nanocolloids

The biphasic character of the nanocolloids was examined by imaging fluorescent dye-loaded particles by CLSM. Figure 4.1a shows a typical collection of particles suspended in water. The CLSM image indicates that the fluorescence-conjugated dextrans incorporated in each phase were effectively retained in the original phase without interfacial diffusion or mixing over the jetting process, thermal reaction, and even after being exposed to water (See Chapter 3 for details). The size distribution of the particles was characterized using dynamic light scattering (Figure 4.1b). Biphasic nanocolloids were suspended in water for 3 days, and their hydrodynamic radius as measured by dynamic light scattering plotted. The distribution is uni-modal with average hydrodynamic radius of 440 nm and S.D. of 290 nm. Given that the size distribution or distribution mode of the suspension did not vary significantly for the examined period of 3 days, it could be inferred that the integrity of the suspension itself was effectively

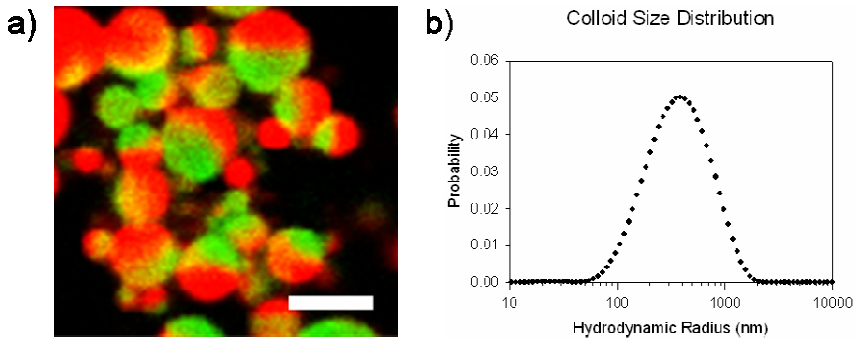

Figure 4.1 Characterization of water-stable biphasic nanocolloids used in the study. Confocal laser scanning micrograph of the biphasic nanocolloids suspended in distilled water (a). Green and red colors are derived from FITC- and Rhodamine B-conjugated dextrans, respectively, where one conjugated dextran was incorporated in one hemisphere of the particles. Scale bar: 2 mm. Size distribution of the particles suspended in phosphate-buffered saline (pH=7.4), measured by the dynamic light scattering (b).

maintained without aggregation formation or dissolution over the 48 h period of interaction with the cells.

Effect of biphasic nanocolloids on HUVEC and NIH 3T3 cell proliferation

Biphasic nanocolloids were added to cell culture at varying doses of 0, 0.01, 0.1, or 1mg biphasic particles/10^6 initially seeded cells for up to 96 h. Cell morphology was monitored every 24 h throughout the culture period. As shown Figure 4.2, for early and late time points of 4 and 96 h, respectively, with or without the highest dose of particles (1 mg/10^6 initially seeded cells), the gross morphology of the cells was not greatly affected by the presence of the particles. Similar results were observed for time points between 4 and 96 h as well as at lower particle doses. Even at the earliest time point of 4 h after addition of the particles, particles were preferentially associated with the murine fibroblasts, whereas those added to HUVECs were more diffusely scattered throughout the cell culture. Although biphasic nanocolloids were fully dispersed and no particle

aggregates were observed, when they were initially introduced to the cells, particles became slightly aggregated at higher doses of biphasic nanocolloids and for longer exposure times (Figure 4.2). This finding is in accordance with similar studies conducted

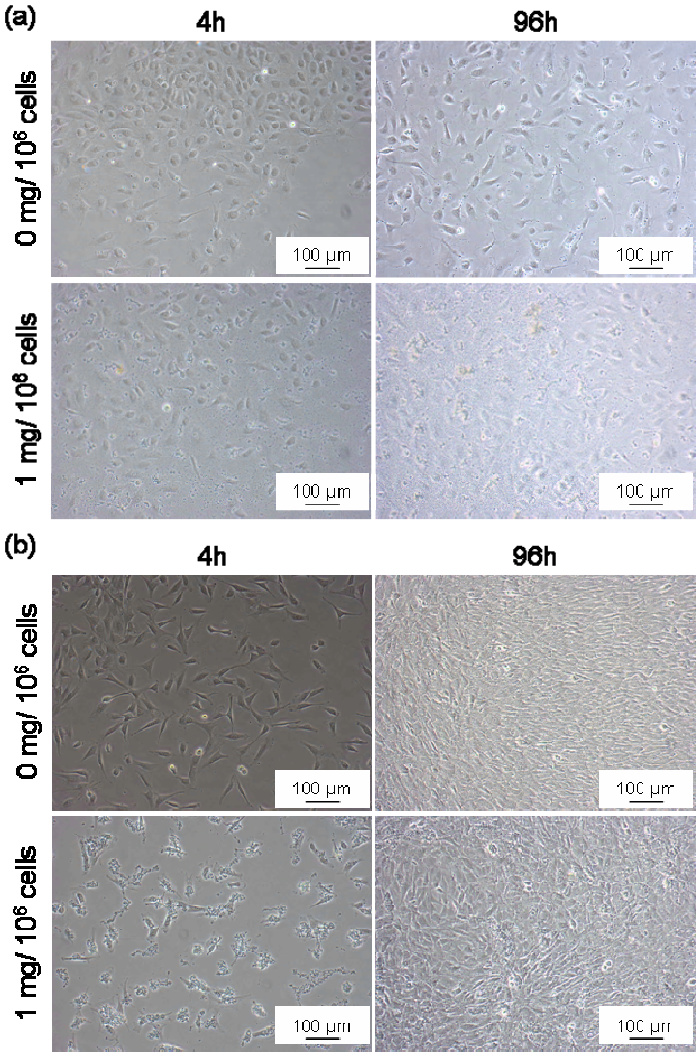

Figure 4.2 Phase contrast micrographs of HUVECs (a) and NIH 3T3 cells (b) in culture with biphasic nanocolloids. Human endothelial cells (HUVECs) or murine fibroblasts (NIH 3T3 cells) were seeded at 2.5×10^4/well in a 24-well TCPS plate. Cells were either left untreated or treated with 1mg biphasic particles/10_6 initial number of cells seeded for up to 96 h. Association of biphasic particles and cells are especially evident for NIH 3T3 cells. Scale bar: 100 mm. This experiment was repeated 3 times and representative micrographs are shown.

with gold nanoparticles. Cell targeting using tiopronin-protected gold particles and functionalized with the GRGDSP peptide has been shown to induce particle aggregation in cell culture systems containing serum.(*49*) In this system, aggregation was attributed to the interaction between the carboxylic groups of the particles and serum proteins.

Although amide and carboxylic acid groups of the biphasic nanocolloids were thermally crosslinked to form imide groups [41], the presence of residual carboxylic acid groups cannot be entirely ruled out. These acid groups could mediate the aggregation of the biphasic nanocolloids to some extent. In applications requiring higher doses of biphasic nanocolloids, further surface modifications using polyethylene glycol may therefore be necessary to prevent aggregation and to ensure uniform cell labeling.

Next, the effect of biphasic nanocolloids on the proliferative capacity of human endothelial and murine fibroblasts was evaluated using a colorimetric proliferation assay (Figure 4.3). In this assay, the amount of formazan product, which is proportional to the number of living cells present in the system, is detected by an absorbance measurement at 490nm. Cells were incubated in the presence of indicated doses of biphasic nanocolloids for 4, 24, 48, 72, and 96 h, and the formation of formazan product was measured at the end of the incubation periods.

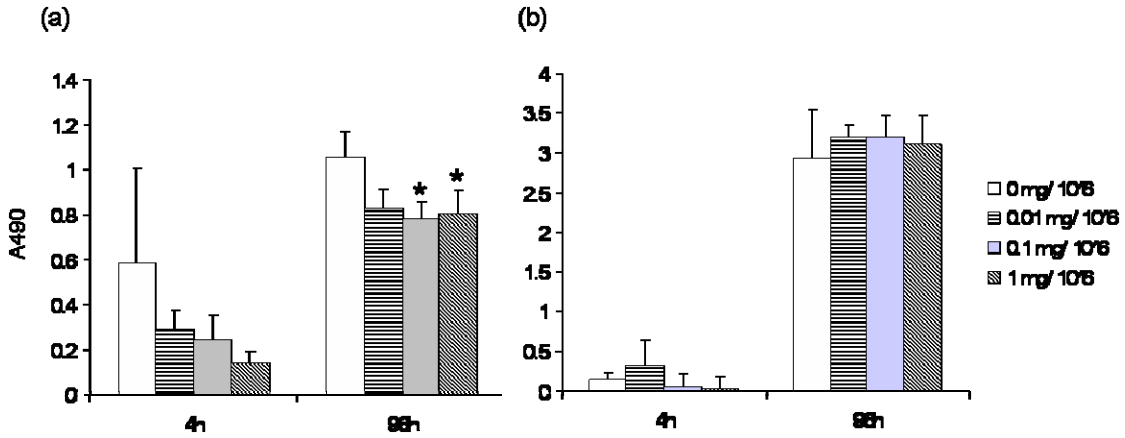

Figure 4.3 Effect of biphasic nanocolloids on HUVEC (a) and NIH 3T3 (b) cell proliferation as measured by a colorimetric assay. Human endothelial cells (HUVECs) or murine fibroblasts (NIH 3T3 cells) were seeded at 2.5×10^4/well in a 24-well TCPS plate, and reagent added after indicated times of treatment to measure proliferation colorimetrically. Within the range tested, addition of biphasic particles affected cell proliferation of HUVECs only at the higher doses at latest time points. * $p \leq 0.05$ compared to 0 mg/10^6 initially seeded cells, n = 3, average ± S.D.

Possible interference from the biphasic nanocolloids on absorbance readings was excluded by transferring the supernatant to a new well for reading using the spectrophotometric plate reader. For both HUVECs and NIH 3T3 cells, number of cells increased with time due to cell proliferation. Only for the highest dose and after 96 h incubation time, proliferation of HUVECs was decreased in the presence of the particles relative to the controls of cells without any particles (Figure 4.3a); however, at the same dose and incubation time, proliferation of NIH 3T3s was not affected by the presence of the particles (Figure 4.3b), as indicated by the lack of significant difference between the cells with and without biphasic nanocolloids. In a comparable study, differential effects of poly(methyl methacrylate) particles on macrophage and fibroblasts have been shown, where macrophages, but not fibroblasts, demonstrated decreased proliferation in response to the polymeric particles.(*50*)

Association of biphasic nanocolloids on HUVEC and NIH 3T3 cells

While phase contrast micrographs of cells in culture in the presence of particles, as shown in Figure 4.2, did suggest cell-nanocolloid association, evidence based on this technique cannot ascertain nor quantify the extent of this association. To explicitly address this question, further studies were conducted using flow cytometry (Figure 4.4). For this purpose, cells were cultured in the absence or presence of biphasic particles containing FITC- and cascade blue-conjugated dextrans in the respective hemispheres at doses of 0.01, 0.1, or 1mg particles/10^6 initially seeded cells for 24 h, washed to remove loosely bound particles, and analyzed by flow cytometry. Cellular events with FITC fluorescence resolved in FL1 were considered to be cells associated with the biphasic particles. For both HUVECs and NIH 3T3s, flow cytometry histograms of analyzed cell population indicated that increasing the initial dose of biphasic nanocolloids resulted in higher mean fluorescence intensity resolved in the FITC channel as well as increased fraction of cell population associated with the fluorescence, indicative of association of particles with the cells, even after washing (Figure 4.4a and 4.4c respectively). Quantification of the cell population associated with biphasic nanocolloids revealed that the majority of the cells became associated with the biphasic nanocolloids; even at the lowest dose of 0.01 mg/10^6 initially seeded cells, over 60% of both human endothelial cell and murine fibroblast populations were associated with the fluorescence arising from the biphasic nanocolloids (Figure 4.4b and 4.4d, respectively). Increase in biphasic nanocolloid association was observed with higher initial biphasic nanocolloid load. At the highest dose of 1 mg/10^6 cells, over 95% of the population was positive for the biphasic nanocolloids. These results suggest that nanocolloids widely associate with cells, which is also corroborated by the phase contrast micrographs in Figure 4.2.

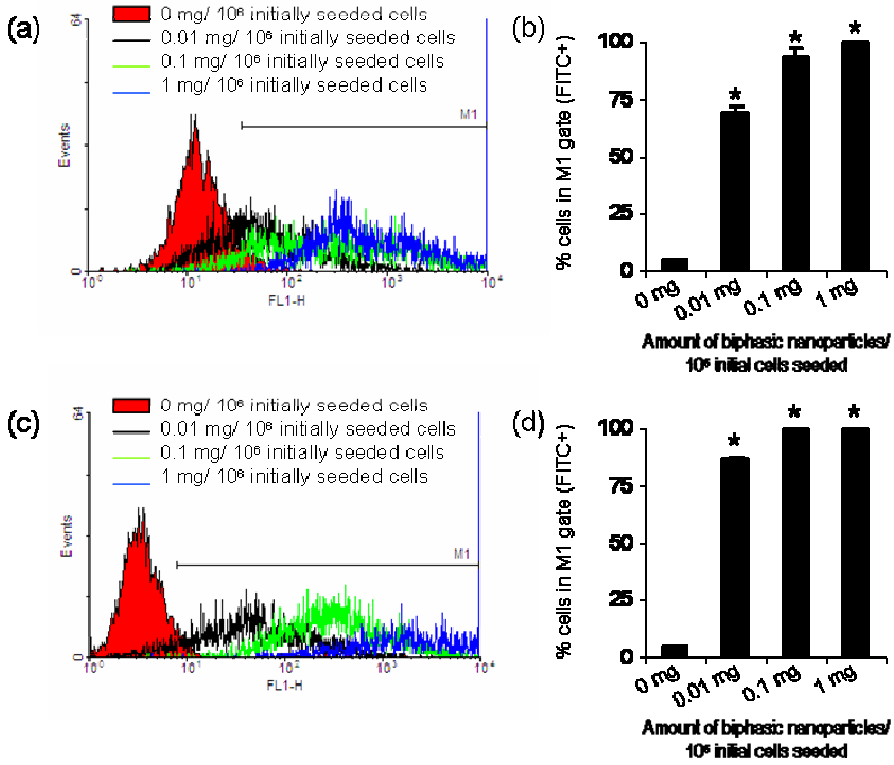

Figure 4.4 Quantification of biphasic nanocolloid association with HUVECs (a, b) and NIH 3T3 cells (c, d). Cells were incubated with the indicated amounts of the biphasic nanocolloids for 24 h, washed, and analyzed by flow cytometry. Histograms of FITC intensity associated with HUVECs (a) and NIH 3T3 cells (c) showed that increasing dose of nanocolloids led to higher fluorescence intensity. Filled histograms represent cellular autofluorescence.Quantification of FITC-positive HUVECs (b) and NIH 3T3 cells (d) indicated that fraction of cells positive for the biphasic nanocolloids increased with increasing nanocolloids dose. This experiment was repeated 3 times and representative histograms are shown. * $p \leq 0.05$ compared to 0 mg/10^6 initially seeded cells, n = 3, average ± S.D.

While flow cytometry results revealed that most of the cells were associated with biphasic nanocolloids, the results from this experiment could not distinguish whether the particles are internalized by the cells or bound to the cell surface through non-specific adhesion. To unambiguously differentiate between particle uptake and cell surface adhesion, further studies were necessary. Therefore, cells were incubated with biphasic nanocolloids loaded with FITC- or rhodamine-conjugated dextran in the respective halves

and visualized using CLSM. As indicated previously, conjugation with dextran prevents the diffusion of the fluorescence across the hemisphere interface, enabling visualization of the distinct hemispheres.

Association of biphasic nanocolloids with cells was observed as early as 4 h after the start of incubation (results not shown). In general, some but not all endothelial cells

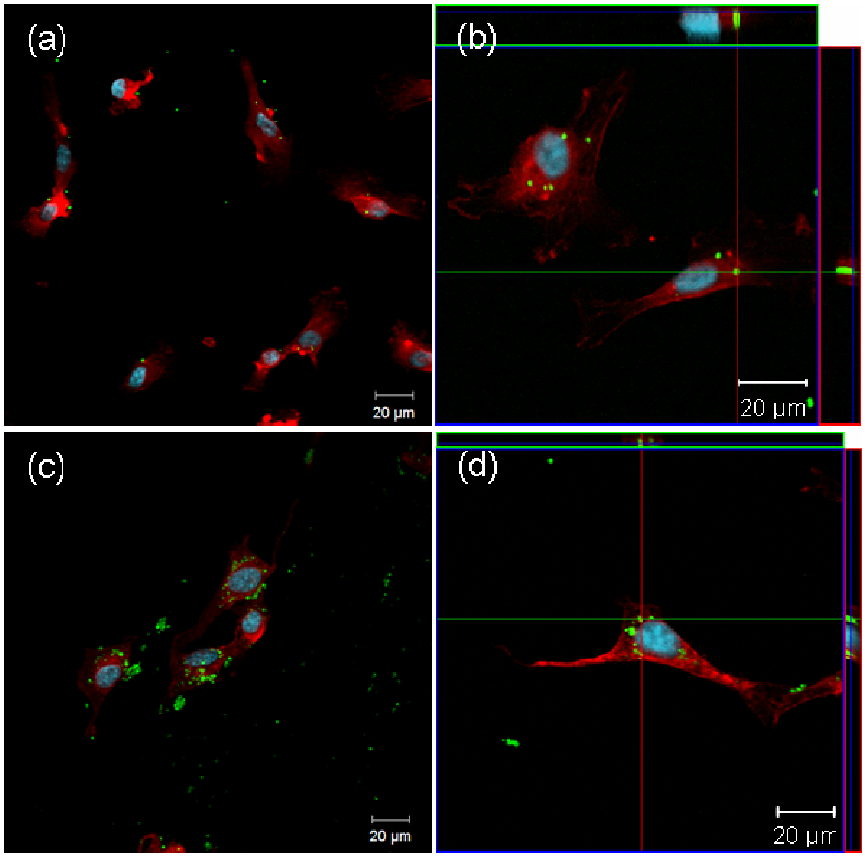

Figure 4.5 Localization of biphasic nanocolloids associated with HUVECs (a, b) and NIH 3T3 cells (c, d). Cells were cultured on coverslips with 1 mg/10_6 initially seeded cells of biphasic nanocolloids. After incubation for 24 h, cells were washed and stained with rhodamine-conjugated phalloidin and counterstained with Hoechst 33342. Compared to HUVECs (a), fibroblasts (c) appeared associated with more biphasic nanocolloids. Orthogonal images reconstructed from Z-stacks indicated that both HUVECs (b) and NIH 3T3 cells (d) are capable of internalizing the biphasic nanocolloids. This experiment was repeated 3 times and representative micrographs are shown.

and fibroblasts were associated with the biphasic nanocolloids. At the same initial biphasic nanocolloid dose, HUVECs were less associated with the biphasic nanocolloids, as compared to NIH 3T3 cells (Figure 4.5a and 4.5c, respectively). To determine whether the biphasic nanocolloids were internalized or not, orthogonal images of endothelial cells and fibroblasts were reconstructed from Z-stacks of CLSM images (Figure 4.5b and 4.5d, respectively).

Independent of the cell type, both, cell surface binding and cell uptake of biphasic nanocolloids were observed. In fact, some particles were enclosed by actin filaments, indicating internalization of the particles, whereas others were not, indicating surface adhesion. In conclusion, both modes of cell/particle interactions are feasible and appear to co-exist. However, caution should be taken when interpreting these data, because particle uptake by cells is not only dependent on surface chemistry,(*51, 52*) but also on cell type, cell density, and particle size.(*53*) In addition, particle phagocytosis by these cells may be influenced by specific experimental conditions. Implementation of further surface modification strategies for biphasic nanocolloids may provide better control over the relative occurrence of surface adhesion vs. internalization. In fact, some success has already been shown with modified gold nanoparticles. When cultured with gold nanoparticles derivatized with ethylenediamine or poly(ethylene glycol) (PEG) bis(3-aminopropyl) terminated, immortalized primary human fibroblasts endocytosed these nanoparticles, whereas the same particles functionalized with GRGDSP peptide attached on the cell surface.(*49*) Using similar surface modification techniques, we expect to greatly reduce or even eliminate internalization or surface binding of biphasic nanocolloids depending on the needs of a specific application. In addition, the use of cell-specific markers may grant control over particle uptake or cell surface binding in a cell-specific manner.

Effect of biphasic nanocolloids on HUVEC and NIH 3T3 cell viability

To characterize the cell viability in response to treatment with biphasic nanocolloids, cells cultured with the fluorescence-loaded biphasic nanocolloids were

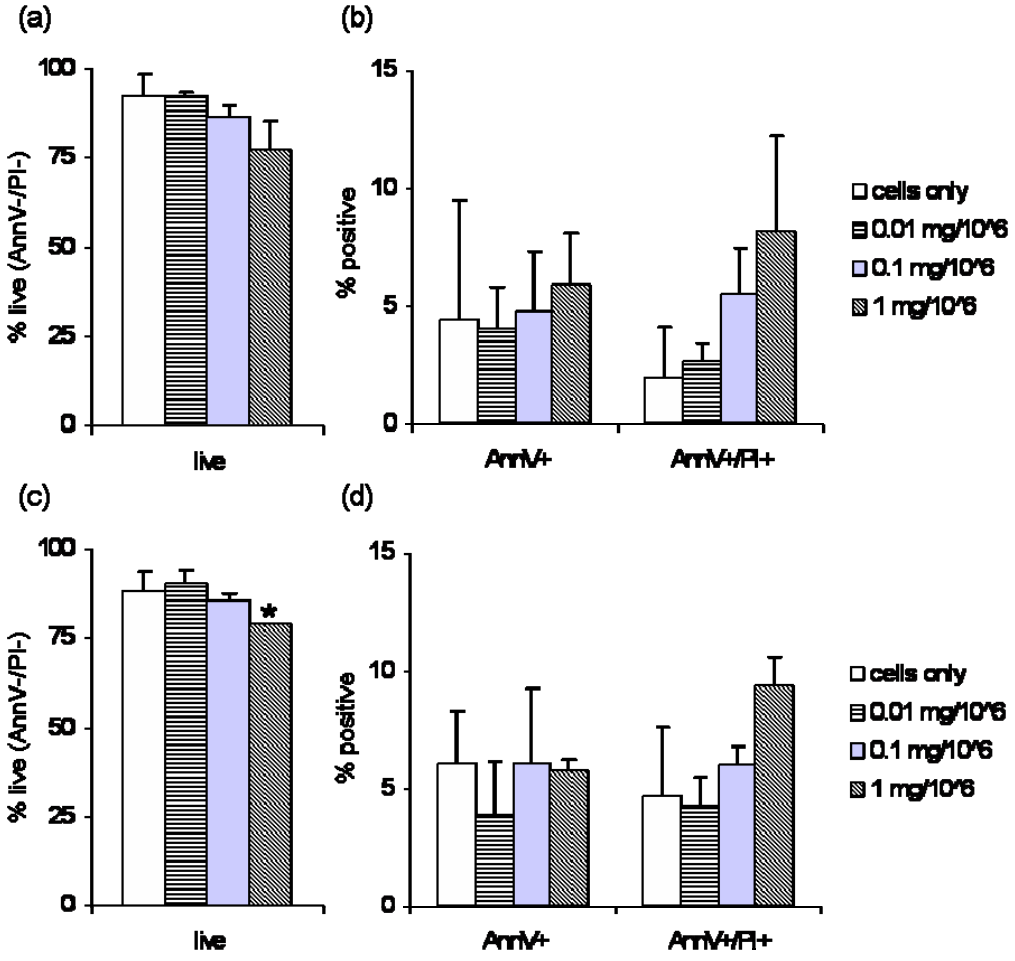

Figure 4.6 Effect of biphasic nanocolloids on HUVEC (a, b) and NIH 3T3 (c, d) cell viability. Cells were cultured in the presence of indicated amounts of the biphasic nanocolloids for 24 h, washed, stained with Alexa fluor 647-conjugated Annexin V and PI, and analyzed by flow cytometry. Statistically significant decrease in the fraction of live cells in the presence of nanocolloids was not detected for HUVECs (a), but was detected at the highest dose for NIH 3T3 cells (c). While a trend higher percentage of dead cells was observed with increasing particle dose for both HUVECs (b) and NIH 3T3 cells (d), they were not a statistically significant level. * $p < 0.05$ compared to 0 mg/10^6 initially seeded cells, n = 3, average + S.D.

analyzed by double staining with Alexa fluor 647-conjugated Annexin V and PI, using flow cytometry. Cells were incubated in the presence of absence of indicated load of particles for 24 h, washed, and then stained. Annexin V binds to exposed phosphatidylserine on apoptotic cells whereas PI enters dead cells with compromised membrane integrity and binds to DNA. In contrast to the proliferation assay, this approach provides quantitative results with respect to the state of cell death. Furthermore, because the cells were cultured with biphasic nanocolloids containing FITC- and cascade blue-conjugated dextrans in the respective hemispheres, cells associated with the biphasic nanocolloids were also tracked by evaluating FITC fluorescence resolved in FL1 channel. Staining of cells with Annexin V and PI showed the general state of cell viability upon treatment with the biphasic nanocolloids. Figure 4.6a and 4.6c show the fraction of population that was alive or negative for Annexin V and PI staining for HUVECs and NIH 3T3 cells, respectively.

Decrease in cell viability was observed for NIH 3T3s only at the highest dose of 1 $mg/10^6$ initially seeded cells, as compare to cells that did not receive any biphasic nanocolloids treatment (Figure 4.6c). In addition, percentages of apoptotic (positive for only Annexin V) or dead cells (positive for Annexin V and PI) were not significantly affected by increasing doses of the particles (Figure 4.6b and 4.6d) Because the cytotoxic potential of biphasic nanocolloids is a major concern of this study, we wanted to confirm these initial data with a second approach. Therefore, cell viability was also measured using release of G6PD from cells cultured in presence or absence of biphasic particles. The difference between the two methods is that PI enters the cells through damaged areas of the cell membrane, while this enzymatic assay relies on detection of release of cytosolic enzyme, G6PD, into the medium. After 24 h of incubation, HUVECs and NIH 3T3 cells that were treated with varying doses of particles did not release increased

amounts of G6PD as compared to cells not treated with any particles (Figure 4.7a and 4.7b, respectively). Moreover, the fluorescence detected in media of cells treated or not with particles was not significantly different from what was detected with media alone. In this case, there was no significant effect of fluorescence interference from the presence of the particles, suggesting that there was no leaching of fluorescent-conjugated dextrans incorporated into the particles (data not shown). In addition, no correlation between initial dose of the particles and G6PD release was observed for both cell types. As expected, significantly increased amounts of G6PD were detected when comparing to the positive controls consisting of lysed cells.

Within the concentration range evaluated, these results suggest a generally low cytotoxic potential of biphasic nanocolloids. Data obtained by the PI assay, but not the

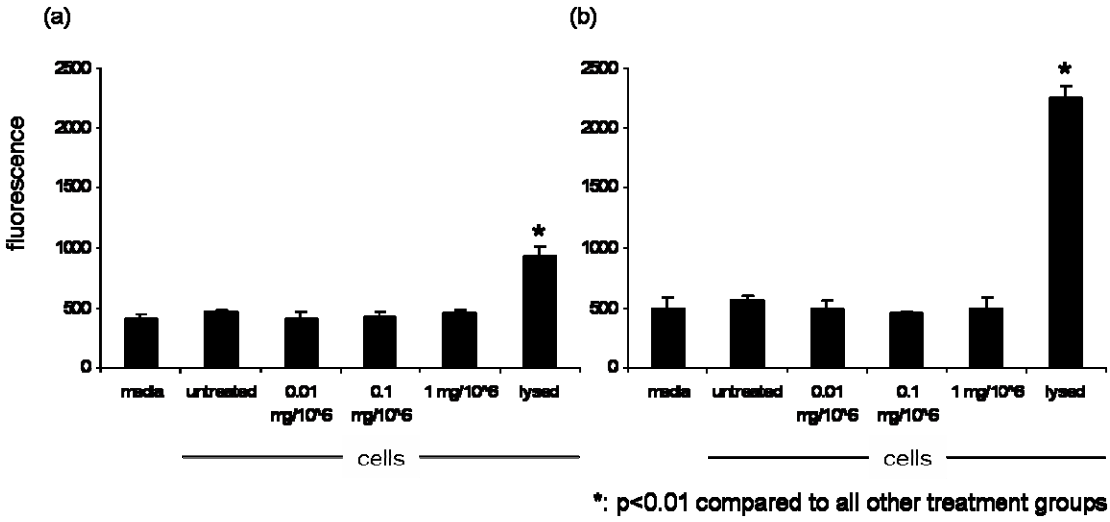

Figure 4.7 Effect of biphasic nanocolloids on HUVEC (a) and NIH 3T3 (b) glucose-6-phosphate dehydrogenase release. HUVECs or NIH 3T3s cells were cultured with or without 0.01, 0.1, or 1mg of biphasic particles/10_6 seeded cells for 24 h. Media was cleared and assessed for G6PD by taking fluorescence measurements every 5 min for 30 min at 37 1C (ex: 544 nm, em: 590 nm). Fluorescent readings at 10 min incubation of the cleared media with substrate are shown* $p \leq 0.01$ compared to 0 mg/10^6 initially seeded cells, n = 3, average ± S.D.

G6PD assay, indicated reduced viability at the highest particle concentration (1 mg particles/106 seeded cells). As cell viability was affected only at the highest dose, biphasic nanocolloid doses tested herein provide a wide range in which these particles could be used as imaging probes. This effect offers flexible use of biphasic nanocolloids depending on the needs of a particular imaging application. However, determining the proper dosage feasible for a given application is critical in the development of these biphasic nanocolloids as imaging probes.

The major polymeric components of the particles tested herein are PAAm-co-AA with 10% PAA residues as well as PAA. Given the commercial use of implantable PAAm hydrogels, such as Aquamid, the intrinsic biocompatibility of the base polymers is not surprising. Compared to the benign bulk properties, effects stemming from sub-micron dimensions and biphasic particle geometries appear less dominant. For comparison, cytotoxicity of 10% and 20% Aquamid tested in a direct contact assay with bovine arterial endothelial or human dermal fibroblast cell cultures using Trypan blue exclusion was reported to be above 90% and 75% for the respective cell types after 4 days.(*54*) Additionally, PAA nanoparticles have been previously explored for ophthalmic and mucosal drug delivery applications.(*46, 47*) Human corneal epithelia cells incubated with PAA nanoparticles showed no change in morphology but a 10% reduction in viability after 2 h incubation.(*46*) Similarly, a human study evaluating tolerance of PAA-based ocular insert showed that the inserts were generally well accepted by the volunteers with respect to a several parameters evaluated including irritation and lacrimation.(*55*)

4.1.4 Conclusions

This first section of Chapter 4 reports on the short time biocompatibility of biphasic nanocolloids, which with further development, may present interesting

candidates as anisotropic imaging probes. A series of noteworthy observations underline this conclusion: (i) exposure of HUVECs and NIH 3T3 cells with biphasic nanocolloids did not greatly affect their cell proliferation; (ii) biphasic nanocolloids were internalized by these cells, but did not greatly decrease cell viability within the doses tested; and (iii) without further surface modification, complete prevention of biphasic nanocolloids uptake by cells may be unlikely.

For any in vivo imaging application, it is paramount that the imaging probes are biocompatible and maintain their integrity in a physiological environment. Without these essential characteristics, further development work seems challenging. While the scope of this biocompatibility study has been limited to a short-term assessment (i.e., exposure times up to 96 h) and does not address functional imaging criteria, it still offers critical insight into the compatibility of these novel particles with biological systems.

With the basic biocompatibility demonstrated, further studies will be aimed at improvement of biphasic nanocolloids as imaging probes through implementation of targeting strategies (See Chapter 4.2). After additional implementation of specificity to promote internalization or surface binding (via receptors or surface markers), these biphasic nanocolloids may establish a flexible polymer particle platform that can be tailored for various imaging modalities using magnetic, optical, or fluorescent properties. The fact that biphasic nanocolloids provide simultaneous access to two compartments that can be independently loaded with different therapeutics as well as imaging moieties, such as dyes or magnetic nanomaterials, and—at the same time—can be selectively surface modified to control orientation relative to the cell surface, supports the vision of unique imaging capabilities. Far beyond simple imaging capabilities, anisotropic nanoparticles may provide further functions, such as self-assembly into three-dimensional tissue constructs or potential to mimic extracellular matrix with subcellular organization

and order, which will be very difficult to achieve with more conventional, isotropic nanoparticles.

4.2 Directional Cell Membrane Labeling

4.2.1 Introduction

Recent successful merge of nanotechnology and biomedical diagnostics has brought about an era of bio-imaging in a single molecular length scale.(*56, 57*) Further advancement of bio-imaging probes is expected, expecially with regards to novel and diverse functionalities.(*58-60*) Examples of this effort include drug delivery vehicles that can be systemically administered and accumulated at the targeted tissues to deliver curing agents as well as contrasting materials for bio-imaging mechanisms.(*61, 62*) For this purpose, quantum dots (QDs),(*63, 64*) metal nanoshells,(*65*) liposomes,(*66, 67*) superparamagnetic nanoparticles,(*68-70*) polymeric surfactants,(*71*) dendrimers,(*72*) and carbon nanotubes(*73, 74*) have been extensively studied.

In Chapter 2, novel method to create multiphasic nanocolloids by use of simultaneous electrohydrodynamic jetting of two or more different solutions was demonstrated.(*36, 75*) It was shown in Chapter 3 that the biphasic nanocolloids produced by electrified co-jetting of poly(acrylamide-*co*-acrylic acid) (PAAm-*co*-AA) solutions could be stabilized against aqueous environment by use of thermal imidization.(*76*) Additionally in the first section of Chapter 4, the short-term (exposure time of 96 hours) *in vitro* biocompatibility of this nanocolloid system was examined as the first step toward

potential biomedical application of unique anisotropy of the nanocolloids.(*77*) The results showed that (i) incubation of HUVECs and NIH 3T3 cells in the presence of biphasic nanocolloids did not greatly affect the cell proliferation; (ii) biphasic nanocolloids were either attached on cell membrane or internalized by the cells without any introduction of ligands for the specific interaction; and (iii) cell-particle association did not greatly decrease cell viability within the doses tested. While the results of initial biocompatibility tests were encouraging, further design and surface modification of the colloids were necessary to prevent the non-specific association and to enhance the directional interaction between the cells and the colloidal particles.

In this section of Chapter 4, anisotropic nanoprobe design that realizes the novel concept of direction-specific bio-labeling of live cell membrane is proposed. Depending on the cells (tissues) to be targeted, many possible applications of the directional association of anisotropic colloids may be proposed. For example, colloidal particles may be intravenously injected; if only one hemisphere of the particles is designed to specifically bind to the endothelial cells, while the entire particle surface is designed to minimize non-specific interactions with other boold cells and serum proteins, the blood vessel lumen will be covered with a layer of directionally-bound particles without a risk of thrombosis or embolism.

Poly(ethylene glycol) (PEG) layer has been extensively studied due to its resistance to the bioadsorption.(*78-90*) In the study herein, the non-specific association between the cells and particles was successfully prevented by introduction of PEG layer onto the particle surfaces. The specific interaction was introduced to a single hemisphere of the particle by selective surface modifications. Series of bio-linkers (biotin-Streptavidin) and antibody molecule for a cell membrane surface protein, PECAM-1 (platelet/endothelial cell adhesion molecules, CD31), was employed for this purpose.

Following the characterization of the novel colloids, directional bio-labeling was successfully demonstrated for the HUVECs by flow cytometry.

4.2.2 Methods

Preparation of biotin modified PAAm-*co*-AA and acetylene modified PAAm-*co*-AA

1-Ethyl-3-(3-dimethylaminopropyl)carbodiimide hydrochloride [EDC, Sigma-Aldrich Inc.] combined with *N*-Hydroxysulfosuccinimide sodium salt [Sulfo-NHS, Fluka Inc.] were used as the coupling agents to activate the carboxylic acid groups of acrylic acid residues in poly(acrylamide-*co*-acrylic acid, sodium salts) (PAAm-*co*-AA) (MW 200 kD, 10% acrylic acid residues, Polysciences, Warrington, PA). The activated ester groups were further modified with amine groups of biotin ethylenediamine hydrobromide [or 1H-Thieno[3,4-d]imidazole-4-pentanamide, N-(2-aminoethyl)hexahydro- 2-oxo-, (3aS,4S,6aR)-N-(2-aminoethyl)biotinamide hydrobromide, Sigma-Aldrich Inc.] or propargyl amine [Aldrich Inc.] to form stable amide linkages. For biotin modification, 100 mg of PAAm-*co*-AA was dissolved in 10 ml of double distilled H_2O (ddH_2O), and 25 mg of biotin ethylenediamine hydrobromide, 192 mg of EDC and 21.7 mg of Sulfo-NHS were subsequently added into the solution and the solution was stirred for 5 hours. Similarly for the introduction of acetylene groups, 250 mg of PAAm-*co*-AA was dissolved in 35 ml of ddH_2O, and 38.5 mg of propargyl amine, 675 mg of EDC and 76.5 mg of sulfo-NHS was added into the solution and the solution was stirred for 4 hours. After the reaction, the excess reagent and the isourea by-product were removed by dialysis (MWCO 3,000) overnight. The final products were lyophilized and appropriate amount was re-dissolved in the preparation of jetting solutions.

Preparation of methyl-PEG-azide

A mixture of 500 mg of polyethylene glycol monomethyl ether mesylate [methyl-PEG-mesylate, MW 5,000, Fluka Inc.] and 65 mg of sodium azide [Sigma-Aldrich Inc.] dissolved in 10 ml of DMF was stirred at 60 °C for 24 h. The polymer product was precipitated by pouring excess ethyl ether onto the DMF solutions and recovered by filtration. The filtrate was dissolved in water and washed by dialysis [MWCO 3,000] overnight. The dialyzed solution was subsequently lyophilized.

Synthesis of monophasic and biphasic nanoparticles

Monophasic and biphasic nanoparticles were fabricated and stabilized by use of the electrified jetting procedure and thermal imidization treatment that have been published.(*2, 5*) For fabrication of monophasic and biphasic nanoparticles with different chemical composition, respective jetting solutions were designed and used for the electrified jetting. All components were dissolved in double distilled H_2O (ddH_2O), and all percentage reported here are weight per volume contents. In brief for monophasic nanoparticles, a mixture of 3 % of PAAm-*co*-AA, 1 % biotin-modified PAAm-*co*-AA, 1 % acetylene-modified PAAm-*co*-AA, and 0.5 % FITC (fluorescein isocyanate)-conjugated dextran (MW 250 kD, Sigma) was used as a jetting solution. For biphasic particles, two pairs of jetting solutions were used: i) a mixture of 4 % PAAm-*co*-AA, 1 % acetylene modified PAAm-*co*-AA and 0.5 % FITC-dextran paired with a mixture solution of 3 % PAAm-*co*-AA, 1% acetylene modified PAAm-*co*-AA, 1 % biotin modified PAAm-*co*-AA and 0.5% Rhodamine B-dextran. ii) a mixture of 4.5 % of PAAm-*co*-AA, 0.5 % acetylene modified PAAm-*co*-AA, and 0.5 % FITC-dextran paired with a mixture of 4.5 % of PAAm-*co*-AA, 0.5 % biotin modified PAAm-*co*-AA, and 0.5 % Rhodamine B-dextran.

Following the electrified jetting, the nanoparticles were incubated at 175°C for 3 hours to induce crosslinking by thermal imidization between carboxylic acid and amide groups to form an imide group. Prior to use, biphasic nanoparticles were suspended in ddH_2O and treated with subsequent selective modifications.

PEGylation of the nanoparticles by Click Chemistry

Typical reaction conditions were as follows: In an 1 ml microtube, 3 mg of nanoparticles were suspended in 600 µl of ddH_2O. A solution of 6 mg methyl-PEG-azide dissolved in 400 µl ddH_2O was added on the particle suspension. A mixture of 60 µl of 0.3 M sodium ascorbate and 60 µl of 0.03 M $CuSO_4 \cdot H_2O$ was subsequently added onto the suspension and the whole suspension was kept at room temperature for 10 hours on a microtube rotator. The suspension was washed with fresh ddH_2O for three times by iteration of centrifugation and re-suspension. The final washing was performed with fresh PBS for further reaction with streptavidin.

Selective modification of biotin with streptavidin

In a microtube, 1 mg of selectively or homogeneously PEGylated nanoparticles were suspended in 1 ml of PBS. 15 µl of streptavidin [Pierce Inc., reconstituted to a concentration of 10 mg/ml] was added onto the suspension and kept for 6 hours at room temperature on a microtube rotator. The final suspension was washed with fresh PBS for three times in a similar manner.

Flow cytometry of HUVECs and particle suspensions

HUVECs (p13, 96.8% viability) were suspended at a concentration of 10^5/ml in 0.5% BSA in HEPES buffer. 500 µl of this cell suspension was stained or not with 10 µl

indicated antibody for 1hr at 4°C. These cells were washed 1x in 0.5% BSA in HEPES, and subsequently incubated with articles (0.5 mg/10^6 cells) for 1 hr at 4°C on hematology mixer. Cells were then washed 1x in 0.5% BSA in HEPES, and analyzed by flow cytometry (FACSCalibur, BD Biosciences). FlowJo (Tree Star, Inc., Ashland, OR, USA) or WinMDI was used for data analysis. For statistical analysis, marker (M1) was set for FITC/PE histogram such that the 5% of population stained with isotype antibody was included. These same markers were used throughout different runs to derive at % of cell population that had bound to particles ("% gated"). Geometric mean fluorescent intensity (gMFI) values were recorded both within and outside of M1 marker. The FITC/FSC(forward scatter) and PE/FSC clearly distinguished the signals from unbound particles from the signals from particles associated with the cells. The unbound particles which appear in low FSC/high fluorescence region were excluded for the statistical analyses.

4.2.3 Results and Discussion

As described above, the previous study showed that the particles associated with the membranes of HUVECs even in the absence of any specific ligands. To achieve directional binding of particles to HUVECs, surface of the entire particle was modified to

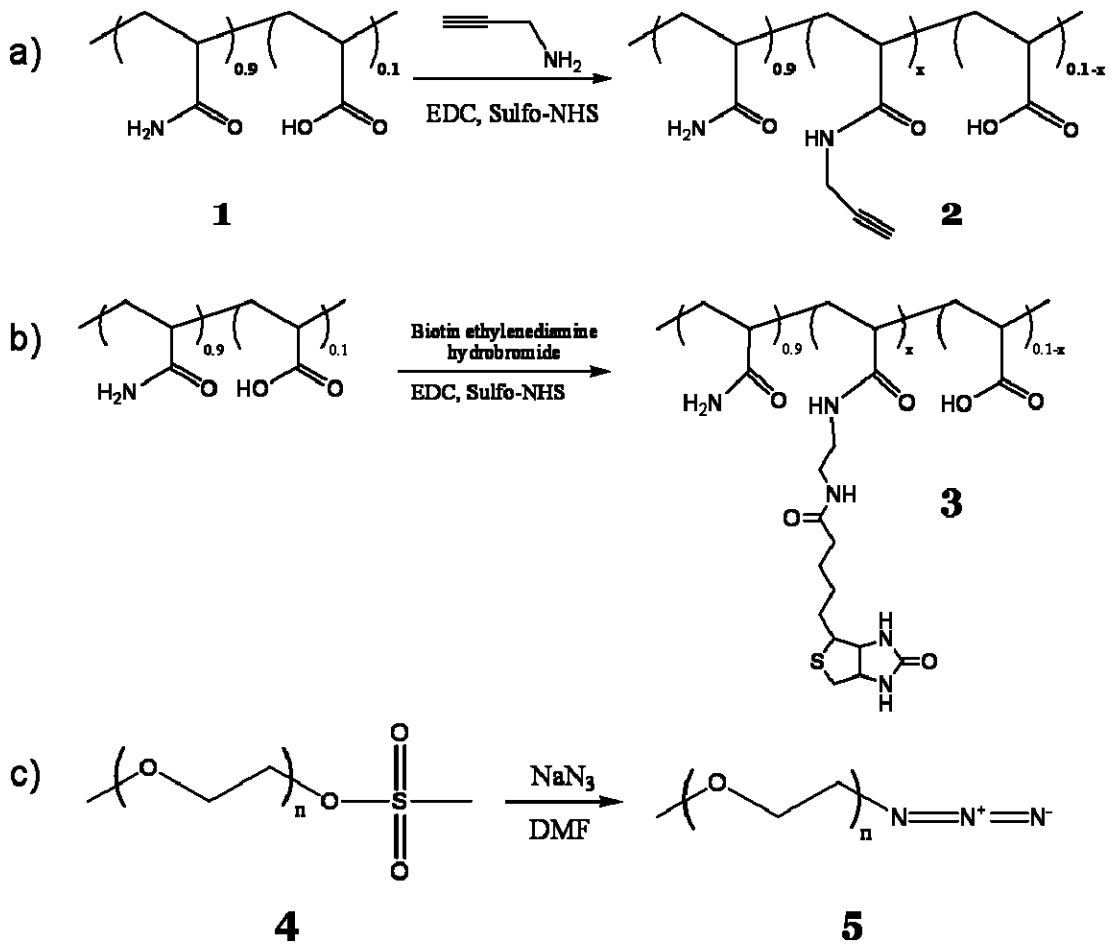

Scheme 4.1 Chemical reactions of the functional polymers employed in the electrified jettings and further surface modifications. Carboxylic acid groups of poly(acrylamide-*co*-acrylic acid) (**1**) were reacted with propargyl amine (a) or biotin ethylenediamine (b) for introduction of acetylene (**2**) and biotin (**3**) moieties into the polymer chains. Poly(ethylene glycol) (**4**) which has methoxy and sulfonyl group at each end was reacted with sodium azide to yield methoxy-PEG-azide (**5**) (c).

minimize non-specific binding, and specific ligand was incorporated into the surface of one hemisphere enhance the specific binding.

As PEG layer prevents non-specific adsorption of biological components such as proteins onto the engineered surfaces,(*81*) we introduced the PEG layer onto the particle surface by Cu(I)-catalyzed Huisgen 1,3-dipolar cycloaddition (Click Chemistry). For this purpose the acrylic acid residues of PAAm-*co*-AA (1) were reacted with propargyl amine by EDC mediated coupling to introduce acetylene groups to the polymer chains (2). PEG chains that contain methyoxy and azide group at each ends (3) were synthesized by a modified method reported previously.(*91*) For the introduction of the specific ligand, the biotin-streptavidin bio-linker was used. Acrylic acid residues of PAAm-*co*-AA were similarly reacted with biotin-ethylenediamine to incorporate biotin groups into polymer chains (4). The reaction schemes and the NMR spectroscopy data are presented in Scheme 4.1 and Figure 4.8, respectively.

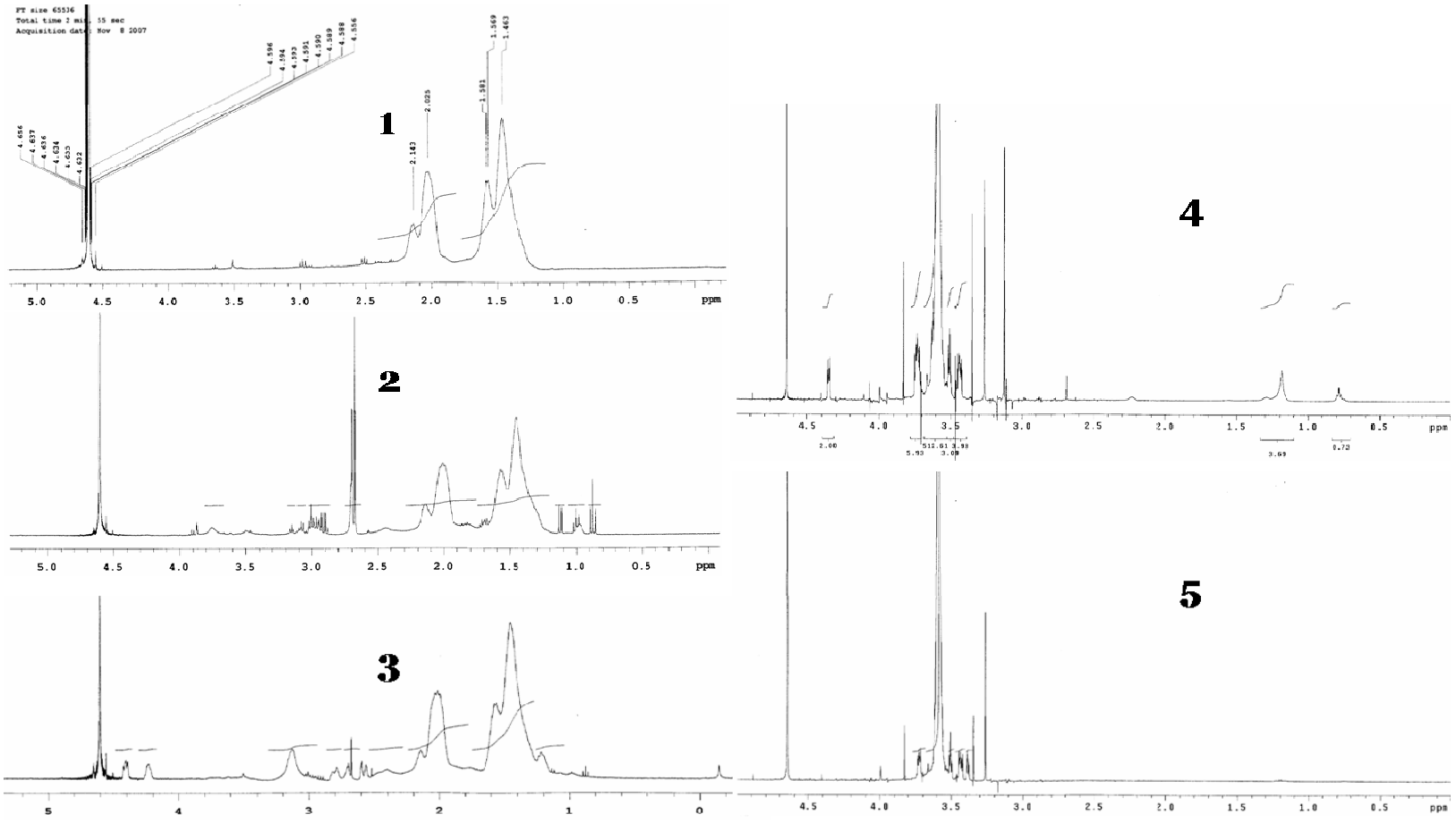

Figure 4.8 ^{1}H nuclear magnetic resonance (NMR) spectroscopies of the polymers before and after the chemical reactions described in scheme 4.1: poly(acrylamide-*co*-acrylic acid) (**1**), poly(acrylamide-*co*-acrylic acid) with acetylene (**2**) and biotin (**3**) moieties, methoxy-poly(ethylene glycol)-sulfonyl (**4**), and methoxy-PEG-azide (**5**).

Scheme 4.2 describes the particles created by electrified co-jetting and further modification reactions by use of above mentioned polymers. For the jetting, acetylene-containing polymer was incorporated in both sides of the jetting solutions, while the biotin-containing polymer was only incorporated in one side. FITC- or Rhodamine B-conjugated dextrans were added to biotin-empty or biotin-containing solutions, respectively, in order to enable examination of the biphasic character of the nanoparticles by confocal laser scanning microscopy (CLSM). Fluorescence-conjugated dextrans incorporated in each phase were effectively separated in each hemisphere of the resulting nanoparticles without significant interfacial diffusion or mixing. It suggests that the difference in chemical composition of each phase was successfully introduced to the biphasic nanoparticle structure in an anisotropic manner, resulting in particles with acetylene on the entire surface, but biotin in only one hemisphere.

After the particles were thermally-crosslinked at 175°C for 3 hours, the re-suspended particles were first reacted with methyl-PEG-azide chains in the presence of Cu(I) for 12 hours at room temperature. After washing excess PEG chains and the catalyst, the particles were suspended in PBS and incubated with streptavidin. Even

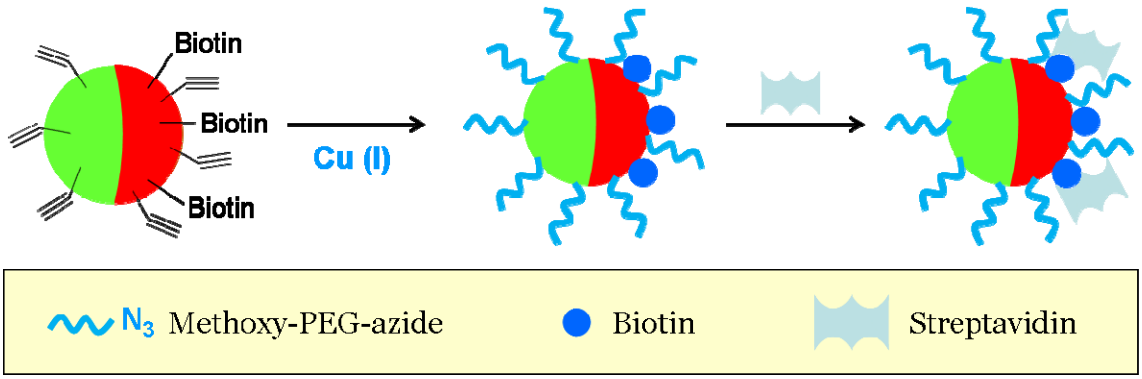

Scheme 4.2 Surface modification of biphasic nanocollodis. As a first step reaction, entire surface was modified with PEG chains by 'Click Chemistry'. Selective modification with streptavidin was followed for one hemisphere containing biotin molecules (blue circle in scheme).

though only one hemisphere contained biotin molecules on the surface, an aggregation of the particles can occur due to the quaternary binding sites of a single streptavidin molecule. In order to prevent this possible aggregation, excess streptavidin was used for the incubation step. The non-specific adsorption of the streptavidin to the biotin-empty side of the particle was designed to be effectively suppressed by the PEG layer.

After the thermal reaction and subsequent chemical modifications, the particles were examined again by CLSM (Figure 4.9). The particles were still well-dispersed without significant aggregations, and the biphasic geometry was maintained. Non-spherical particles and some broken pieces of the particles were scarcely observed. These damages may have been incurred during sonication and washing steps, but the fraction of broken particles was very low.

In order to ensure the selective presence of the streptavidin exclusively in one side of the particle surface, we performed similar modifications of the particles, where FITC-dextran were added to both sides, and used TRITC-conjugated streptavidin molecules to

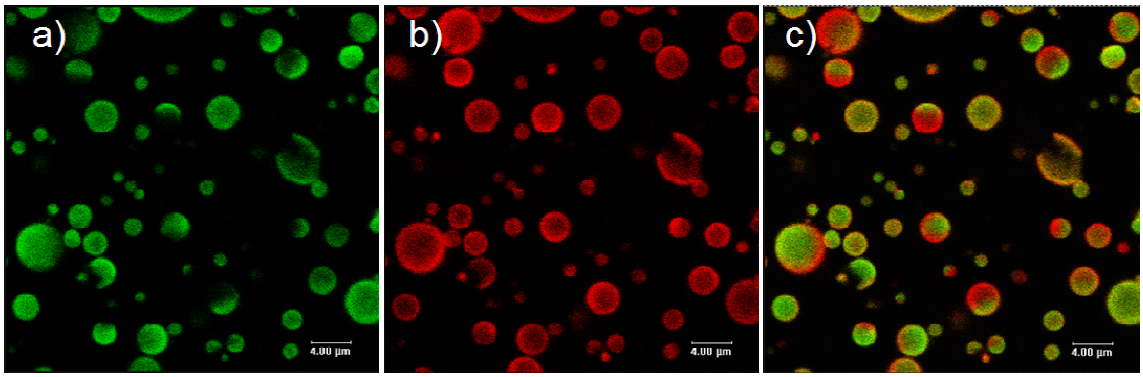

Figure 4.9 Confocal laser scanning microsopy of biphasic nanocollodis after the thermal imidization and two surface modification reactions (PEGylation and streptavidin conjugation). FITC- (a) and Rhodamine B- (b) conjugated dextrans were originally incorporated in each side of jetting solutions and observed in separate channels. Overlay of those two channel (c) confirmed the biphasic character of the nanocolloids. Scale bars are 4 microns.

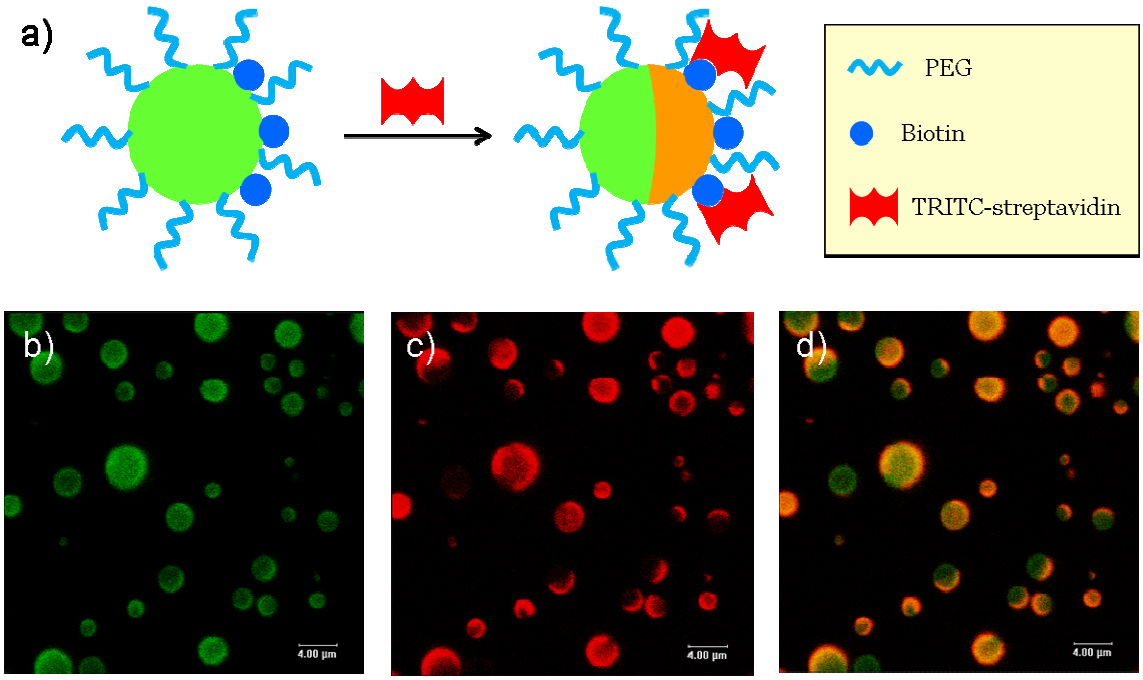

Figure 4.10 Selective modification of stpreatavidin onto hemisphere of the colloidal particles. a) Schematic description of the modification. Pegylated particles containing biotin moieties in one hemispherical surface were incubated with TRITC-streptavidin. Confocal laser scanning microsopy of the resulting biphasic nanocollodis showed FITC signals from the entire particle (b) but TRITC signal from selected areas of the particles (c). Overlay of those two channel (d) confirmed the selective modification by strepatavidin. Scale bars are 4 microns.

bind to the single side with the biotin moieties. The scheme of these modifications and the CLSM images of the resulting particles are shown in Figure 4.10. As expected, FITC signal came from the dextrans incorporated homogeneously in a given particle, while the TRITC signal was observed only in one hemisphere of the particle to which the streptavidin was selectively bound.

In order to realize the specific association of the particles to the HUVEC membrane, biotinylated antibody against membrane molecule PECAM-1 (CD31) was utilized. PECAM-1/CD31 is expressed in endothelial cell membrane and regulates binding of endothelial cells (ECs) to other ECs and to leukocytes.(*92*) Experimental

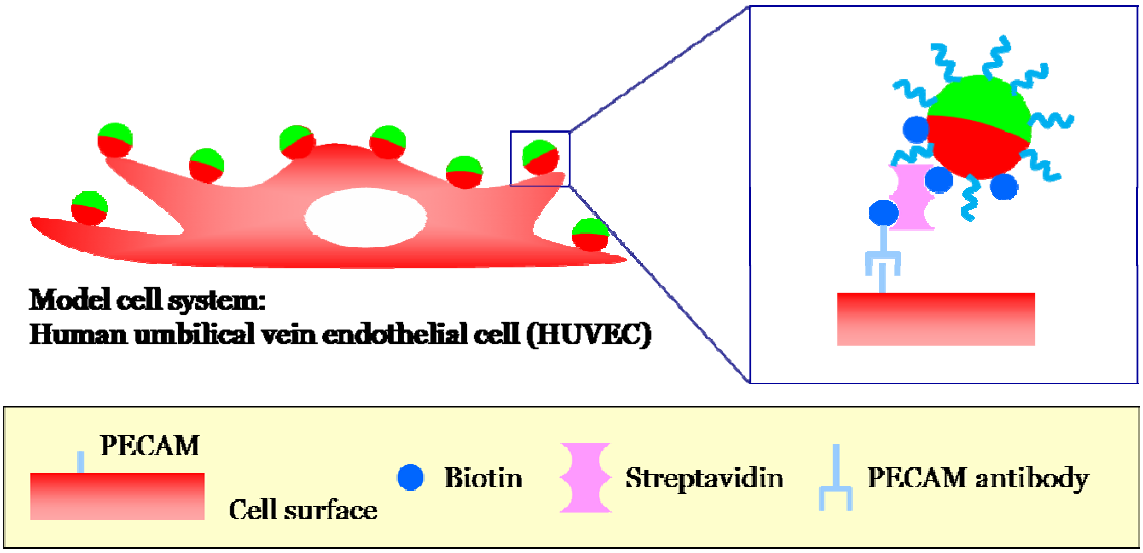

Scheme 4.3 Direction-specific labeleing of cell membrane by use of biphasic nanocollodis. Antibody molecules for PECAM (platelet/endothelial cell adhesion molecule) expressed in model HUVECs (human umbilical vein endothelial cells) were employed for the conjugation between the particles and cell membrane.

design of direction-specific association of the biphasic particles to HUVECs via biotinylated PECAM antibody is shown in Scheme 4.3.

Before the particles were incubated with the HUVECs, the expression of the PECAM on the cell membrane was confirmed by flow cytometry. As shown in Figure 4.11, the HUVECs that were incubated with FITC-conjugated PECAM antibody showed

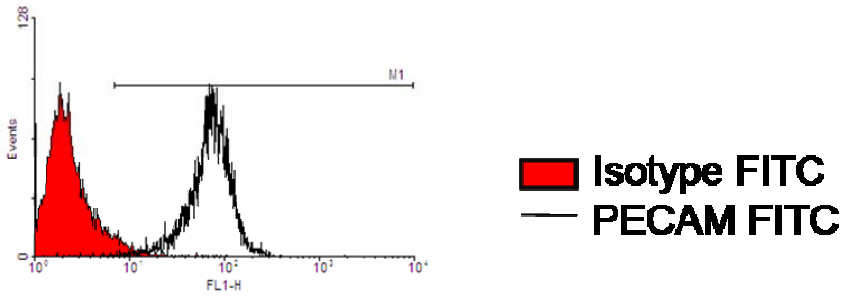

Figure 4.11 Expression of PECAM on HUVEC membrane tested by flow cytometry. HUVECs stained with FITC-conjugated PECAM antibody presented higher FITC fluorescence than HUVECs treated with FITC-conjuaged isotype control anibody (negative control group).

higher FITC fluorescence compared to that of of the HUVECs treated with FITC-conjugated isotype control antibody.

To investigate the effect of particle association to HUVECs by flow cytometry, the possible cell uptake of the particles was precluded by incubating HUVECs with the

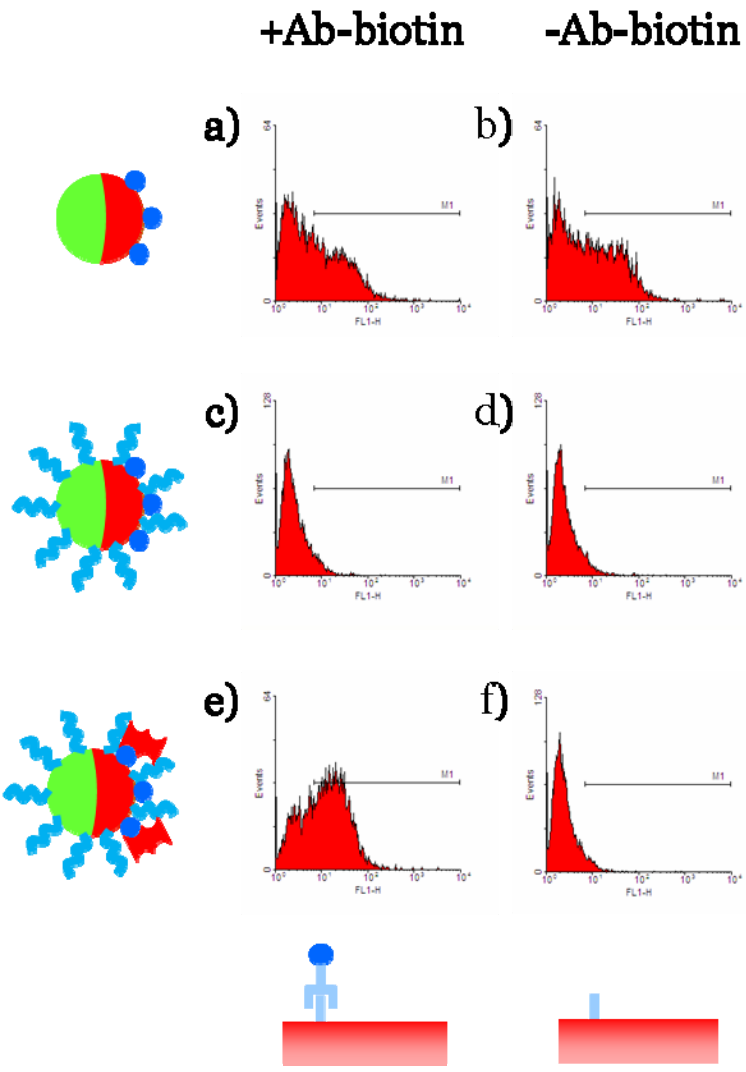

Figure 4.12 Flow cytometry data of HUVEC suspensions after incubations with biphasic particles with different surface characteristics: non-modified (a, b), pegylated without streptavidin (c, d), pegylated with streptavidin in one hemisphere. Three groups of particles were examined in the presence of PECAM antibody(a, c, e) or isotype-antibody (b, d, f) molecules.

particles at lower temperature of 4 ^{o}C. At this low temperature, the cells are still alive but with limited activities, so the active endocytosis is suppressed. Figure 4.12 shows a typical example of flow cytometry results showing number of events (cell count) versus FITC signals, for six different experimental groups. First, the non-specific adsorption of the non-modified biphasic particles to cells was observed, regardless of antibodies with which the cells were stained. However, when the surface of the particle was modified with PEG chains, the non-specific association of the particle was greatly suppressed. Again, the antibodies used to stain the cells had no effect on this minimization of non-specific binding. When the particles with the streptavidin molecules conjugated in single hemisphere were used, the particles bound to the cells only when they were stained with PECAM antibody but not with the isotype control antibody. This suggests specific interaction between the streptavidin on the particle surface and the biotin moieties on the cell membrane, resulting in labeling of the biphasic particles onto the HUVEC membrane. HUVECs treated with isotype antibody were not labeled and showed fluorescent profile comparable to that of PEGylated particles without the streptavidin moelecules.

Similar series of flow cytometry experiments were repeated three times and the results were statistically analysed and summarized in Figure 4.13. Two different values, % gated cell population and geometric mean fluorescent intensity were chosen to analyze the data. Regardless of the parameter evaluated, the trend indicated effective reduction of non-specific binding upon PEGylation and specific binding of streptavidin-modified particles to the cells only in the presence of biotinylated PECAM antibody.

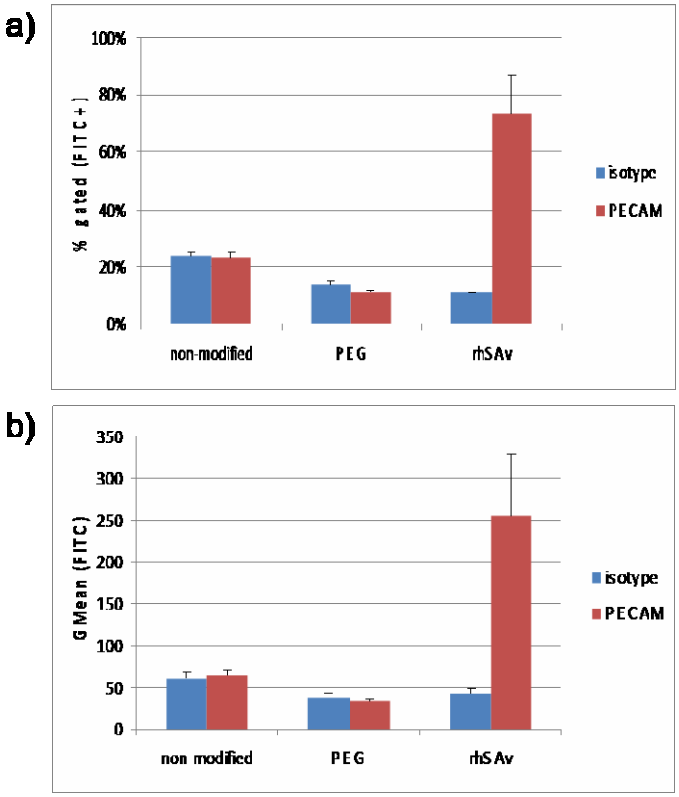

Figure 4.13 Flow cytometry results summarized for two different parameters: % gated cell population (a) and geometric mean value (b). For '% gated' values, marker was set for FITC histogram such that the 5% of population stained with isotype antibody was included, and the population inside of this marker was taken as the value. Geometric mean fluorescent intensity (gMFI) values were recorded both within and outside of M1 marker.

From this series of experiments, it is concluded that i) PEGylation of the particles was effective in suppressing the non-specific adsorption of the particles to HUVEC membrane, ii) biotin-PECAM antibody served as the targeting ligands on the HUVEC membrane, and iii) the particles with PEGylated layer and streptavidin molecules on the surface were associated with the cell membrane via specific interaction. As the streptavidin was exclusively present in one hemisphere of the particle, the results suggest that the specific association was direction-specific.

4.2.4 Conclusions

The novel concept of direction-specific cell membrane labeling was proposed and successfully demonstrated by development of anisotropic nanocolloids. Further modification of the biphasic nanocolloids composed of poly(acrylamide-*co*-acrylic acid) which was described in Chapter 3, was performed. To suppress the non-specific association, PEG layer was introduced by 'Click Chemistry'. Using HUVECs as a cellular model system, non-specific and specific associations were demonstrated by use of PECAM antibody. Flow cytometry results showed that the specific interaction between the biphasic particles and the HUVEC membrane, implying direction-specific labeling. Direct visualization of this direction-specific labeling was not performed in this study. In future work, these direct observation of direction-specific labeling may be designed in conjuction with inclusion of appropriate imaging contrast agents into the particles and use of characterization techniques with resolution of sub-micron scale.

References

1. A. G. Cuenca *et al.*, *Cancer* **107**, 459 (2006).
2. D. F. Emerich, C. G. Thanos, *Biomol Eng* **23**, 171 (2006).
3. K. K. Jain, *Trends Biotechnol* **24**, 143 (2006).
4. L. E. van Vlerken, M. M. Amiji, *Expert Opin Drug Deliv* **3**, 205 (2006).
5. M. V. Yezhelyev *et al.*, *Lancet Oncol* **7**, 657 (2006).
6. S. Warner, *The Scientist* **18**, 38 (2004).
7. A. S. Arbab *et al.*, *Radiology* **229**, 838 (2003).
8. A. K. Gupta, M. Gupta, *Biomaterials* **26**, 3995 (2005).
9. Q. A. Pankhurst, J. Connolly, D. K. Jones, J. Dobson, *J Phys D: Appl Phys* **36**, R167 (2003).
10. R. Handgretinger *et al.*, *Bone Marrow Transplant* **21**, 987 (1998).
11. R. Weissleder, H. C. Cheng, A. Bogdanova, A. Bogdanov, *J Magn Reson Imaging* **7**, 258 (1997).
12. U. Schoepf, E. M. Marecos, R. J. Melder, R. K. Jain, R. Weissleder, *BioTechniques* **24**, 648 (1998).
13. M. D. Chavanpatil, A. Khdair, J. Panyam, *J Nanosci Nanotechnol* **6**, 2651 (2006).
14. Y. Chen, G. Dalwadi, H. A. Benson, *Curr Drug Deliv* **1**, 361 (2004).
15. S. Kommareddy, S. B. Tiwari, M. M. Amiji, *Technol Cancer Res Treat* **4**, 615 (2005).
16. J. Kreuter, *Eur J Drug Metab Pharmacokinet* **19**, 253 (1994).
17. T. G. Cotter, M. Al-Rubeai, *Trends Biotechnol* **13**, 150 (1995).
18. P. Lutjens *et al.*, *Acta Haematol* **112**, 172 (2004).
19. N. Malikova, I. Pastoriza-Santos, M. Schierhorn, N. A. Kotov, L. M. Liz-Marzan, *Langmuir* **18**, 3694 (2002).
20. L. Manna, D. J. Milliron, A. Meisel, E. C. Scher, A. P. Alivisatos, *Nat Mater* **2**, 382 (2003).
21. Z. L. Zhang, S. C. Glotzer, *Nano Lett* **4**, 1407 (2004).
22. J. F. Hulvat, S. I. Stupp, *Adv Mater* **16**, 589 (2004).
23. T. Teranishi, Y. Inoue, M. Nakaya, Y. Oumi, T. Sano, *J Am Chem Soc* **126**, 9914 (2004).
24. Z. Bao *et al.*, *Chem Mater* **14**, 24 (2002).
25. V. N. Paunov, *Langmuir* **19**, 7970 (2003).
26. E. Hugonnot, A. Carles, M. H. Delville, P. Panizza, J. P. Delville, *Langmuir* **19**, 226 (Jan, 2003).
27. H. Takei, N. Shimizu, *Langmuir* **13**, 1865 (1997).
28. O. Cayre, V. N. Paunov, O. D. Velev, *Chem Commun* **18**, 2296 (2003).
29. L. Nagle, D. Fitzmaurice, *Advanced Materials* **15**, 933 (Jun, 2003).
30. Y. Yin, Y. Lu, Y. Xia, *J Am Chem Soc* **123**, 771 (2001).
31. M. Giersig, T. Ung, L. M. LizMarzan, P. Mulvaney, *Advanced Materials* **9**, 570 (Jun, 1997).

32. H. W. Gu, R. K. Zheng, X. X. Zhang, B. Xu, *Journal of the American Chemical Society* **126**, 5664 (May, 2004).
33. A. Pfau, R. Sander, S. Kirsch, *Langmuir* **18**, 2880 (2002).
34. S. Reculusa *et al.*, *Chem Mater* **14**, 2354 (2002).
35. H. Yu *et al.*, *Nano Letters* **5**, 379 (Feb, 2005).
36. K. H. Roh, D. C. Martin, J. Lahann, *Nature Materials* **4**, 759 (Oct, 2005).
37. J. M. Chapman *et al.*, *J Pharm Sci* **73**, 1482 (1984).
38. J. H. Maguire, K. H. Dudley, *Anal Chem* **49**, 292 (1977).
39. S. De, D. W. Miller, D. H. Robinson, *Pharm Res* **22**, 766 (2005).
40. W. G. Kreyling, M. Semmler-Behnke, W. Moeller, *J Aerosol Med* **19**, 74 (2006).
41. A. Magrez *et al.*, *Nano Lett* **6**, 1121 (2006).
42. L. Babes, B. Denizot, Y. Tanguy, J. J. Le Jeune, P. Jallet, *J Coll Int Sci* **212**, 474 (1999).
43. R. A. Rogers *et al.*, *Environ Health Perspect* **107**, 367 (1999).
44. V. M. Silva, N. Corson, A. Elder, G. Oberdorster, *Toxicol Sci* **85**, 983 (2005).
45. J. A. Champion, S. Mitragotri, *Proc Natl Acad Sci U S A* **103**, 4930 (2006).
46. T. K. De *et al.*, *J Microencapsul* **21**, 841 (2004).
47. T. K. De, A. S. Hoffman, *Artif Cells Blood Substit Immobil Biotechnol* **29**, 31 (2001).
48. M. Hornof, E. Toropainen, A. Urtti, *Eur J Pharm Biopharm* **60**, 207 (2005).
49. J. M. de la Fuente, C. C. Berry, M. O. Riehle, A. S. Curtis, *Langmuir* **22**, 3286 (2006).
50. L. C. Jones, M. Tucci, F. C, *Biomed Sci Instrum* **42**, 223 (2006).
51. C. C. Berry, S. Wells, S. Charles, A. S. Curtis, *Biomaterials* **24**, 4551 (2003).
52. A. K. Gupta, C. C. Berry, M. Gupta, A. S. Curtis, *IEEE T Nanobiosci* **2**, 255 (2003).
53. W. Zauner, N. A. Farrow, A. M. Haines, *J Cont Rel* **71**, 39 (2001).
54. E. Zarini *et al.*, *Plast Reconstr Surg* **114**, 934 (2004).
55. M. Hornof, W. Weyenberg, A. Ludwig, A. Bernkop-Schnurch, *J Cont Rel* **89**, 419 (2003).
56. R. Weissleder, U. Mahmood, *Radiology* **219**, 316 (May, 2001).
57. C. H. Contag, M. H. Bachmann, *Annual Review of Biomedical Engineering* **4**, 235 (2002).
58. M. Ferrari, *Nature Reviews Cancer* **5**, 161 (Mar, 2005).
59. I. Brigger, C. Dubernet, P. Couvreur, *Advanced Drug Delivery Reviews* **54**, 631 (Sep, 2002).
60. W. J. Parak *et al.*, *Nanotechnology* **14**, R15 (Jul, 2003).
61. B. N. G. Giepmans, S. R. Adams, M. H. Ellisman, R. Y. Tsien, *Science* **312**, 217 (Apr, 2006).
62. W. B. Cai, X. Y. Chen, *Small* **3**, 1840 (Nov, 2007).
63. M. Bruchez, M. Moronne, P. Gin, S. Weiss, A. P. Alivisatos, *Science* **281**, 2013 (Sep, 1998).
64. W. C. W. Chan, S. M. Nie, *Science* **281**, 2016 (Sep, 1998).
65. L. R. Hirsch *et al.*, *Annals of Biomedical Engineering* **34**, 15 (Jan, 2006).

66. V. P. Torchilin, *Nat Rev Drug Discov* **4**, 145 (2005).
67. V. Torchilin, M. I. Papisov, *J Liposome Res* **4**, 725 (1994).
68. R. Weissleder *et al.*, *Radiology* **175**, 489 (May, 1990).
69. D. D. Stark *et al.*, *Radiology* **168**, 297 (Aug, 1988).
70. A. K. Gupta, M. Gupta, *Biomaterials* **26**, 3995 (Jun, 2005).
71. V. P. Torchilin, *J Microencapsul* **15**, 1 (Jan-Feb, 1998).
72. M. J. Liu, J. M. J. Frechet, *Pharmaceutical Science & Technology Today* **2**, 393 (Oct, 1999).
73. S. S. Wong, E. Joselevich, A. T. Woolley, C. L. Cheung, C. M. Lieber, *Nature* **394**, 52 (Jul, 1998).
74. R. R. Meyer *et al.*, *Science* **289**, 1324 (Aug, 2000).
75. K. H. Roh, D. C. Martin, J. Lahann, *Journal of the American Chemical Society* **128**, 6796 (May, 2006).
76. K. H. Roh, M. Yoshida, J. Lahann, *Langmuir* (2007).
77. M. Yoshida, K. H. Roh, J. Lahann, *Biomaterials* **28**, 2446 (May, 2007).
78. P. Harder, M. Grunze, R. Dahint, G. M. Whitesides, P. E. Laibinis, *Journal of Physical Chemistry B* **102**, 426 (Jan, 1998).
79. H.-W. Jun, J. L. West, *Journal of Biomedical Materials Research, Part B: Applied Biomaterials* **72B**, 131 (2005).
80. F. Zhang, E. T. Kang, K. G. Neoh, P. Wang, K. L. Tan, *Section Title: Pharmaceuticals* **22**, 1541 (2001).
81. P. Kingshott, H. J. Griesser, *Section Title: Surface Chemistry and Colloids* **4**, 403 (1999).
82. B. Shi, C. Fang, Y. Pei, *J Pharm Sci* **95**, 1873 (2006).
83. W. Feng, S. Zhu, K. Ishihara, J. L. Brash, *Biointerphases* **1**, 50 (2006).
84. F. Hu, K. G. Neoh, L. Cen, E.-T. Kang, *Biomacromolecules* **7**, 809 (2006).
85. M. Q. Zhang, T. Desai, M. Ferrari, *Biomaterials* **19**, 953 (May, 1998).
86. J. K. Gbadamosi, A. C. Hunter, S. M. Moghimi, *FEBS Lett* **532**, 338 (2002).
87. P. Calvo *et al.*, *Pharmaceutical Research* **18**, 1157 (2001).
88. J. A. O'Shaughnessy, *Clin Breast Cancer* **4**, 318 (Dec, 2003).
89. R. Gref *et al.*, *Colloids Surf B Biointerfaces* **18**, 301 (Oct 1, 2000).
90. S. Stolnik *et al.*, *Pharm Res* **11**, 1800 (Dec, 1994).
91. D. A. Ossipov, J. Hilborn, *Macromolecules* **39**, 1709 (Mar, 2006).
92. F. R. Pu, R. L. Williams, T. K. Markkula, J. A. Hunt, *Biomaterials* **23**, 2411 (2002).

CHAPTER 5

ANISOTROPIC ENCAPSULATION OF SUPERPARAMAGNETIC NANOCRYSTALS IN POLYMERIC BIPHASIC NANOCOLLOIDS

5.1 Introduction

As introduced in Chapter 1, Janus-type microspheres have been designed and synthesized as potential building blocks whose dipole alignment are controllable by external force field. Electric dipolar character was introduced to bichromal microspheres by spinning disk techology and flow focusing method.(*1*) These biphasic microspheres were trapped in oil-filled cavities of thin-layered elastomer on top of the transparent electrodes, and their alignment was successfully controlled by electric field generated by the electrodes, which shows the potentials in novel display device or electronic paper.

Very different approach was pursued by Anker *et al.* for the control of biphasic microsphere alignment, leveraging magnetic dipoles.(*2*) They deposited metal layer on the hemisphere of polystyrene microspheres 4.4 μm in diameter containing ferromagnetic materials. Magnetization was made so that the metal coated side is the microspheres south pole. The alignment control over the biphasic geometry was demonstrated for the potential use of those microspheres as optical probes.

Unique physical and chemical properties of nanocrystals including semiconducting quantum dots, metal nanoparticles, and magnetic nanoparticles have been attracting an increasing interest with researchers. The polymer-nanocrystals

composite structure has a great potential for many practical applications, such as photonic and electronic devices, storage devices, and biomedical materials. Electrified jetting has been widely used to create nanofibers of polymer-nanoparticle composites,(*3*) especially magnetic nanofibers which have been produced by the incorporation of iron oxide nanoparticles.(*4, 5*) In these previous composite structures, the nanocrystals are randomly or homogeneously encapsulated.

In the previous chapters, it has been shown that anisotropic material distribution in nano-objects can be achieved by electrified co-jetting of multiple jetting solutions in side-by-side geometry.(*6, 7*) In this chapter, the electrified co-jetting process is also applied to fabricate anisotropic polymer-nanocrystal composite geometry. With an intention to induce directional functionality, superparamagnetic iron oxide nanocrystals were encapsulated selectively in one hemisphere of a polymeric nanocolloid by use of side-by-side electrified co-jetting. Magnetite (Fe_3O_4) nanocrystals (NCs) with diameters of 5 to 20 nm were synthesized by co-precipitation of ferrous and ferric ions. For the side-by-side dual jetting geometry, the nanocrystal suspension mixed with a polymer solution was used as a jetting solution for one side in parallel with a corresponding polymer only solution in the other side simultaneously.

For the successful electrified co-jetting, the magnetite nanocrystals must be well suspended in the jetting solution. The stabilization of the nanoparticle suspension should be achieved by use of appropriate stabilizer for different polymer solutions. Four different polymers, poly(acrylamide-*co*-acrylic acid) (PAAm-*co*-AA), polyacrylic acid (PAA), polyethylene glycol (PEG), and poly(lactic-*co*-glycolic acid) (PLGA), and three different stabilizing mechanism for the magnetite nanocrystal suspensions were employed. The resulting particles generated by co-jettings of each solution pairs were characterized by transmission electron microscopy.

Among the pairs of polymer solutions and magnetite nanocrystal suspensions, aqueous solutions of poly(acrylamide-*co*-acrylic acid) and polyacrylic acid-stabilized magnetites was selected for the futher characterization. These magnetic nanocolloids with unique anisotropy can be useful for novel display device, magnetically controlled biomedical imaging or targeted drug delivery.

5.2 Methods

Materials

Ferric chloride hexahydrate ($FeCl_3$·6H2O), ferrous chloride tetrahydrate ($FeCl_2$·$4H_2O$), poly(acrylic acid) (PAA, MW 250k), Poly(lactic-*co*-glycolic acid) (PLGA, MW 50k-75k, lactic acid: glycolic acid = 85:15), Polyethylene oxide (PEO, MW 600k and 10k), FITC-dextran (MW 70k) and rhodamine B-dextran (MW 70k) were purchased from Sigma-Aldrich, Inc. USA. Poly(acrylamide-co-acrylic acid) (PAAm-co-AA, MW 200k, 10% acrylic acid residues) was purchased from Polysciences, Inc. USA. 2-methoxy(polyethyleneoxypropyl)trimethoxysilane (MW 460-590) was purchased from Gelest Inc. USA. All reagents were used without further purification.

Synthesis of Magnetite NCs stabilized by oleic acid(*8, 9*)

1.08 g of ferric chloride hexahydrate ($FeCl_3·6H_2O$) and 0.398 g of ferrous chloride tetrahydrate ($FeCl_2·4H_2O$) were dissolved in 20 ml of distilled water. In a separate flask, 0.5 ml of oleic acid was mixed into the 200 ml of 0.5 M NaOH solutions in distilled water. The iron solution was added slowly into the alkali solution while the

mixture solution is vigorously stirred under Argon gas purging. The temperature of the reaction vessel was kept at 95 ^{o}C with reflux for one hour. The nanoparticles modified with oleic acid precipitated after the reaction. The powders were washed with fresh distilled water and acetone for three times each. For the TEM experiment, the nanoparticles were dispersed in chloroform by sonication for one minute. 50 μ l of the suspension droplet was put on top of carbon-film-coated copper grid and dried.

Synthesis of Magnetite NCs stabilized by PEG(*10*)

Bare magnetite nanocrystals were synthesized by conventional co-precipitation method first before the surface was treated with PEG. In brief, 4 g of NaOH was dissolved in 200 ml of ddH_2O (0.5M) in a reaction flask. A mixture solution of 0.1M of ferrous and 0.2M ferric ions was prepared separately by dissolving 1.08 g of $FeCl_3$·6H2O and 0.398 g of $FeCl_2$·4H_2O into 20 ml of ddH_2O. When the orange colored iron ion solution was added into the alkali solutions under vigorous stirring, black precipitates formed immediately. All the solution preparations and the co-precipitation reaction were performed under Argon gas purging in order to prevent potential oxidation. After the reaction was kept for 1 hour at room temperature, the nanoparticles were decanted by use of permanent magnet and the supernatant was discarded and changed with fresh ddH_2O. This washing step was performed 3 times.

About 1 g of synthesized nanocrystal washed by ddH_2O multiple times was finally suspended in 10 ml of ethanol. After 50 ml of toluene was added, the total suspension was condensed by rotary evaporator in order to get rid of trace of ethanol and water. After 50 ml of extra toluene was added onto the suspension, 1 ml of 2-[methoxy(polyethyleneoxy)propyl]trimethoxysilane (MW 460-590 g/mol) was added. The mixture suspension was stirred at 80^{o}C for 2 hours. After sonication for 5 minutes,

the modified nanocrystals were washed with fresh toluene 2 times. The centrifuged nanoparticles were kept in ethanol.

Synthesis of Magnetite NCs stabilized by PAA

Magnetite nanocrystals were synthesized by a modified method of two previous reports.(*8, 11*) First, mixed aqueous solutions of ferrous chloride (0.1M), ferric chloride (0.2M) and PAA (1%, w/v) were prepared by stirring while purging with Ar gas. After 30 minutes of stirring, the pH of the solution was increased to above 10 by adding 0.1 M NaOH solution. The solution was aged for an hour subsequently, while being kept under inert conditions. Then the NC suspension was washed with fresh distilled water three times after magnetic decantation and centrifugation, before it was mixed with additional polymers for the electrified jetting.

Preparation of Jetting Solution

After Synthesis, NC suspensions were washed with fresh solvents and re-suspended before they were mixed with the polymers. As the completely dried NCs were not successfully re-suspended, the centrifuged NCs were diluted with appropriate volume of solvents to control their final concentrations to be in the range of 0.2~0.5 % (w/v).

PLGA was dissolved in mixture solvents of chloroform and DMF with or without the OA-stabilized magnetite NCs. Two different pairs of jetting solutions were prepared. For the first pair, 5% (w/v) of PLGA was dissolved in a mixture solvent (chloroform : DMF = 95 : 5 by v/v). For the second, 2.5% (w/v) of PLGA was dissolved in a mixture of chloroform and DMF (85:15).

For PEO-based solutions, polymers with two different molecular weights were dissolved in water with or without the PEG-stabilized magnetite NCs. For the higher

molecular weight PEG (MW 600kD), 3 % (w/v) solution was prepared and mixed with magnetite NCs. Even though the suspension was far more stable than the case with the bare magnetites, NC aggregates tend to form and precipitate during the jetting process. When the same PEG-stabilized magnetites were suspended in 5% (w/v) solution of shorter PEG (MW 10kD), the suspension didn't show any precipitation formation even after storage for days. After the re-suspension of NCs, 0.5% (w/v) of long chain PEG (MW 600kD) was added to achieve stable jetting behavior. The pair solutions without the magnetite NCs were also prepared with same concentrations of polymers.

Similarly, PAAm-co-AA or PAA was directly added into the PAA-stabilized nanocrystal suspensions with the final concentrations of 5% (w/v) and 10% (w/v) respectively, and dissolved by continuous stirring and a subsequent sonication step. An aqueous solution of each polymer of the same concentration without the nanocrystals was also prepared and used for the other side of the jetting solution. For the CLSM analysis, 0.5% (w/v) of rhodamine B-dextran and 0.5% (w/v) of FITC-dextran were added to the jetting solutions with and without the nanocrystals, respectively.

Side-by-Side Electrified Co-Jetting

We followed the same method of our previous reports on the electrified co-jetting.(*3*, *4*) Two syringes loaded with a specific jetting solution were set up side-by-side and the flow rate was controlled by a single syringe pump. A dual channel tip ((FibriJet® SA-0105, Micromedics, Inc., MN, USA) was connected to the two syringes. Positive voltage was applied with a high potential generator (ES30P, Gamma High Voltage Research, Inc., USA) between the dual capillaries and a piece of aluminum foil (about 10 square inches) as a collecting substrate.

Characterization

JEOL 2010F was operated at the accelerating voltage of 200 kV for transmission electron microscopy. The nanocolloids were directly jetted on top of a carbon-coated copper grid (Ted Pella, Inc. USA). SP2 CLSM (Leica, USA) was used for confocal microscopy. Ar/ArKr laser at 488 nm and GreNe laser at 543 nm were used to excite FITC and rhodamine B, respectively. The characteristic emission signals for the dyes were collected in separate wavelength windows. Thermogravimetric analysis (TGA) was performed by a Perkin-Elmer Pyris 1 TGA. Scanning rate was 10 ^{o}C/min. Air and N_2 gas were purged during the analysis of PAA-based and PAAm-*co*-AA-based particles, respectively.

5.3 Results and Discussion

As discussed above, the final aims of the research in this chapter are two folds. The first is to demonstrate that material distribution control by electrified co-jetting can be applied for the anisotropic encapsulation of functional nanoparticles. The second is to create a functional anisotropic building block whose orientation can be controlled by external force. In order to achieve these goals simultaneously, design of the building block is required to select the appropriate properties of nanoparticles to be encapsulated among many.

In order to use magnetic field as the controlling force field, superparamagnetic nanocrystal was selected as the appropriate candidate for the anisotropic encapsulation (Scheme 5.1). The superparamagnetic properties originate from the small size of the

crystal. The whole particle behaves as a single crystal domain, and the size is small enough that the magnetization direction fluctuates randomly due to the comparable thermal energy (kT) at room temperature. When a magnetic field is applied to the collection of superparamagnetic particle, all the particles' magnetic moments align along the external field. However that magnetization of the particle vanishes and become randomized when the external field is taken away. If these superparamagnetic nanocrystals are encapsulated in one hemisphere of a bigger nanocolloidal particle, the nanocrystals will be magnetized along the external field regardless of the particle's initial orientation. When an appropriate field gradient is applied, each nanocrystal will be pulled close to the highest field with a certain force, and the biphasic building block will reach to the minimum magnetic potential energy state when all the nanocrystals are

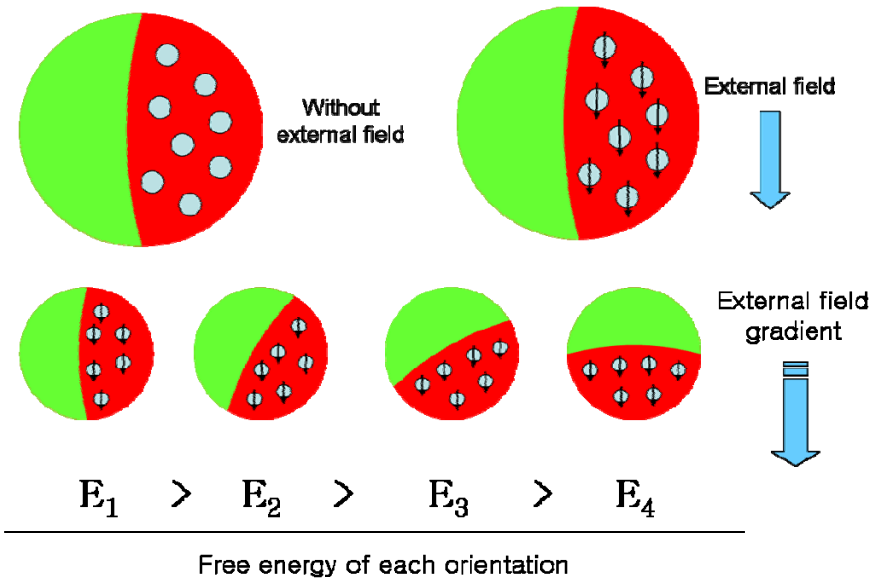

Scheme 5.1 Design of biphasic nanocolloids containing superparamagnetic nanocrystals in an anisotropic manner. The magnetite nanocrystal becomes magnetized along the direction of external magnetic field regardless of the original orientation of the biphasic particle. In the presence of magnetic field gradient, the orientation of the particle will rotate until the pole containing magnetites face to the direction of highest magnetic field density.

positioned at their most possible proximity to the highest field, i.e. when the hemisphere containing magnetic nanocrystals position toward the highest field point.

Magnetite (Fe_3O_4) is one of the phases of iron oxide which has a cubic inverse spinel structure with O^{2-} ions forming fcc closed packing, Fe^{2+} ions positioning in octahedral sites, and Fe^{3+} ions occupying half in octahedral and half in tetrahedral sites.(*12*) Its great magnetic properties have been used for many applications including magnetic recording media,(*13*) biomedical imaging,(*14, 15*) drug delivery,(*16, 17*) bioseperation,(*18, 19*) and ferrofluid.(*20*) And it's been reported that the magnetite nanocrystals have superparamagnetic properties when their diameter is smaller than 20 nm.(*8, 11, 21, 22*)

In addition to the appropriate magnetic properties of the NCs, the characteristics of their suspension are critical for the application of the suspension as the jetting solution. First requirement of the suspension is the stability. If the NCs are not stabilized by a

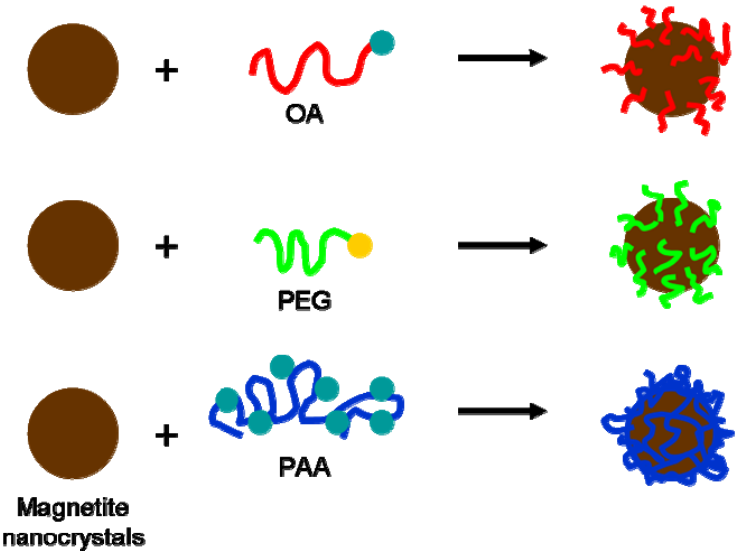

Scheme 5.2 Magnetite nanocrystals (NCs) synthesized and used for the electrified co-jetting. Polyacrylic acid (PAA) and oleic acid (OA) are stabilizing the surface of the NCs by electrostatic interaction, whereas polyethylene glycol (PEG) was bound to the surface of NCs with covalent bonding (silanization).

certain mechanism, they tend to form aggregates and precipitate due to their increased surface-surface interactions, which will be detrimental for the homogeneous encapsulation of the NCs in the final objects and for the stable electrified jetting for long time periods (~hours). Feasibility of the electrified jettings of magnetite NC suspensions was tested for three different stabilizing agents (Scheme 5.2). First, the magnetite nanocrystals that were synthesized in the presence of oleic acid was intended to be mixed in more hydrophobic organic solvents. And bare magnetite particles were synthesized and post-modified with short (MW 460-590 g/mol) PEG chains by silanization for the suspensions in aqeous solutions of longer PEG chains (MW 600 kD and 10 kD). Lastly, the magnetite was synthesized in the presence of polyacrylic acid. These PAA-stabilized nanocrystals could be suspended in aqeous solutions of polyacrylic acid and/or poly(acrylamide-co-acrylic acid).

Figure 5.1 shows the TEM images of synthesized magnetite NCs coated with different stabilizing agents. First, the magnetite stabilized with oleic acid (a and b) showed average diameter of 7.0 nm and standard deviation of 1.8 nm, which is the medium size and the smallest size distribution among the magnetites with different

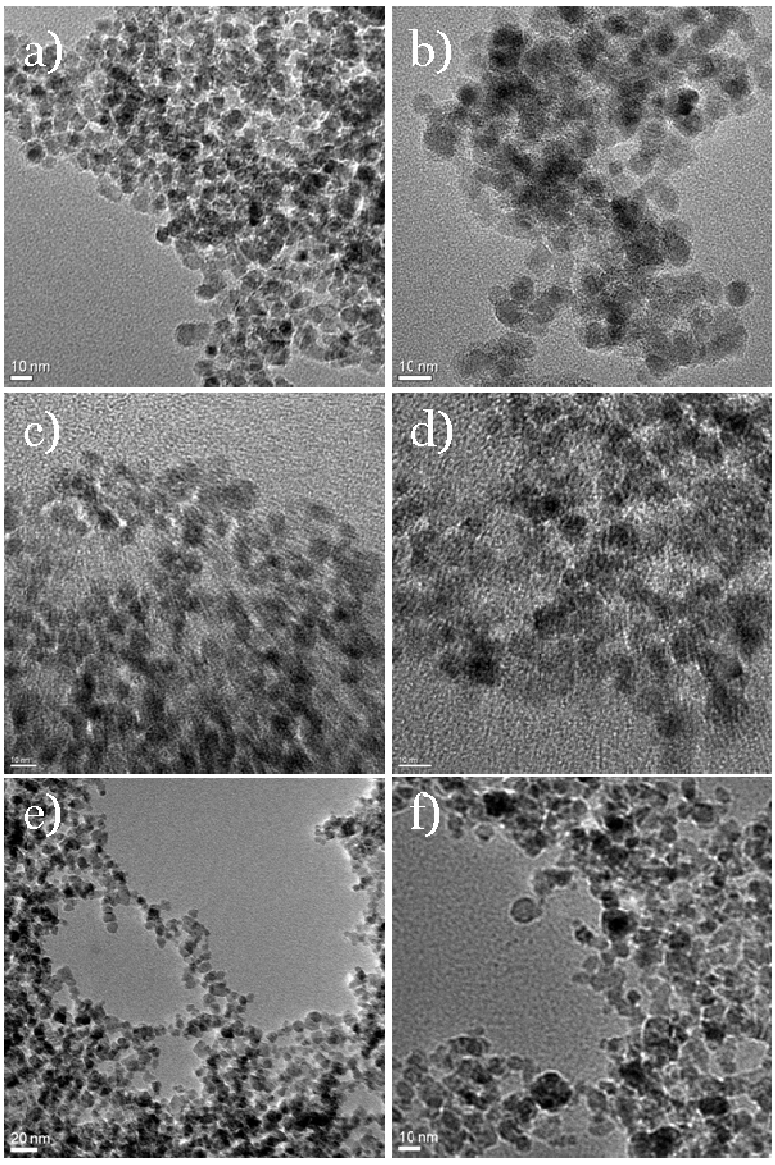

Figure 5.1 Transmission electron (TEM) micrographs of magnetite nanocrystals (NCs) synthesized and stabilized by oleic acid (a, b), polyethylene glycol (c, d), and polyacrylic acid (e, f). Scale bars: (a-d, f) 10 nm, (e) 20 nm.

stabilization layer. PEG-stabilized nanocrystals (c and d) were the biggest in size (average diameter of 11.8 nm with std of 2.4 nm), which is probably due to the fact that these nanocrystals were synthesized in the absence of stabilizing agent and stabilized by post-modification. Lastly, the magnetite synthesized in presence of poly-acrylic acid (e and f) showed averge diameter of 6.6 nm with standard deviation of 2.5 nm. It has been reported that the size of the magnetite nanocrystals can be controlled by changing the concentrations of the stabilizing polyelectrolytes used for the synthesis.(*11*) However, it is difficult to infer what incurred the differences between each magnetite NCs described above without further systematic investigation, because size and size distribution of these NCs could be dependent on many synthesis parameters such as ionic strength, temperature, precipitation speed in addition to the stabilizing agents. Nevertheless, it was found that the size of the synthesized nanocrystals are small enough to be superparamagnetic regardless of the utilized stabilizing agents.

No stable magnetite suspensions could be prepared with the bare magnetite NCs

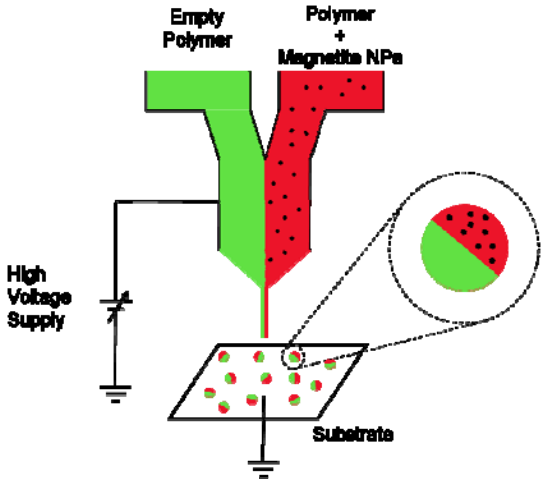

Scheme 5.3 Electified co-jetting of polymer only solution and poymer solution containing magnetite nanocrystals. If the anisotropy introduced by jetting capillaries is maintained, the resulting nanocolloids contain nanocrystals in an anisotropic manner.

in any of the polymer solutions tested. Without the stabilizaiton, the bare magnetite NCs formed big aggregates and precipitated within minutes even after vigorous sonication. However the selected stabilizing layers for each polymer solutions were very effective, so every solution prepared for the jetting didn't show any precipitation of NCs over many hours of electrified jetting.

Scheme 5.3 shows the experimental setup of the electrified co-jetting process with magnetite nanocrystal suspension as a jetting liquid. When high electrical voltage was applied to the pendant droplet, a thin liquid jet was ejected from the interface between the two jetting solutions. If the anisotropic distribution of the nanocrystals is preserved until the jet is disintegrated with simultaneous drying, the resulting nanocolloids would also possess nanocrystals selectively in one hemisphere as shown in the resulting nanocolloids in the scheme.

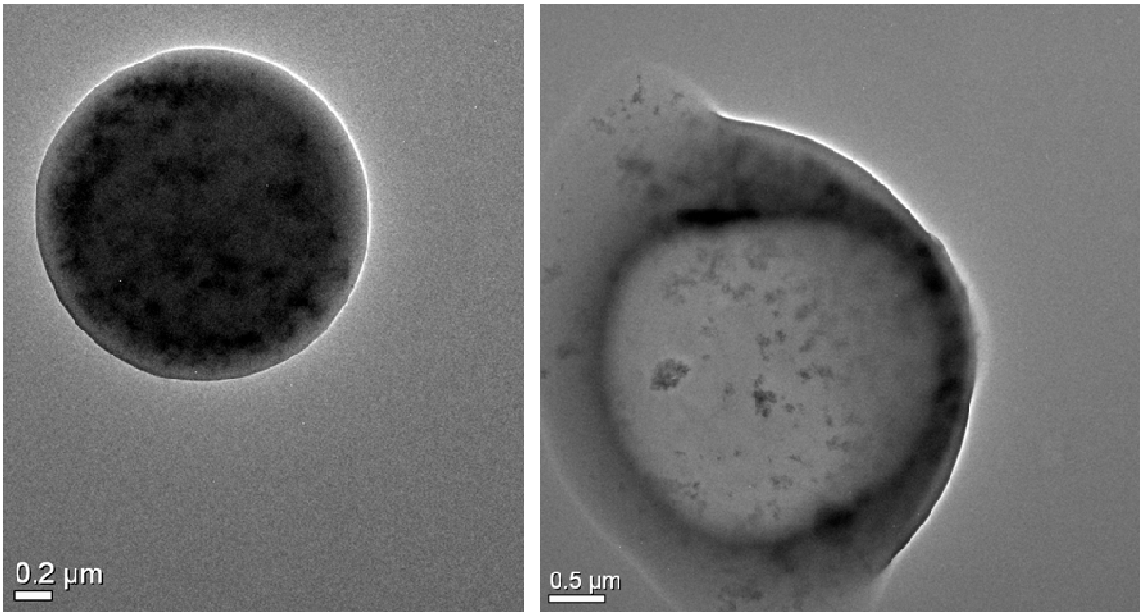

Figure 5.2 Transmission electron (TEM) micrographs of the biphasic nanocolloids based on poly(lactide-*co*-glycolide) containing magnetite nanocrystals that are stabilized with oleic acid. Polymer concentration in mixed solvent of chloroform and DMF was 5% (w/v).

Figure 5.2 and Figure 5.3 show the typical TEM images of the nanocolloids made from the co-jetting of OA-stabilized magnetite NCs mixed in PLGA solutions. When 5.0 % (w/v) polymer solutions were used (Figure 5.2), the resulting polymeric particles were relatively big (a few microns in diameter). Even though the magnetite encapsulation seems to be homogeneous, the anisotropy of encapsulation was scarecely observed, which might be due to the reduced conductivity and viscosity of the solutions compared to the case of aqeous solutions. The recirculating meridional motion(*23*) and spontaneous swirl motion(*24*) of the liquid have been reported to occur in the cone of cone-jet mode, especially, the conductivity and the viscosity of the jetting solution are low.

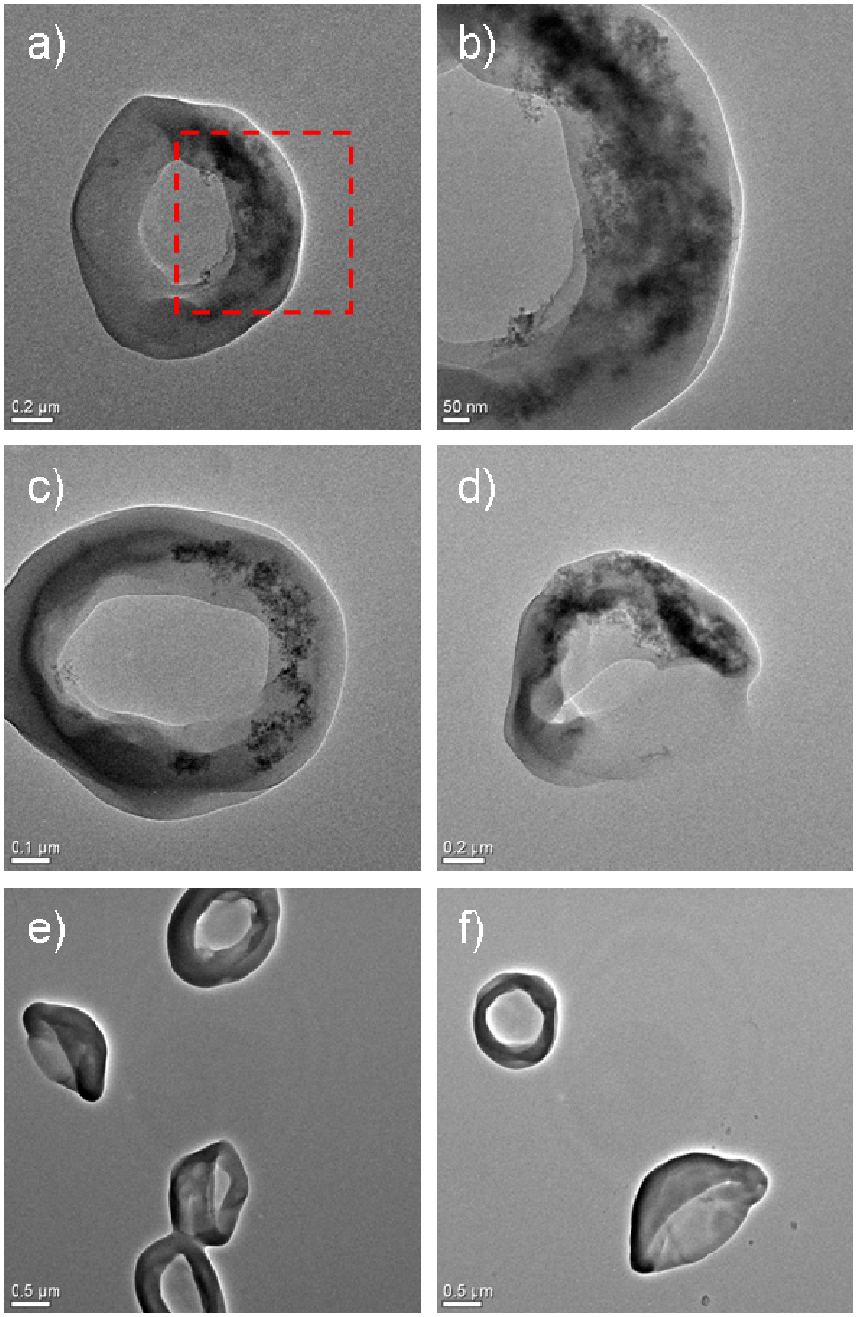

Figure 5.3 Transmission electron (TEM) micrographs of the biphasic nanocolloids based on poly(lactide-*co*-glycolide) containing magnetite nanocrystals that are stabilized with oleic acid. Polymer concentration in mixed solvent of chloroform and DMF was 2.5% (w/v). Clear anisotropic encapsulation was observed in a small number of doughnut-like particles (a-d), whereas most of the other particles are empty (e, f). Scale bars: 200 nm (a, d), 50 nm (b), 100 nm (c), 500 nm (e, f).

When the polymer concentration was further diluted to 2.5 %, differences were observed both in terms of size and shape of the polymeric particles. As shown in Figure 5.3, the major population of the resulting particles show doughnut-like morphology rather than spherical shape, with reduced diameters (less than one micron in diameter). In a small number of particles, clearly anisotropic encapsulation was observed (Figure 5.3a-d). In these particles, almost exact one half of the doughnut-like shape is filled with quite dense magnetite NCs whereas the other half is empty. Figure 5.3b is enlarged image of the magnetite NCs-containing side of the particle which is marked as dotted square in Figure 5.3a. The magnetite NCs seem to be aggregated at a certain degree, which might be the reason why the magnetite NCs are so dense in these particles. However the major population of the particles turned out to be totally empty (Figure 5.3e-f). So it is highly probable that lower concentration of PLGA polymers made the NC suspension less stable and the slight aggregate formation prohibited the homogeneous encapsulation of the NCs and rather rendered concentrataed encapsulation in small number of particles.

The PEGylated magnetite NCs were suspended in aqueous solutions of PEOs of two different molecular weights, and used in the electrified co-jettings. Regardless of the molecular weight of used polymers (PEOs), the peglated NCs could be stabilized far better than the bare magnetites in the same solution. When the NCs were mixed in 3 % aqueous solution of relatively high molecular weight PEO (MW 600kD), aggregation of NCs were observed after 3 hours of storage at room temperature. When the above suspension was electrified co-jetted with empty 3% PEG solution, a quite stable biphasic jetting was achieved. (0.08 ml/hr, 5 kV, 30 cm). The clear interfaces between the phases lasted several seconds after the jet comes out of the cone.

The TEM micrographs of the resulting particles showed anisotropic encapsulation of dense magnetite aggregates in a small number of particles (Figure 5.4a-b), whereas the

major portion of the particles are empty. When the same magnetites are suspended in 5 % aqueous solution of smaller molecular weight PEO (MW 10kD), the suspension didn't form aggreages and didn't precipitate over an observed period of 24 hours. The particles

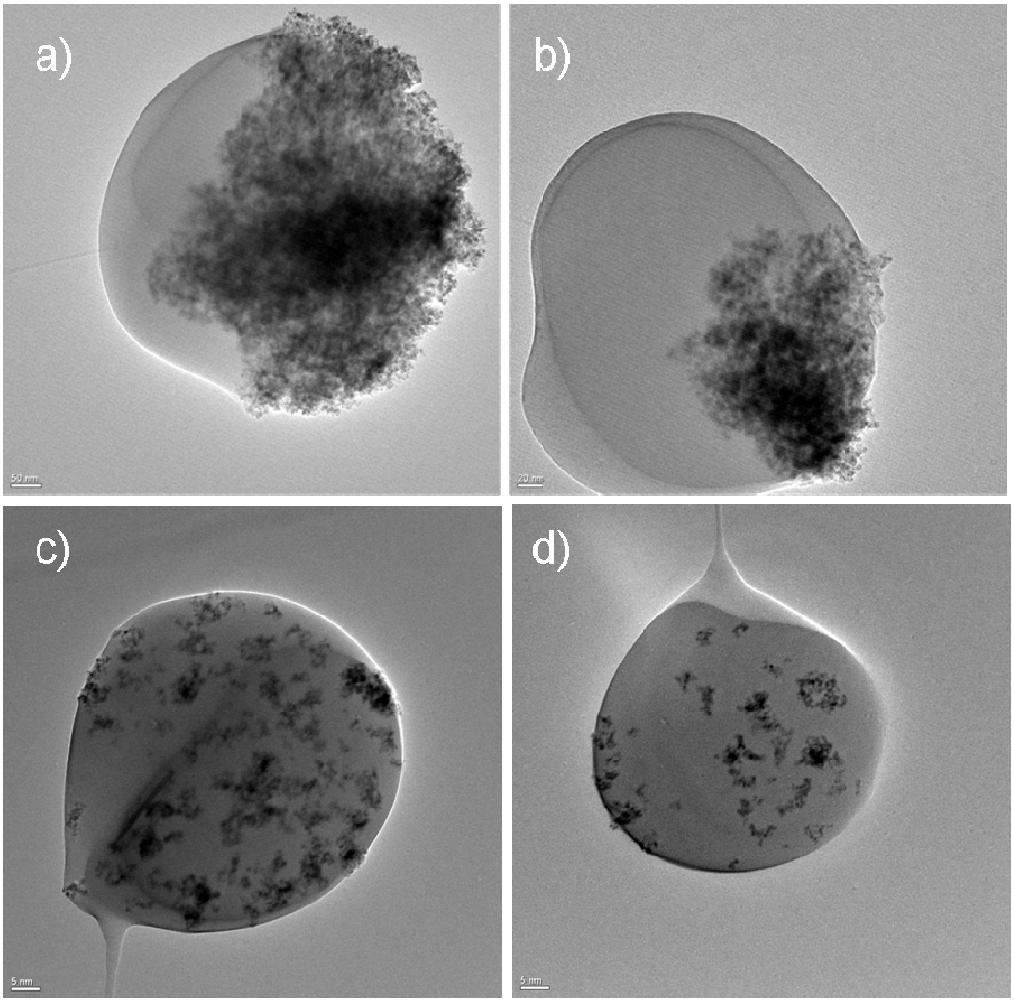

Figure 5.4 Transmission electron (TEM) micrographs of the biphasic nanocolloids based on polyethylene oxide (PEO) containing magnetite nanocrystals that are stabilized with polyethylene glycol. When the magnetite NCs were suspended in longer PEO (MW 600 kD) solutions, anisotropic encapsulation was observed in a small number of particles with big aggregates of magnetites, whereas the most of the other particles are empty (a, b). When the NCs were suspended in shorter PEO (MW 10 kD) solutions, the resulting particles become smaller and the magnetites were better dispersed in most of the polymeric particles. However the anisotropy was hardly observed (c, d).

produced from the co-jetting of this more stable magnetite suspension and the empty polymer solution yielded far more homogeneous encapsulation of the NCs in polymer particles. However, the anisotropic encapsulation was hardly observed, which again might be owing to the fact that smaller molecular weight polymer solutions possess reduced viscosities (Figure 5.4c-d).

Lastly, the magnetite NCs stabilized with PAA was suspended in 5.0 % (w/v) of PAAm-*co*-AA solution in water and used for the electrified co-jetting with empty solution of 5.0 % PAAM-*co*-AA solution in the other side. Figure 5.5 shows typical examples of TEM images of the resulting nanocolloids. As intended, the nanocrystals are encapsulated not randomly or homogeneously. In many polymeric particles with diameters of several hundred nanometers, NCs were observed. Even though the TEM image is 2-dimensional transmission of the objects, anisotropic encapsulation of the NCs were observed in mojor portion of the populations. This was true for both nanocolloids

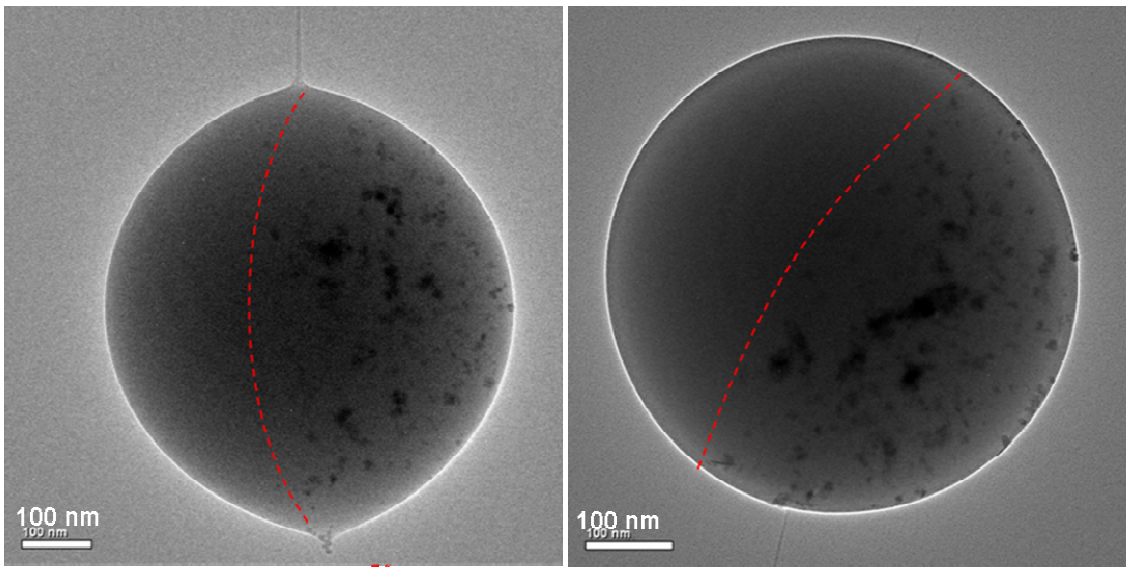

Figure 5.5 Transmission electron (TEM) micrographs of the biphasic nanocolloids based on poly(acrylamide-*co*-acrylic acid) containing magnetite nanocrystals that are stabilized with polyacyrlic acid. The encapsulation is clearly anisotropic as indicated by red dotted line. Scale bars are 100 nm.

made of PAAm-*co*-AA and PAA. However, it is worthy to note not every particle in TEM images showed this anisotropic geometry, and the volume fraction of empty phase in a particular particle was not always identical to those of others. This might be attributed either to the 2-dimensional character of TEM images or to the imperfect co-jetting behavior.

These nanocolloids would be very useful if dyes or drugs could also be also loaded in biphasic manner. In order to test this, dextran molecules conjugated with two fluorescent dyes were incorporated in each side of jetting solutions. The resulting nanocolloids were suspended in immersion oil (Leica, USA) and examined by confocal microscopy (Figure 5.6). The overlay image of emission signals from the two dyes

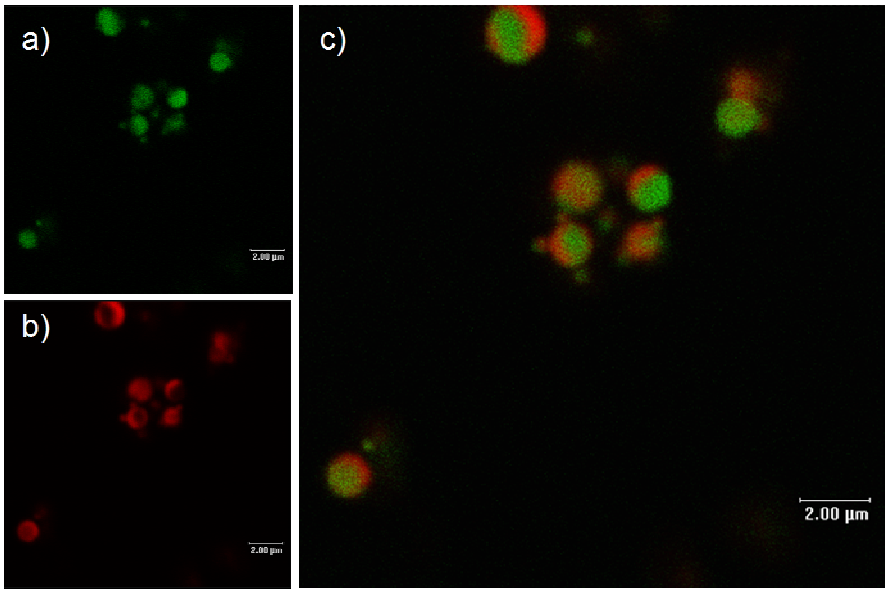

Figure 5.6 Confocal laser scanning micrographs of the biphasic nanocolloids based on polyacrylic acid (PAA) containing magnetite nanocrystals that are stabilized with PAA. Each side of the particles is color coded by selectively encapsulating FITC- and Rhodamine B-conjuaged dextrans. Rhodamine B-dextran was incorporated in the solution containing magnetite nanocrystals. The resulting nanocolloids were suspended in a Leica® oil and imaged for the emission wavelength of FITC (a) and Rhodamine (b) for the separate channels. Overlay of the two (c) clearly shows anisotropy.

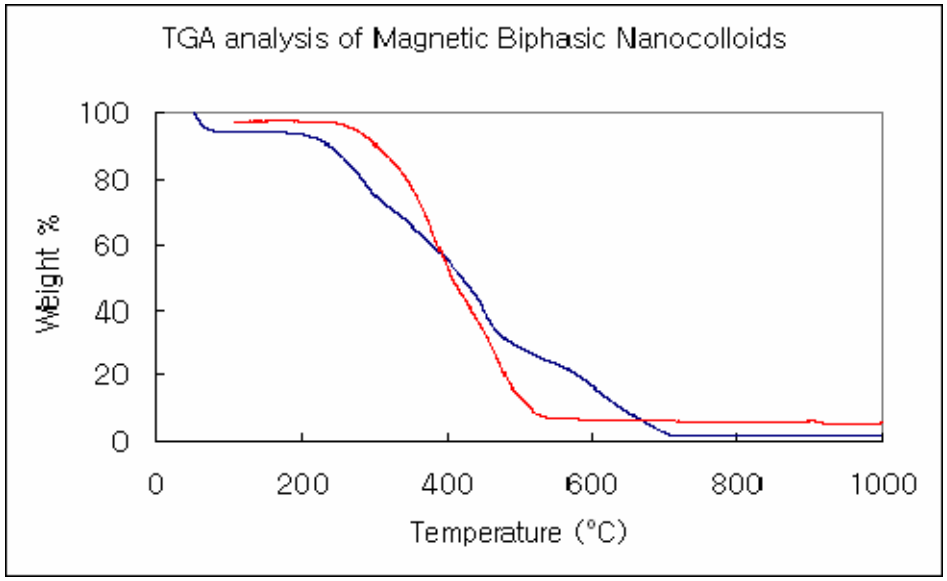

Figure 5.7 Thermal gravimetric analysis of magnetite-polymer composite bipasic nanocollodis. The red line is for the nanocolloids made of poly(acrylamide-*co*-acrylic acid) and the blue line is obtained from the nanocolloids made of poly(acrylic acid). The final values of the magnetite weight % were determined to be 5.65% and 1.55% for red and blue lines, respectively.

confirms that the nanocolloids are color-coded, also in an anisotropic manner.

As the anisotropic encapsulation of magnetite was demonstrated the most successfully for the PAAm-*co*-AA and PAA based nanocollodis, the loading contents of the magnetite NCs in those polymeric nanocolloids were examined by thermal gravimetric analysis (TGA). Figure 5.7 shows the typical example of TGA graphs of the polymer-magnetite composite nanocolloids. The weight fraction of the magnetite was determined to be controllable for about 1.0 ~ 5.0 %.

For a certain loading content (*f*, weight fraction of the magnetite in total polymer-magnetite composite particle), an average number of magnetite NCs encapsulated per polymer particle (N_1/N_2, where N is number of crystals or particles, subscript *1* is for magnetite nanocrystals and subscript *2* is for polymer particles) can be calculated, if the average diameter of magnetite NCs is given. Equation 5.1 shows how *f* can be expressed.

$$\frac{N_1 M_1}{N_2 M_2} = \frac{N_1 d_1^3 \rho_1}{N_2 d_2^3 \rho_2} = f$$ (Equation 5.1),

where M is average weight, d is diameter and ρ is density of the magneite nanocrystals (subscript 1) or polymeric particles (subscript 2).

For the magneite NCs with average diameter of 10 nm (d_1 = 10 nm), putting density ratio between the magnetite and polymer as 5 will allow us to plot N_1/N_2 versus d_2 for certain f values (Figure 5.8). The experimental data points were obtained by couting the number of NCs per polymeric particle by use of TEM micrograph image. Loading contents determined by TGA (1 %) roughly matched with the caculations, for the data points are between the lines of 0.5% and 1%.

The force that would be applied to a single magnetite NC by a certain magnetic field and magnetic field gradient is determined by equation 5.2

$$F_{NC} = \frac{V\chi}{\mu_o} \nabla(B^2)$$ (Equation 5.2),

where V is the volume of the magnetite NC, χ is susceptibility of the magnetite, μ_0 is the vacuum permeability, and B is the magnetid field strength.

Therefore for a polymer-magnetite composite particle that contains the magnetite NCs with an average diameter, the force that could be applied to a biphasic nanoparticle (BNP) under a certain magnetic field and field gradient would be determined by equation 5.3.

$$F_{BNP} = (N_1/N_2)\, F_{NC} \qquad \text{(Eqation 5.3)}$$

In order to design a electromagnetic device to control the alignment of the biphasic nanoparticles (BNPs) containing magnetite nanocrystals, consideration for the magnetic field and field gradient generation should be made in conjunction with the

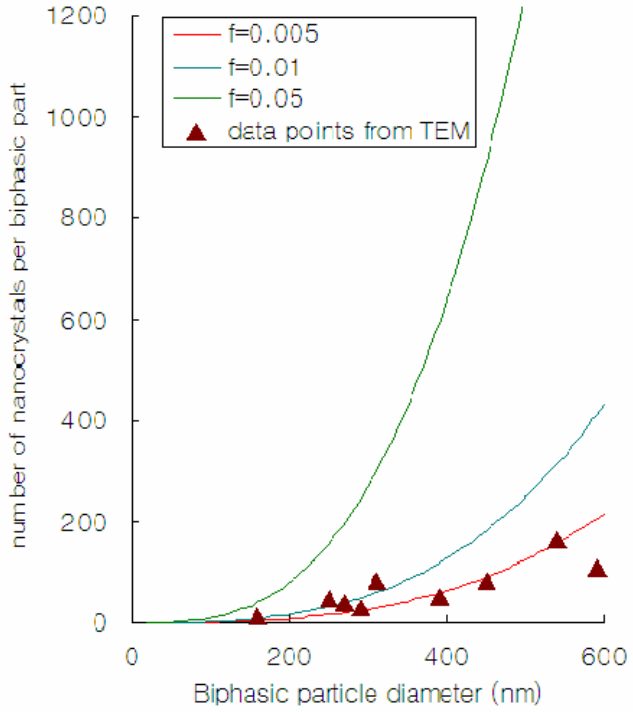

Figure 5.8 Number of nanocrystals per polymeric particle (N_1/N_2) vs. diameter of polymeric particle (d_2) for a given loading contents (f). The line was drawn for the magnetite nanocrystals with diameter (d_1) of 10 nm. The experimental data points were obtained by counting the number of crystals from TEM micrographs. The loading content matches roughly to the TGA analysis data ($f = 0.01$). The number of nanocrystals per polymeric particle is highly dependent on the size of the resulting polymeric particles.

appropriate design of the BNPs, especially in terms of magnetite loading contents and the size of the particles.

5.4 Conclusions

Electrified co-jetting was applied for the production of polymeric nanocolloids containing magnetic nanocrystals in the anisotropic manner. This research shows that anisotropic encapsulation of various functional nanomaterials inside of polymeric colloids is possible by a well-designed electrified co-jetting process. By leveraging and modifying conventional co-precipitation methods, superparamagnetic magnetite nanocrystals (diameter of less than 10 nm), that is coated and stabilized by PAA, OA, and PEG, were synthesized. Their suspension in the jettig polymer solution showed far better stability than the bare magnetite suspension. The nanocolloids based on PAAm-*co*-AA in this study showed the best homogeneous encapsulation in an anisotropic manner. These PAAm-*co*-AA nanocolloids could further be crosslinked by simple thermal treatment,(*25*) which could be useful for an application where polymeric nanocolloids need to be exposed to an aqueous environment. Considering that various dyes or drugs can also be loaded in each phase, these magnetic nanocolloids with novel geometry can be useful for display device, magnetically controlled biomedical imaging or targeted drug delivery.

It seems that the selection of the polymer solutions for a certain nanocrystal and its stabilization mechanism is critical for the successful electrified co-jetting. Stability of the suspension in the jetting polymer solution is important for every resulting colloidal particles to possess identical number of nanocrystals for a given diameter (homogeneous encapsulation). The conductivity and viscosity are critical parameter to control the liquid

motion inside of Taylor cone. If the liquid motion is vigorous enough to perturb the biphasic interface, the co-jetting cannot be successful. The instabilities originated from the imbalance between those physical properties of two jetting solutions should be minimized by optimization.

Detailed characterization and the application study of these nanocolloids in conjunction with optimization in the amount of encapsulation of nanocrystals and in the size of nanocolloids is proposed for the future work.

References

1. http://www2.parc.com/hsl/projects/gyricon/.
2. J. N. Anker, R. Kopelman, *Applied Physics Letters* **82**, 1102 (Feb, 2003).
3. I. S. Chronakis, *Journal of Materials Processing Technology* **167**, 283 (2005).
4. S. T. Tan, J. H. Wendorff, C. Pietzonka, Z. H. Jia, G. Q. Wang, *ChemPhysChem* **6**, 1461 (Aug, 2005).
5. Y. Zhu, J. C. Zhang, J. Zhai, L. Jiang, *Thin Solid Films* **510**, 271 (Jul, 2006).
6. K. H. Roh, D. C. Martin, J. Lahann, *Nature Materials* **4**, 759 (Oct, 2005).
7. K. H. Roh, D. C. Martin, J. Lahann, *Journal of the American Chemical Society* **128**, 6796 (May, 2006).
8. D. K. Kim, M. Mikhaylova, Y. Zhang, M. Muhammed, *Chemistry of Materials* **15**, 1617 (Apr, 2003).
9. D. K. Kim, Y. Zhang, W. Voit, K. V. Rao, M. Muhammed, *Journal of Magnetism and Magnetic Materials* **225**, 30 (Apr, 2001).
10. Y. Zhang, N. Kohler, M. Q. Zhang, *Biomaterials* **23**, 1553 (Apr, 2002).
11. S. Si *et al.*, *Chemistry of Materials* **16**, 3489 (Sep, 2004).
12. R. M. Cornell, Schwertmann, U., *The iron oxides: structure, properties, reactions, occurrence, and uses* (VCH, New York, 1996), pp.
13. K. Yamaguchi, K. Matsumoto, T. Fujii, *Journal of Applied Physics* **67**, 4493 (May, 1990).
14. D. Portet, B. Denizot, E. Rump, J. J. Lejeune, P. Jallet, *Journal of Colloid and Interface Science* **238**, 37 (Jun, 2001).
15. C. Sun, R. Sze, M. Q. Zhang, *Journal of Biomedical Materials Research Part A* **78A**, 550 (Sep, 2006).
16. A. K. Gupta, C. C. Berry, M. Gupta, A. S. Curtis, *IEEE T Nanobiosci* **2**, 255 (2003).
17. R. Jurgons *et al.*, *Journal of Physics-Condensed Matter* **18**, S2893 (Sep, 2006).
18. S. Miltenyi, W. Muller, W. Weichel, A. Radbruch, *Cytometry* **11**, 231 (1990).
19. J. M. Perez, F. J. Simeone, Y. Saeki, L. Josephson, R. Weissleder, *Journal of the American Chemical Society* **125**, 10192 (Aug, 2003).
20. A. I. Anton, *Journal of Magnetism and Magnetic Materials* **85**, 137 (Apr, 1990).
21. T. Neuberger, B. Schopf, H. Hofmann, M. Hofmann, B. von Rechenberg, *Journal of Magnetism and Magnetic Materials* **293**, 483 (May, 2005).
22. S. H. Sun, H. Zeng, *Journal of the American Chemical Society* **124**, 8204 (Jul, 2002).
23. I. Hayati, A. I. Bailey, T. F. Tadros, *Nature* **319**, 41 (Jan, 1986).
24. A. Barrero, A. M. Ganan-Calvo, J. Davila, A. Palacio, E. Gomez-Gonzalez, *Physical Review E* **58**, 7309 (Dec, 1998).
25. K.-H. Roh, J. Lahann, *Section Title: Chemistry of Synthetic High Polymers* **47**, 957 (2006).

CHAPTER 6

CONCLUSIONS

6.1 Suggested Future Directions

6.1.1 Optimization of the Electrified Co-Jetting Process

Liquid motion inside of multiphasic jetting cone

As discussed in the previous chapters, the critical requirement for the successful application of electrified co-jetting with jetting capillaries of side-by-side geometry is that the liquid-liquid interface must be sustained throughout the jetting process, from where the liquid jet must be ejected out. When there is no other mixing mechanisms involved except the simple diffusion, we can create sufficiently long-lasting interface over the jetting process by leveraging macromolecules' slow diffusion rate, as shown in Chapter 2 and 3 in details. However if there is fast liquid motion inside of the cone during the jetting process, this condition doesn't hold any more.

For the electrified jetting of a single liquid, the liquid motion inside of the cone has been investigated. It is relatively well known that there is a meridional recirculating motion for the jetting of a liquid with relatively low conductivity.(*1*) This motion has an axis-symmetry (meridional), so this motion itself wouldn't be very detrimental for the interface. However when the cone is composed of two or more different liquids, it is

highly probable that the axis-symmetry is easily broken, considering the liquid motion is originated from the tangential force which in turn is dependent upon the physical properties of each of the jetting liquids.

Furthermore, there is a spontaneous swirl motion of liquid inside the cone during the electrified jettings of liquids with low conductivity and low viscosity.(*2*) Without a viscosity high enough to dampen down the fast meridional motion, the spontaneous turbulent flow is unavoidable. Therefore, it seems intrinsically difficult to apply these jetting liquids that have high Reynolds number during the jetting process into the simultaneous jetting of multiple liquids without compromising the interfaces. However it is worth looking for additional stabilizing mechanisms which can be useful for counteracting with the instabilities of the cone and thus maintaining the liquid-liquid interface.

Therefore, the basic studies on the critical parameters of the jetting solutions related to the liquid motions inside of jetting cone is suggested for development of quasi-universally applicable electrified co-jetting process.

Size distribution

One of the imminent obstacles to use the multi-phasic nano-objects produced from the electrified jetting in the real-world applications would be their broad size distribution. For the end-production of a narrow size distribution, essentially two different approaches are possible: i) optimization of the jetting process and ii) filtration or sorting of the nano-objects.

If the focus is made for the discussion of process optimization, the reasons of broad size distribution is the objective to tackle. The broad size distribution of the nano-objects generated by the electrified jetting process can be attributed to intrinsic instability

of the process, fast drying under uncontrolled environment, and factors from the jetting liquid. First, the intrinsic instability of the process can be suppressed by modifying the process with additional stabilizing mechanisms. The probable approach would be the combination of the electrified jetting process with microfludic co-flow method. (*3, 4*) Second, the heterogeneity originated from the fast drying involved in the process can be regulated by efforts to control the environmental conditions surrounding the jet. The vapor pressure of the solvent used, humidity, and temperature would become the most obvious controlling parameters. Third, it seems probable that the size distribution of the polymer chains in a solution might be another reason for the broad size distribution of the resulting nano-objects. Using solutions of polymers with narrow polydispersity index for the electrified jetting would resemble the electrified jetting of low molecular weight liquids with defined molecular weights (such as water and oils). Polymer solutions behave differently from the liquid with a low molecular weight during the jetting process, especially due to the complex nature of viscoelasticity. However in electrified jetting of dilute limit, such as where the molecular ions are produced for the mass spectrometry, (*5, 6*) the control over size distribution will certainly be beneficial for narrower size distributions.

6.1.2 Extension of Electrified Co-Jetting Process

Multibore needle – multiphasic and compartmentalization

In this thesis, co-jetting process was proven to be applied up to three different jetting solutions that are placed in side-by-side way. And it is hard to find the reasons that this process cannot be applied to multiple solutions of more than three.

Essentially if the jetting capillaries are designed to feed many different solutions in a parallel way, they are applicable for the electrified co-jetting process. The possible number of combinations to assemble the position of each capillary becomes larger as the number of capillaries grows.

It is noteworthy that the number of types of jetting liquids can be controlled regardless of the total number of the capillaries. This implicates that we can control the relative fraction and position of each phase in the final objects by simply controlling the relative number and position of capillaries used for that specific jetting solutions. In other words, two more axes in the design for the smart building blocks (relative position and fraction of one phase to the others) can be introduced to by use of these multibore jetting capillaries.

Multiphasic nanofiber

In this thesis, focus was made for the production of biphasic/triphasic nanocolloids. However as mentioned in Chapter 1, the process is intrinsically applicable for the production of multiphasic nanofiber. In fact, the pseudo-universality of the electrified co-jetting process can be better postulated in the case of co-electrospinning than in co-electrospraying. The jetting solutions used for the electrospinning usually bear higher viscosity, which in turn is beneficial for maintaing the liquid-liquid interface owing to the reasons discussed above with regard to the liquid motions inside of the cone.

6.1.3 Potential Applications

Biomedical probes

In this thesis, platforms for utilizing biphasic nanocolloids for biomedical applications were devised. By use of these platforms, real-world biomedical applications can be further pursued. Biphasic nanocolloids can be applied in the field of drug delivery systems, cellular probes for *in-vitro* and *in-vivo* experiments, or *in-vivo* biosensors with drug targeting capability. Intrinsic complexity of biphasic character endows these objects multifunctionality.

When one phase of the colloidal particle is exploited for cell targeting by use of cell-specific antibody, as demonstrated in the work of directional labeling of cell membrane in Chapter 4, recognizing and sensing or even drug carrying can be achieved by the other phase. If we combine the concept of anisotropic encapsulation of nanocrystals presented in Chapter 5 into the work of Chapter 4, very many new possibilities may come out.

When the magnetite encapsulation described in Chapter 5 is directly combined with biolabeling, the nanocolloids can become a unique MRI probe. In the meantime, quantum dots are emerging new materials for biological labeling and are rapidly substituting traditional organic dyes and fluorescent proteins due to their unique advantageous characteristics such as high luminescence and long stability. When these quantum dots are selectively encapsulated inside of the biphasic particles, new probing and sensing mechanisms can be devised by combining the biphasic character and an appropriate physical mechanism (e.g. fluorescent resonance energy-transfer, FRET). For sensors or probes based on FRET, size control and interface design between the donor and acceptor considering the Föster distance will be the critical issue.

The use of two different cell-specific antibodies that are conjugated in each phase of biphasic nanocolloids would make these unique materials serve as bio-glue. These multiphasic nano-objects can be used to orient cells in a biomimicry fashion for novel tissue engineering.

Active layer for a photovoltaic device

Over the past decade, photovoltaic cells using semiconducting polymers have been steadily improved in power conversion efficiency. However the overall power conversion efficiency of organic solar cells are not comparable to their inorganic counterparts. Though there has been rigorous research in this area, few studies have put much effort on using the superior processing ability of organic materials, especially polymers, for the purpose of improving the efficiency of these devices. The overall efficiency of these devices can be enhanced by improving either light-harvesting capacity or the charge transfer process.

The non-woven mesh membrane of nanofibers directly produced by electrospinning has very high surface area compared to those of conventional uniform film layers.(*7*) Considering that the typical depth of optical absorption is far below micron scale, it is obvious that photo-harvesting capacity would be proportional to the surface-to-volume ratio of the effective layer, which is greatly enhanced when the layer is composed of fibers with a nanometer scale diameter.

In addition, the biphasic nanofiber membrane is more advantageous than a conventional blending system for generating heterojunctions between electron donor and acceptor. The electron-hole pairs (excitons) should be split before they recombine, and the electron acceptor-donor interface should be near a 10 nm length scale. Since Halls *et al.* reported interpenetrating networks of two polymer mixtures of donor and acceptor,(*8*)

many studies have been made on these blending of two components. However these so-called bulk heterojunctions have several limitations. Some regions made by random blending are too large for excitons to diffuse to the interface and each charge carrier phase can be interrupted by the other before it reaches the electrode. Exciton recombination due to these problems is still the major challenge for enhancing the energy conversion efficiency of organic solar cell device. In contrast, our biphasic nanofibers have a controllable phase dimension, whose diameter can go down to tens of nanometers. So theoretically almost every exciton generated by both phase can meet the interface before it recombines. These pseudo-molecular level heterojuction interfaces realized by the biphasic configuration of nanofibers will give a novel way to improve the exciton-splitting process. Additionally, since each phase forms a 1-dimensional object, each acts as a charge carrier uninterrupted by the other until it contacts the electrode.

6.2. Concluding Remarks

In this thesis, electrified co-jetting was proposed as a new method to control the material distribution in nanometer-scale. As a result, biphasic nanocolloids were synthesized by selective encapsulation of two different bio-macromolecules in each of the individual phases of an individual particle. In order to expand the versatility of those biphasic nanocolloids, selective tethering of ligands to the surface of individual phases was demonstrated. And the possible extension in the number of co-jetting capillaries was examined by employing three side-by-side capillaries for the production of triphasic nanocolloids.

Thermal imidization reaction was employed to crosslink the biphasic nanocolloids made of poly(acrylamide-*co*-acrylic acid) and polyacrylic acid. After the thermal treatment, the nanocolloids were stable in aqueous environment for the tested multiple weeks without dissolution or aggregation. As the first step toward the potential biological applications of these biphasic nanocolloids, the cyto-compatibility was tested. For the each cellular model system, human umbilical vein endothelial cells (HUVECs) and murine fibroblasts (NIH 3T3), presence of biphasic nanocolloids didn't affect their cell proliferation. The biphasic nanoparticles were either internalized by or adsorbed to these cells even without the specific interactions introduced. But this non-specific association of the biphasic nanocolloids and cells did not greatly decrease the cells' viability within the doses tested. The complete prevention of this non-specific association seems unlikely without further surface modification.

Polyethylene glycol layer was then introduced to the surface of the biphasic naocollodis by use of 'Click Chemistry', which was shown to greatly reduce the non-specific association. Combined with selective modification of specific ligands, a concept

of directional labeling of the biphasic nanocolloids onto the HUVEC membrane was successfully demonstrated.

Finally electrified co-jetting was successfully applied for encapsulating functional nanocrystals into polymeric nanocolloids in anisotropic manner. Suspensions of superparamagnetic magnetite nanocrystals that are coated and stabilized with oleic acid, polyethylene glycol, and polyacrylic acid were synthesized and utilized as the jetting solutions. Transmission micrographs of the resulting nanocolloids showed that the best anisotropic encapsulation was made for poly(acrylamide-co-acrylic acid) and polyacrylic acid-based nanocolloids containing polyacrylic acid-stabilized magnetite nanocrystals. Discussions for the optimization both in the amount of encapsulation of nanocrystals and in size of the biphasic nanocolloids were made.

As part of the conclusions, some future research directions for the better utilization of the electrified co-jetting were proposed. In order to achieve successful anisotropic multi-phasic co-jetting for a broader range of jetting liquids, efforts should be made to suppress the instabilities in the various fluid motions related to the cone-jet mode. If the process is optimized to generate anisotropic nanocollodis with narrower size distributions, there would be far more possible opportunities in biomedical, electronic and ink applications.

References

1. I. Hayati, A. I. Bailey, T. F. Tadros, *Nature* **319**, 41 (1986).
2. A. Barrero, A. M. Ganan-Calvo, J. Davila, A. Palacio, E. Gomez-Gonzalez, *Physical Review E* **58**, 7309 (1998).
3. T. Nisisako, T. Torii, T. Takahashi, Y. Takizawa, *Advanced Materials* **18**, 1152 (2006).
4. A. S. Utada *et al.*, *Science* **308**, 537 (2005).
5. J. B. Fenn, M. Mann, C. K. Meng, S. F. Wong, C. M. Whitehouse, *Science* **246**, 64 (1989).
6. J. B. Fenn, M. Mann, C. K. Meng, S. F. Wong, C. M. Whitehouse, *Mass Spectrometry Reviews* **9**, 37 (1990).
7. I. D. Norris, M. M. Shaker, F. K. Ko, A. G. MacDiarmid, *Synthetic Metals* **114**, 109 (2000).
8. J. J. M. Halls *et al.*, *Nature* **376**, 498 (1995).